UNIVERSITY OF PALERMO
DEPARTMENT OF ENGINEERING

UNIVERSITY OF BELGRADE
SCHOOL OF ELECTRICAL ENGINEERING

Maja B. Trumić

STIFFNESS ESTIMATION AND ADAPTIVE CONTROL FOR SOFT ROBOTS

Doctoral Dissertation

Palermo/Belgrade, 2021

УНИВЕРЗИТЕТ У ПАЛЕРМУ
ДЕПАРТМАН ЗА ТЕХНИКУ

УНИВЕРЗИТЕТ У БЕОГРАДУ
ЕЛЕКТРОТЕХНИЧКИ ФАКУЛТЕТ

Маја Б. Трумић

ЕСТИМАЦИЈА КРУТОСТИ И АДАПТИВНО УПРАВЉАЊЕ КОД ПОПУСТЉИВИХ РОБОТА

Докторска дисертација

Палермо/Београд, 2021

Supervisors

Dr. **Adriano Fagiolini**
Assistant Professor
Department of Engineering, University of Palermo, Italy

Dr. **Kosta Jovanović**
Assistant Professor
School of Electrical Engineering, University of Belgrade, Serbia

Thesis Committee

Dr. **Alessandro De Luca**
Full Professor
Department of Computer, Control and Management Engineering
The Sapienza University of Rome, Italy

Dr. **Slobodan Vukosavić**
Full Professor
School of Electrical Engineering, University of Belgrade, Serbia

Dr. **Cosimo Della Santina**
Assistant Professor
Department of Cognitive Robotics, Delft University of Technology, Netherlands

Dr. **Antonio Chella**
Full Professor
Department of Engineering, University of Palermo, Italy

This Ph.D. thesis has been realized within the Agreement for Joint Supervision of a Doctoral Thesis between the University of Belgrade, the University of Palermo and Maja Trumić. At the University of Palermo, Maja has been enrolled in the International Doctoral Program on "Information and Communication Technologies" (Cycle 33), and at the University of Belgrade she has been enrolled in the Ph.D. program "Electrical and Computer Engineering" on the topics of Robotics and Automation.

Thesis Evaluators at the University of Belgrade

Dr. **Alessandro De Luca**
Full Professor
Department of Computer, Control and Management Engineering
The Sapienza University of Rome, Italy

Dr. **Slobodan Vukosavić**
Full Professor
School of Electrical Engineering, University of Belgrade, Serbia

Dr. **Cosimo Della Santina**
Assistant Professor
Department of Cognitive Robotics, Delft University of Technology, Netherlands

Dr. **Antonio Chella**
Full Professor
Department of Engineering, University of Palermo, Italy

Dr. **Željko Đurović**
Full Professor
School of Electrical Engineering, University of Belgrade, Serbia

Dr. **Filippo D'Ippolito**
Assistant Professor
Department of Engineering, University of Palermo, Italy

Thesis Evaluators at the University of Palermo

Dr. **Željko Đurović**
Full Professor
School of Electrical Engineering, University of Belgrade, Serbia

Dr. **Filippo D'Ippolito**
Assistant Professor
Department of Engineering, University of Palermo, Italy

Acknowledgements

I am very grateful for meeting numerous truly amazing people during my Ph.D. studies who have significantly enriched my life.

First, I would like to express my deepest gratitude to Dr. Adriano Fagiolini for his infinite support and encouragement, for sharing with me the visionary ideas for control of robots that made me remain highly motivated throughout every day of studies, and for dedicated, invaluable, and focused guidance that allowed me to finish studies in time. Without his persistent help and incredibly kind and friendly nature merged with a genius mind, Ph.D. studies would not be such a joyful experience. Moreover, I would never learn ice-skating.

I would also like to extend my deepest appreciation to Dr. Kosta Jovanović for his infallible guidance and intuition within the field of soft robotics. His solution-oriented approach, constantly optimistic perspective, and a strong belief in final results have not only positively affected my research, but also shaped me as a person and a professional. Being the role model for me and, indeed, generations of engineering students in Serbia, Kosta has transferred various soft skills for which I am very grateful.

Moreover, I am sincerely thankful to Prof. Antonio Bicchi for lending me pneumatic robot GioSte which allowed timely validation and publication of results, as well as for the insightful suggestions throughout my Ph.D. studies. The research results of Prof. Alessandro De Luca and Dr. Fabrizio Flacco have been the important pillars of my Ph.D. studies. Therefore, the kindness and patience of Prof. De Luca, his valuable advice, and fruitful discussions have been of high significance and support for me.

It has been a great pleasure to collaborate with Dr. Cosimo Della Santina and Dr. Giorgio Grioli on the topics within my thesis. Huge thanks to Cosimo for introducing me to the fantastic world of soft-bodied robots and sharing the new perspective on soft robot control and modeling. Moreover, it has been a great experience working on the noninvasive stiffness estimation with Giorgio, one of the pioneers in determining stiffness in soft robot joints.

Numerous professors that I met during my studies have been a source of great motivation and support for me. In this regard, I am very grateful for Prof. Andrea Serrani's inspiring lectures about adaptive control, for Prof. Maurizio Cirrincione's technical help regarding robot GioSte and for being an example of how to fully live a life, for the huge understanding by Prof. Aleksandar Rodić and Prof. Goran Kvaščev, for the life and robotics lessons by Prof. Veljko Potkonjak, for the encouragement by professors Slobodan Vukosavić, Dejan Popović, Milica Janković, Željko Đurović, Branko Kovačević, Aleksandar Rakić, Branko Malešević, Ivana Jovović, and Tatjana Lutovac on Belgrade side and professors Ilenia Tinnirello, Laura Giarré, Giovanni Garbo, Stefano Mangione, and Pierluigi Gallo on Palermo side. Special thanks to my first supervisor Prof. Stevica Graovac who has always believed in me and Prof. Tomislav Šekara for introducing me to the scientific world, as well as to my supervisors in the previous company Bosch, Volker Henrichs and Rüdiger Ruddies, for pushing me to aim at the highest. Furthermore, I would like to warmly thank Sanja Vujnović, Aleksandra Marjanović, Predrag Tadić, and Jovana Petrović for their kind moral support throughout my entire studies.

The Ph.D. studies have been a fantastic period thanks to my colleagues and office-mates Branko Lukić, Nikola Knežević, Zaviša Gordić, and Vladimir Petrović. They have given me significant practical and moral support, discussed often with me soft robotics, and tremendously helped with the administration. Especially helpful to me in the beginning was the technical support by skillful Predrag Todorov and four students from the University of Palermo: Francesco Pravatà, Fabio Corso, Giorgio Gullo, and Alessandro Augello. I owe as well gratitude to Ricardo Mengacci and Franco Angelini for the discussions on soft robotics and to the other Centro Piaggio members Prof. Lucia Pallottino, Federico, Sariah, Gemma, Chiara,

Gianluca and Giuseppe for a great time at conferences.

During this journey, I received financial support that facilitated my mobility, allowed me to visit conferences and follow courses by eminent professors. Therefore, I am very grateful to the University of Palermo, the Ministry of Education, Science and Technological Development of Serbia, the European Embedded Control Institute, and Zoran Đinđic Foundation. Following bilateral doctoral studies included a lot of additional administrations. I am very grateful for the assistance and availability of Milena Šikanić from the University of Belgrade, Milena Damjanović and vice dean Predrag Ivaniš from the School of Electrical Engineering, and Dr. Carmelo Priolo from the University of Palermo.

Furthermore, I would like to thank a lot my friends. First, many thanks to Milica Jovanović, my dear friend who has always been very supportive and a successful problem-solver. I would like to extend the gratitude for the joyful moments in Belgrade to Dragana, Tamara, Stefan, Igor, Milan, Dušan, Milica, Đuka and the employees of the restaurant Mihajlo. Special thanks go to Dejan Zlatanović for being a true friend. When in Palermo, my free time has always been quite interesting thanks to all people who at one point belonged to the Holy Light choir, Alessandro who put an effort in teaching me ice-skating, my flatmates from Via Gorizia and Via Ernesto Paci. Sincere thanks go to Signor Mammina and Giovanni Garraffa for teaching me Sicilian. Moreover, my huge gratitude goes to Amalia and Davide for hosting me in Fornacette and temporarily in Palermo.

Lastly, I have been truly blessed to receive immense support from my family, particularly from my mother Biserka and my brother Ivan. Thank you for all the patience.

Belgrade, April 21, 2021

Maja Trumić

Dissertation title: Stiffness Estimation and Adaptive Control for Soft Robots

Abstract: Although there has been an astonishing increase in the development of nature-inspired robots equipped with compliant features, i.e. soft robots, their full potential has not been exploited yet. One aspect is that the soft robotics research has mainly focused on their position control only, while stiffness is managed in open loop. Moreover, due to the difficulties of achieving consistent production of the actuation systems for soft articulated robots and the time-varying nature of their internal flexible elements, which are subject to plastic deformation over time, it is currently a challenge to precisely determine the joint stiffness.

In this regard, the thesis puts an emphasis on stiffness estimation and adaptive control for soft articulated robots driven by antagonistic Variable Stiffness Actuators (VSAs) with the aim to impose the desired dynamics of both position and stiffness, which would finally contribute to the overall safety and improved performance of a soft robot. By building upon Unknown Input Observer (UIO) theory, invasive and non-invasive solutions for estimation of stiffness in pneumatic and electro-mechanical actuators are proposed and in the latter case also experimentally validated. Beyond the linearity and scalability advantage, the approaches have an appealing feature that torque and velocity sensors are not needed.

Once the stiffness is determined, innovative control approaches are introduced for soft articulated robots comprising an adaptive compensator and a dynamic decoupler. The solutions are able to cope with uncertainties of the robot dynamic model and, when the desired stiffness is constant or slowly-varying, also of the pneumatic actuator. Their verification is performed via simulations and then the pneumatic one is successfully tested on an experimental setup. Finally, the thesis shows via extensive simulations the effectiveness of adaptive technique applied to soft-bodied robots, previously deriving the sufficient and necessary conditions for the controller convergence.

Keywords: robotics, soft robotics, variable stiffness actuators, modeling, stiffness estimation, unknown input observers, adaptive control
Scientific field: Electrical and Computer Engineering
Scientific subfield: Robotics and Control Systems

Наслов докторске дисертације: Естимација крутости и адаптивно управљање код попустљивих робота

Апстракт: Иако се данас изузетно интензивно ради на развоју робота инспирисаних природом које одликује еластична структура, њихов пуни потенцијал још увек није искоришћен. Са једне стране, истраживања у области попустљивих робота су углавном фокусирана само на управљање њиховом позицијом, док се крутост регулише у отвореној спрези. Поред тога, због потешкоћа у постизању конзистентне производње актуатора и променљиве природе њихових еластичних елемената, који су временом подложни пластичној деформацији, тренутно је изазов прецизно одредити крутост зглобова робота.

У циљу доприноса побољшању перформанси и безбедности рада попустљивих робота, теза приказује допринос процени крутости и адаптивног симултаног управљања позицијом и крутости антагонистичких актуатора променљиве крутости (ВСА). Ослањањући се на теорију опсервера непознатих улаза (УИО), предложена су инвазивна и неинвазивна решења за процену крутости у пнеуматским и електромеханичким актуаторима и експериментално верификована у случају друге групе актуатора. Поред линеарности и скалабилности, ови приступи имају привлачну особину да сензори момента и брзине нису потребни.

Теза предлаже иновативне системе управљања који поседују адаптивни компензатор и динамички декуплер. Предложене методе управљања демонстрирају могућност да компензују несигурности динамичког модела робота без обзира да ли је он погоњен електричним или пнеуматским актуаторима. Након симулација, развијено управљање је верификовано и на пнеуматском роботу. На крају тезе, обимне симулације показују ефикасност адаптивне технике када се примени на роботе са флексибилним линковима, претходно изводећи довољне и потребне услове за конвергенцију контролера.

Кључне речи: роботика, попустљиви роботи, актуатори променљиве крутости, моделирање, естимација крутости, адаптивно управљање
Научна област: Електротехника и рачунарство
Научна подобласт: Роботика и управљачки системи

Titolo della tesi: Stima della rigidezza e controllo adattivo per *soft* robot

Sommario: Nonostante la sorprendente crescita nello sviluppo dei robot ispirati alla natura, tra cui i cosiddetti *soft* robot, il potenziale di questi sistemi, che hanno intrinseche capacità di adattamento, non è ancora stato sfruttato a pieno. La ricerca ha principalmente considerato il controllo in retroazione della posizione dei giunti del robot, lasciando la gestione della cedevolezza di questi ultimi ancora in anello aperto. Peraltro, le attuali limitazioni nel processo di produzione degli attuatori a cedevolezza variabile e l'inevitabile variabilità nel tempo degli elementi elastici costitutivi, i quali sono soggetti ad usura e deformazione plastica, rendono il problema della determinazione precisa della rigidezza di giunto ancora oggi una sfida.

In tale ambito, questa tesi pone l'accento sulla stima della rigidezza e sul controllo adattativo dei soft robot, considerando in primis i sistemi articolati e pilotati da attuatori a cedevolezza variabile (VSA) in configurazione antagonista. Ciò viene fatto con l'obiettivo primario di imporre *simultaneamente* una dinamica desiderata sia per la posizione che per la rigidezza e, conseguentemente, di migliorare la sicurezza fisica e le prestazioni di un soft robot.

Basandosi sulla teoria degli osservatori ad ingresso sconosciuto (UIO), in questo lavoro vengono proposte soluzioni, invasive e non, che consentono di stimare la rigidezza nei robot con attuatori pneumatici o elettromeccanici, soluzioni che nel secondo caso vengono anche validate sperimentalmente. Oltre al vantaggio della linearità e della scalabilità, le suddette soluzioni hanno l'interessante caratteristica di non richiedere l'uso di sensori di coppia o velocità.

Sfruttando così la disponibilità di una stima della rigidezza, il lavoro descrive inoltre dei metodi innovativi per il controllo robusto dei soft robot articolati, il cui schema include un compensatore adattativo e un disaccoppiatore dinamico. Detti metodi possono gestire le incertezze nella conoscenza del modello dinamico del robot e, quando il riferimento della rigidezza è costante o lentamente variabile, anche quelle relative all'attuatore pneumatico. La loro verifica è valutata attraverso delle simulazioni e, nel caso pneumatico, anche per via sperimentale.

Infine, la tesi mostra come estendere le tecniche di controllo adattativo ai sistemi robotici con cedevolezza distribuita lungo l'intero corpo del robot, garantendo formalmente la convergenza del controllore. L'efficacia di questa tecnica adattativa è mostrata attraverso una estensiva simulazione.

Parole chiave: robotica, *soft* robotica, attuatori a cedevolezza variabile, modellistica, stima della rigidezza, osservatori ad ingresso sconosciuto, controllo adattativo.
Macro-ambito scientifico: Ingegneria elettrica e informatica
Settore scientifico: Robotica e sistemi di controllo.

Contents

Introduction

At the mention of industrial robots, usually bulky, heavy, and rigid manipulators come to mind. Their installation in factories has begun in the 1980s marking the beginning of the modern age of robotics, where robots switched humans in almost all repetitive and exhausting yet simple and precise tasks. For safety reasons, most industrial robots are placed inside cages where they perform tasks such as welding, assembling, and grinding without any interference from a human operator. In this way, a clear borderline between human and robot roles is drawn.

The aspiration of the robotics society in the last three decades, however, has been the development of robots that will be more human-like in both mechanical and cognitive sense and, as such, capable of operating within the anthropic environment. Indeed, creating a shared human-robot workplace would have positive social and economic influence (Ajoudani et al. (2018)) while human-robot collaboration would radically improve the health of manufacturing workers if robots would assist them, for example, in carrying heavy equipment (Cherubini et al. (2016)). Moreover, the physical interaction with a robot increases the bonding and attenuates the stress of a human (Willemse and van Erp (2019)). These insights, accompanied by the endeavor to achieve or even surpass human dexterity and promptness in performing motion and manipulation tasks, have fostered the development of soft robotics.

The term *soft robot* will be used to denote the robots whose era started with the intentional introduction of flexible elements inside them aiming at mimicking the actuation mechanism of biological systems. Even though rigid robots can become human-friendly by exploiting collision detection and avoidance software (Haddadin et al. (2017)), perception (Flacco et al. (2012b)), and active compliance (Albu-Schäffer et al. (2007b)), soft robots have the advantage of light-weight structure, high force-to-weight ratio, energy efficiency, and the infinite bandwidth. Thanks to these properties, soft robots have shown promising aspects where safety, robustness, and adaptability are the main concern (Rus and Tolley (2015), Van Ham et al. (2009)). So far, the idea of soft robot design has led to the development of effective prosthetic devices such as tendon-driven robotic hands (Piazza et al. (2017)) and exoskeletons (Karavas et al. (2015)). However, while robots with software-enabled compliance have already been quite developed and has become part of the industry, there is still a panorama of open questions about soft robots – robots with intrinsic and passive compliance.

In general, these systems can be divided into two groups: soft articulated robots whose elastic elements are concentrated within joints and soft-bodied robots with the elasticity distributed along the links (De Luca and J. Book (2016)).

Part of the research focuses on soft articulated robots whose essential feature is the ability to change, besides position, also their stiffness – the inverse of the compliance - in real-time. Such potential, similar to the one that humans have, can be achieved with several different mechanisms. Among them, variable stiffness actuators (VSAs) in the antagonistic setup, either electrically or pneumatically powered, seem to be most auspicious in typical applications (Grioli et al. (2015)). The pneumatic variant has benefits due to the higher power-to-weight ratio and simplicity of the mechanism (Bicchi and Tonietti (2002), Albu-Schäffer et al. (2007a)) while the electric ones are prominent for their compactness, silence, and the fact that no external

devices are required (such as air or fluid compressors) (Wolf et al. (2016)). On the other side, inspired by nature and endowed with morphological flexibility and compliance, robots with flexible links, more precisely – soft-bodied continuum robots, are advantageous with respect to the articulated ones for their capacity to adapt to the harsh terrain, move within confined spaces, achieve rapid movements, and smoothly manipulate objects (Rus and Tolley (2015); Polygerinos et al. (2017)).

Motivation

To ensure the safety of a human-robot collaboration one has to be continuously aware of the soft robot stiffness. This requirement is described with the danger index defined by Ikuta et al. (2003), where it is suggested that the index shall be a product of several factors, such as distance between robot and human, their relative velocity, and finally the inertia and stiffness of a robot. However, stiffness is not measurable, meaning that its value cannot be determined by using a sensor. In this case, one can either perform extensive experimentation and identification, in order to obtain an accurate stiffness model, or can rely on datasheets from the manufacturers. Even in the case that the provided datasheets are initially reliable, the continuous wear induced by the impact of forces acting on the elastic elements, the temperature drifts, and the torque hysteresis eventually result in additional inaccuracies (Ruderman et al. (2014)). This motivates the development of online stiffness estimators, which also become crucial for closed-loop stiffness control.

Effective control of stiffness at the joint or end-effector level is the key enabler for the VSA benefits that arise in various tasks, such as when performing cyclic movements for dribbling a ball (Haddadin et al. (2018)), during explosive actions of autonomous hammering (Garabini et al. (2011)), for safe human-robot interaction (De Santis et al. (2008)), and indeed in many others. Different solutions of position and stiffness control have already been explored, including backstepping (Petit et al. (2015)), LQR-based gain scheduling (Sardellitti et al. (2012)), adaptive control (Tonietti and Bicchi (2002)), sliding mode control (Best et al. (2016b)), all with the assumption that an accurate and reliable stiffness estimate is available. So far, since stiffness is not measurable, its regulation is mostly performed in open-loop by leveraging on model-based computation. The initiative to close the loop on both position and stiffness, achieving the decoupled control of those variables and imposing the desired motion dynamics, has first been addressed by exploiting static and dynamic feedback linearization (Palli et al. (2008)), however, the high control gains have deterred its applicability. This has simultaneously motivated the development of online stiffness estimators and control techniques for soft articulated robots that are robust to model uncertainties, such as those based on adaptive techniques.

Robust control techniques have a promising application also within the field of soft-bodied robots. The recent conclusion that soft robot dynamics can be connected to the one of an augmented rigid robot by satisfying certain kinematic and dynamic constraints (Della Santina et al. (2020b)), has opened the door for applying classical control techniques on the theoretically infinite-dimensional soft-bodied robots. Therefore, the cumbersome necessity to perform an extensive identification procedure in order to find dynamic parameters of soft continuum robots prior to applying model-based control laws has inspired the consideration of adaptive-based approaches.

Thesis contributions

The research within the thesis has been devoted to the development of algorithms that will enhance the capabilities of soft robots. The starting goal has been to design the control law that can ensure the simultaneous and decoupled closed-loop control of both position and stiffness in robot joints without requiring accurate knowledge of robot dynamic parameters.

Since stiffness is not measurable, the first line of the research has been directed towards designing online stiffness estimators. To the best of the author's knowledge, in the thesis the first online stiffness estimator for joints actuated by pneumatic VSAs is proposed and its performance has been validated in the simulation environment. Moreover, the estimation of stiffness in joints of electro-mechanically driven robots has been achieved in an innovative way by using unknown input observer theory, both invasively and non-invasively, being accompanied by the simulation and experimental verification of the proposed estimators. As a result, the design of an invasive stiffness estimator differs from the state-of-the-art solutions in a way that it neither requires information about the velocity of drives, nor tuning of any other parameters except the ones of the Recursive Least Square algorithm. The original work on this topic has been published by the author in (Fagiolini et al. (2020), Trumić et al. (2019)). Furthermore, the presented non-invasive estimator improves the latest results since it does not lean on information from force/torque sensors and does not suffer from the observability issues.

The commonly applied approaches for the control of soft robots are closing the loop only on position, while stiffness is regulated in open loop. Contrarily, the limelight of the thesis is to design the control that can simultaneously ensure that both the position and stiffness have the desired dynamics. In this regard, the results by the author in (Trumić et al. (2018), Trumić et al. (2020c)) have presented the very first experimental verification of closing the loop on both position and stiffness of pneumatically driven robots, which is achieved via decoupled nonlinear adaptive control, while the broader perspective is discussed in (Trumić et al. (2020)). Moreover, comparison to feedback linearization approach is shown in (Trumić et al. (2020b)). The thesis continues with the solution for the decoupled adaptive control of electrically driven soft articulated robots, which takes into account also the actuator dynamics. Finally, sufficient and necessary conditions for designing adaptive control of soft-bodied robots are discussed and the formulation of the adaptive control in the context of soft robots is shown. The non-theoretical contribution of this topic comprises simulations that show the performance of adaptive control when applied to different instances of soft robots (Trumić et al. (2020a)).

The main contributions are the following:

- A PCC-based model for a generic three-dimensional soft robot, ensuring kinematic and dynamic equivalence with the original system and having no representation singularities and discontinuities;
- An invasive stiffness estimator for pneumatically and electro-mechanically driven soft articulated robots based on the theory of delayed Unknown Input Observers, which requires neither apriori knowledge about stiffness model nor measurement of motors velocities;
- A non-invasive stiffness estimator for electro-mechanically driven soft articulated robots based on the theory of delayed Unknown Input Observers, that lacks the necessity of force/torque measurements and does not experience observability issues;
- Experimental validation of the invasive and non-invasive stiffness estimators performed on the electro-mechanically driven soft articulated robot;
- A robust closed-loop position and stiffness controller for pneumatic soft articulated robots, which is based on the nonlinear adaptive control theory. Decoupling position and stiffness control is achieved by using control degrees of freedom associated with the null-space of the actuator matrix;

- A simulation and experimental validation of the proposed technique which shows the performance and comparison with open-loop based solutions and feedback linearization method;
- A robust cascade-based closed-loop position and stiffness controllers for electro-mechanical soft articulated robots, which address also dynamics of the actuator and which are based on the proportional-derivative (PD) controller plus feedforward term and nonlinear adaptive control theory. Decoupling is achieved via the corresponding matrix which maps the flexibility torques into the desired position and stiffness dynamics;
- Simulation validation of the proposed controllers and the comparison in cases when the integral term is added.
- A robust closed-loop position controller for a soft-bodied robot, which is based on the nonlinear adaptive control theory;
- Extensive simulation validation - including 3D and non-constant curvature soft robots - proving the effectiveness and the robustness of the controller.

The related publications by the author are:

International journals:

Fagiolini A, **Trumić M** and Jovanović K (2020) An input observer-based stiffness estimation approach for flexible robot joints. *IEEE Robotics and Automation Letters* 5(2): 1843-1850, DOI: 10.1109/LRA.2020.2969952.

Trumić M, Jovanović K and Fagiolini A (2020) Decoupled nonlinear adaptive control of position and stiffness for pneumatic soft robots. *The International Journal of Robotics Research*, In press DOI: 10.1177/0278364920903787.

Trumić M, Della Santina C, Jovanović K and Fagiolini A (2020) Adaptive control of soft robots based on an enhanced 3D augmented rigid robot matching. *IEEE Control Systems Letters (L-CSS)*, In press, DOI: 10.1109/LCSYS.2020.3047737.

International conferences:

Trumić M, Jovanović K and Fagiolini A (2020) Comparison of model-based simultaneous position and stiffness control techniques for pneumatic soft robots. In: *International Conference on Robotics in Alpe-Adria Danube Region*. Springer, pp. 218-226, DOI: 10.1007/978-3-030-48989-2_24

Italian and Serbian national conferences:

Trumić M, Jovanović K and Fagiolini A (2020) Towards safer collaboration - closing the loop on position and stiffness of soft articulated robots. In: *Italian Robotics and Intelligent Machines Conference*, In press.

Trumić M, Jovanović K and Fagiolini A (2019) Flexibility torque estimation in articulated soft robots, Automatica.it 2019, Ancona, Italy
(http://www.automatica2019.it/programma/programma-tecnico/sessioni-interattive/)

Trumić M, Jovanović K and Fagiolini A (2018) Kernel-based nonlinear adaptive control of stiffness and position in pneumatic soft robots, Automatica.it 2018, Florence, Italy
(http://sidra2018.dinfo.unifi.it/programmma/sessioni-interattive/)

Trumić M, Jovanović K and Fagiolini A (2018) Adaptivno upravljanje robotom sa elastičnim pogonom, 62^{nd} ETRAN conference, pp. RO1.1 377-380, June 2018, Palić, ISBN: 978-86-7466-752-1.

Thesis overview

The thesis is divided into three parts: modeling, stiffness estimation, and adaptive control of soft robots.

Summary of Part I

The first part introduces the reader to the mechanisms of state-of-the-art soft robotic setups and provides their mathematical description.

Chapter 1 gives an overview of different soft articulated robots, highlighting ones with the antagonistic variable stiffness actuation, and briefly reports on various soft-bodied robots.

Chapter 2 presents the mathematical description of soft articulated robots with the variable stiffness actuators driven by either pneumatic or electro-mechanic drive.

In **Chapter 3** dynamics of soft-bodied robots is modeled under the assumption of piecewise constant curvature. The author contributes by developing an augmented formulation for a soft robot in three-dimensional space, that is described by an improved parameterization, thus avoiding singularity and discontinuity issues (Trumić et al. (2020a)). Besides, the chapter presents the model of a soft inverted pendulum with affine curvature.

Summary of Part II

The second part proposes novel techniques for stiffness estimation in soft articulated robots. Recalling that stiffness is not measurable, there is no sensor that can retrieve its value. However, to be aware of the value of stiffness is crucial not only for guaranteeing safe human-robot collaboration, but also for designing the control techniques which close the loop on both position and stiffness.

Chapter 4 introduces the main concept of stiffness estimation, as well as state-of-the-art techniques.

Chapter 5 outlines the general theory of delayed unknown input observers and recursive least square algorithms, which are fundamental for determining the analytic expressions of stiffness and flexibility torque.

In **Chapter 6** an invasive approach is performed to find stiffness in both pneumatically and electro-mechanically actuated robot joints. First, the flexibility torque acting on the robot joint is determined by considering it as an unknown input to the system. Then, coefficients of stiffness and flexibility torque polynomial approximations are obtained via recursive least square algorithm. Part of this chapter has been published by the author in (Trumić et al. (2019), Fagiolini et al. (2020)).

Chapter 7 presents a non-invasive approach, which is appealing for the reason that only information on link and drives positions are necessary. Herein, a delayed UIO and RLS algorithms are used to directly reconstruct the first time derivative of the flexibility torque, which by definition contains the information on stiffness.

Summary of Part III

The third part addresses the adaptive control of soft robots. To manage a soft robot presents an immense challenge due to the existence of intrinsic flexible and nonlinear elements as well as the elastic coupling between the motors and links positions in the case of soft articulated robots. Thus, the solutions proposed in this part tackle these challenges by coping with model uncertainties and ensuring the decoupling property.

Chapter 8 reviews the previously achieved results in controlling soft robots.

Chapter 9 presents the principles of nonlinear adaptive control.

In **Chapter 10** the decoupled nonlinear adaptive control is proposed to ensure the simultaneous and independent closed-loop control of both position and stiffness for pneumatically driven flexible joint robots. The results within this chapter have been published by the author in (Trumić et al. (2020c), Trumić et al. (2020), Trumić et al. (2020b), Trumić et al. (2018)).

Chapter 11 proposes a cascade-based decoupled adaptive control for robots with the electro-mechanic actuation which also considers the dynamics of actuators. The inner loop controller ensures asymptotic tracking of the desired motors positions, while the outer-loop one enables tracking of the desired position and stiffness trajectories.

Finally, **Chapter 12** tackles the dynamic control of soft-bodied manipulators. More precisely, it shows how to formulate the adaptive control calculations and describe the necessary and sufficient hypotheses for convergence. Results from this chapter have been published by author Trumić et al. (2020a).

Part I

Modeling

What distinguishes a mathematical model from, say, a poem, a song, a portrait or any other kind of "model" is that the mathematical model is an image or picture of reality painted with logical symbols instead of with words, sounds or watercolors.

John L. Casti

Chapter 1

Introduction

To model a soft robot, one should either consider that flexibility is concentrated within joints as in soft articulated robots or distributed along the link, which is the case of soft-bodied ones. Before proceeding to the mathematical description of soft articulated and soft-bodied robots, this chapter presents a review of the existing hardware solutions.

In that light, the compliance in robots can either be achieved by programming the stiffness (*active compliance*) or introducing the flexible elements (*passive compliance*) within their actuators. The latter ones are then divided into three groups according to the actuation mechanism: single actuated flexible transmission (SAFT), antagonistic variable stiffness actuators (aVSA), and serial variable stiffness actuators (sVSA), and described in more details by Flacco (2012). Figure 1.1 depicts the instances of rigid robots with active compliance and soft articulated robots powered by the before-mentioned actuators.

Within this thesis, the attention has been dedicated to the second group – antagonistic variable stiffness actuators, which are used to drive robots shown in Fig. 1.2. Being inspired by the way biceps and triceps antagonistically actuate human elbow, these actuators endow a compliant robot with a wider range of the achievable Cartesian stiffness compared to the SAFT ones and have a less complex mechanism than the one of serial VSAs. More precisely, the antagonistic mechanism is based on the following logic: the position of the arm is changed by extending one muscle and simultaneously contracting the antagonistic one while stiffness varies by simultaneous contraction or relaxation of both muscles. To replicate such a system on robots, it is necessary to ensure the possibility to vary stiffness in real-time, which is only possible if the nonlinear spring is used (this is easily shown by finding stiffness via its definition, i.e. by calculating partial derivative of elastic force with respect to the elongation (Van Ham et al. (2009)). For this reason, the first solutions of antagonistic VSAs included springs with quadratic and exponential characteristics, or McKibben muscles that naturally have nonlinearity, (Fig. 1.3 a). Since such *simple* arrangement of antagonistic VSAs requires that each motor (or muscle in pneumatic case) can generate the maximum torque at the link, novel and energy-efficient designs emerged in form of *bidirectional* VSAs that allowed the agonist and antagonist motors to support each other (Fig. 1.3 b). However, due to the high coupling between position and stiffness, the control of such actuators becomes challenging.

In this regard, Chapter 2 provides the mathematical descriptions of pneumatic and electric antagonistic VSAs, also comprising the first-order dynamic equation for stiffness, which are later used to derive the decoupled control laws of position and stiffness.

A step further towards mimicking nature is made in the field of soft-bodied robots. The rapid development of computationally powerful devices, soft materials, and wearable electronics triggered the various conceptions of such robots, with some of the most interesting solutions being shown in Fig. 1.4. Chapter 3 presents the piecewise constant curvature model of a general soft-bodied robot in three-dimensional space as well as its description assuming affine curvature.

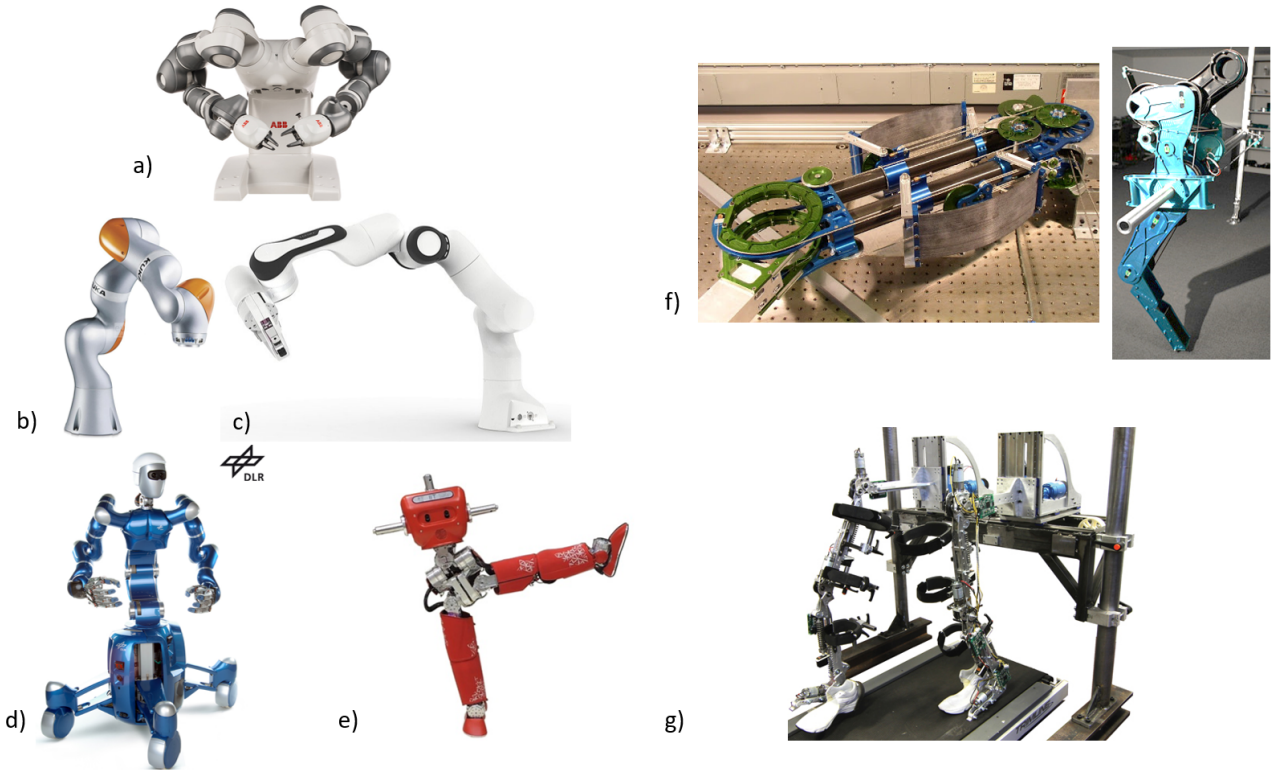

Figure 1.1: Active compliance: (a) Dual-arm 7 axis collaborative YuMi of ABB (figure from ABB (2019)); (b) Collaborative KUKA LBR iiwa 7 axis manipulator (figure from KUKA (2015)); (c) Cost-efficient 7 axis Panda manipulator of Franka Emika (figure from Franka Emika (2011));
SAFT: (d) Rollin' Justin whose arms are DLR Light-Weight-Robot III 7 axis manipulators. Elasticity in joints is introduced via harmonic drives as presented by Hirzinger et al. (2002) (figure taken from DLR (2007)); (e) The HeiCub humanoid robot (iCub version from Heidelberg university) whose knees and ankles are driven by series elastic actuators and which is described by Hu et al. (2016) (figure taken from University of Heidelberg (2018));
sVSA: (f) The actuator with mechanically adjustable series compliance AMASC (right) used for the biped BiMASC (left) (figures from Hurst et al. (2010) and Dynamic Robotics Laboratory (2007)); (g) The Mechanically Adjustable Compliance and Controllable Equilibrium Position Actuator MACCEPA used within exoskeleton ALTACRO (figure from Cherelle et al. (2010))

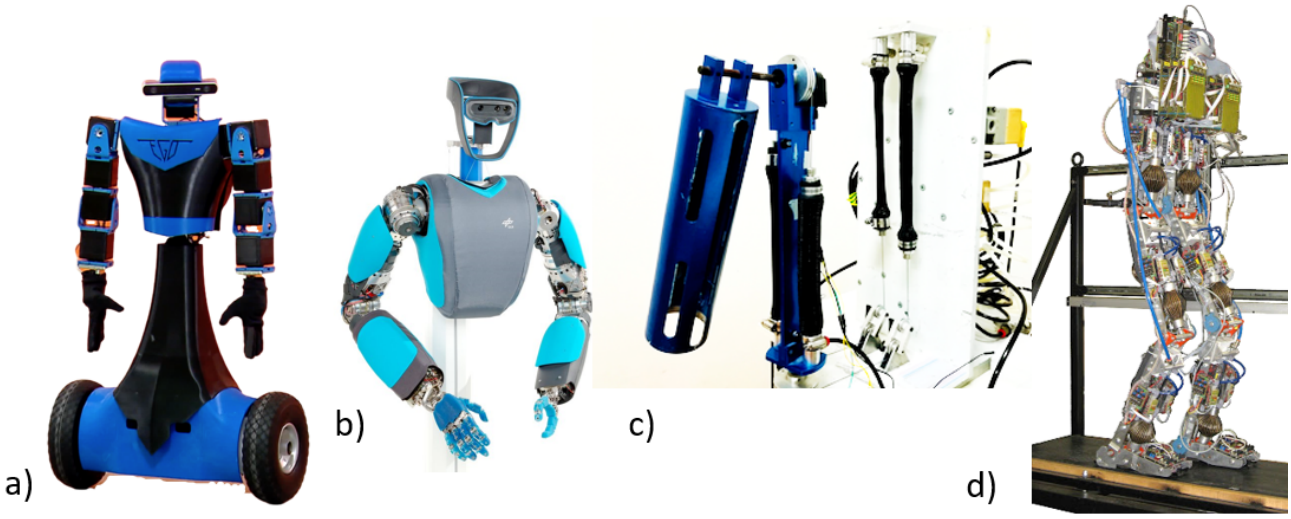

Figure 1.2: Antagonistic electromechanical VSAs: (a) ALTER-EGO is a soft dual arm mobile robot whose arms are actuated by *qbmove* antagonistic variable stiffness actuators. It is developed in Centro Piaggio at the University of Pisa by Lentini et al. (2019) (figure from Centro Piaggio (2018)); (b) The antropomorphic robot David from DLR with bidirectional antagonistic variable joints (BAVS) for wrist and forearm rotation described by Grebenstein et al. (2011) (figure from DLR (2007));
Antagonistic pneumatic VSAs: (c) The soft pneumatic manipulator GioSte with antagonistic setup of McKibben muscles; (d) The pneumatic biped Lucy actuated by antagonistic pleated pneumatic artificial muscles (figure from Verrelst et al. (2005))

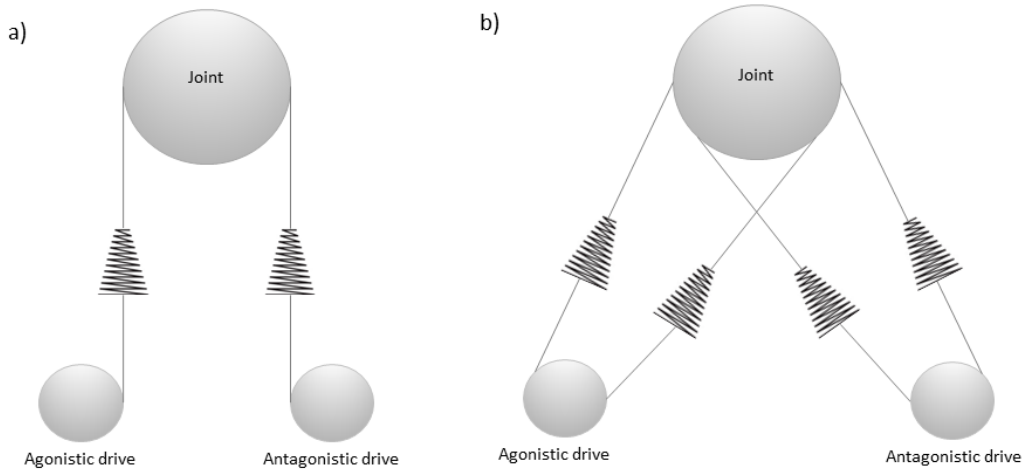

Figure 1.3: Configurations of antagonistic VSAs: (a) simple and (b) bidirectional

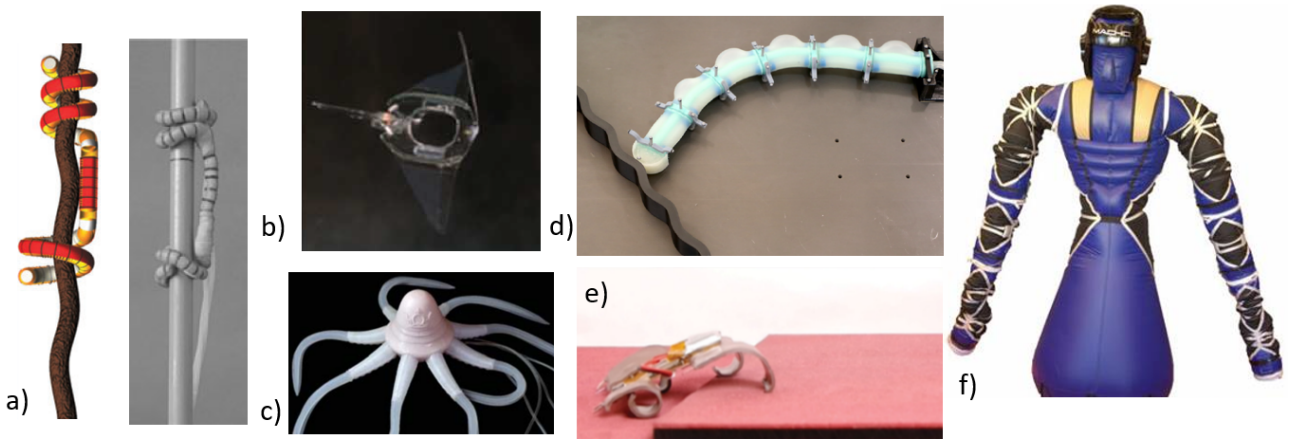

Figure 1.4: Soft-bodied robots: (a) Soft rod-climbing robot inspired by winding locomotion of snake (figure from Liao et al. (2020)); (b) Ray-inspired fast-moving soft electronic fish (figure from Li et al. (2017)); (c) Octopus inspired robot (figure from Fras et al. (2018)); (d) Worm-like soft robot (figure from Della Santina et al. (2020b)); (e) Reptilian-like soft electrically actuated quadruped (figure from Huang et al. (2019)); (f) King Louie - inflatable humanoid soft robot (figure from Best et al. (2016a))

Chapter 2

Soft articulated robots

To derive a model of soft articulated robots, i.e. flexible joint robots, which is applicable for analysis and control, certain approximation assumptions have to be made. First of all, since robot joints considered in this research have nonlinear stiffness characteristics, the mapping between transmission deflection and flexibility torque has to be smooth and invertible. Furthermore, it is assumed that the actuator of the i-th robot link is mounted on link $i-1$, which is indeed the case for the robots mentioned below.

Being equipped with the possibility to vary their stiffness, soft robots subject to gravity are in danger of crashing if the obtained stiffness is too small. Therefore, it is assumed that the lowest stiffness of the joint is greater than the upper bound of gravity forces gradient.

Additionally, concerning electro-mechanically driven robots, it stands that rotor inertial matrix is diagonal, such that the rotor position does not affect a robot inertia matrix, gravity vector, as well as the angular velocity of a rotor center of mass, which actually only depends on the own spinning of a rotor.

Consider a soft robot with discrete points of elasticity coinciding with its n joints, which is used in applications requiring simultaneous regulation of joint position and stiffness. Having denoted with $q = (q_1, \cdots, q_n)^T$ and $\sigma = (\sigma_1, \cdots, \sigma_n)^T$ the robot's position and stiffness vectors, respectively, in which q_i and σ_i are the i-th joint angle and stiffness variables, a full model of the robot describing these vectors dynamics is required. As it is known, the link side dynamics is given by the differential equation:

$$B(q)\,\ddot{q} + C(q,\dot{q})\,\dot{q} + G(q) = \tau + \tau_{ext}\,, \tag{2.1}$$

where $B(q) \in \mathbb{R}^{n\times n}$ is the inertia matrix, $C(q,\dot{q}) \in \mathbb{R}^n$ is the vector of Coriolis, centrifugal, and damping terms, $G(q) \in \mathbb{R}^n$ is the vector of gravity forces, $\tau = (\tau_1, \cdots, \tau_n)^T$ is the elastic torque vector, and $\tau_{ext} \in \mathbb{R}^n$ is the vector of external torque loads.

For model in Eq. 2.1 a set of properties holds. The ones of the interest for the control laws derived in the thesis are listed below.

Proposition 1. *The inertia matrix $B(q)$ is symmetric positive definite and bounded:*

$$\lambda_1 I_n < B(q) < \lambda_2 I_n \quad \forall q\,,$$

where λ_1 and λ_2 are positive scalars.

Proposition 2. *The matrix $\dot{B}(q) - 2C(q,\dot{q})$ is skew symmetric, hence, it stands*

$$q^T\left(\dot{B}(q) - 2C(q,\dot{q})\right) q = 0\,.$$

Proposition 3. *The left-hand side of link position dynamics can be expressed as a linear combination of regressor and parameters, i.e.*

$$B(q)\,\ddot{q} + C(q,\dot{q})\dot{q} + G(q) = Y(q,\dot{q},\ddot{q})\pi\,,$$

2.1 Pneumatically actuated soft articulated robots

The class of pneumatically driven robots with so-called McKibben artificial muscles in antagonistic configuration, where every joint i is actuated by a pair of muscles, a_i and b_i, attached to a pulley of radius R_i is schematically shown in Fig. 2.1. The i-th pair of muscles are respon-

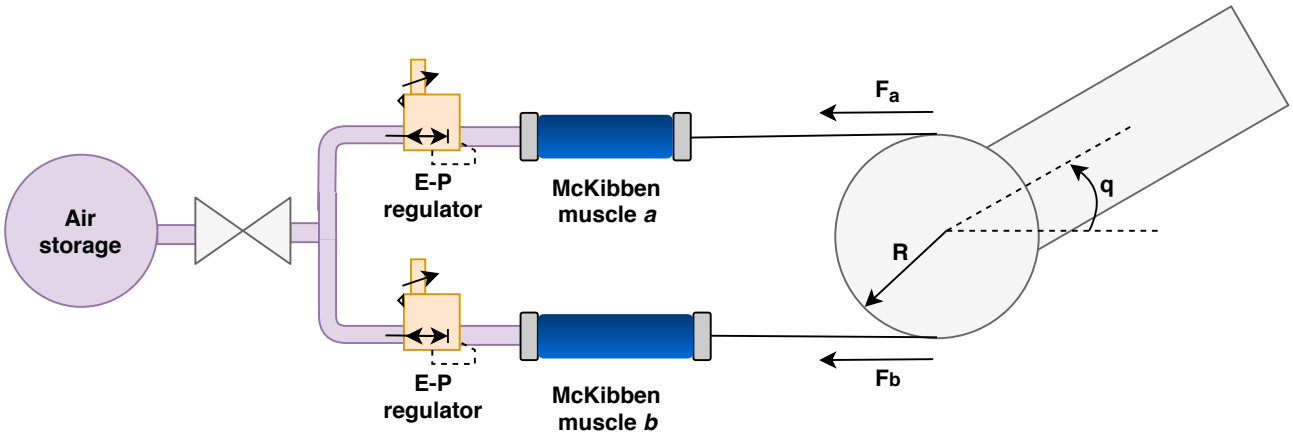

Figure 2.1: Depiction of a 1-DoF soft robotic arm actuated by a pair of McKibben artificial muscles in antagonistic configuration. Air pressure in the muscles is controlled by electro-pneumatic regulators and induces muscle contractions, thus allowing position and stiffness control of the robot's link.

sible for providing the torque τ_i required for motion of the i-th joint, according to the static equation:

$$\tau_i = \tau_{i,a} - \tau_{i,b} = R_i F_{i,a}(q_i) - R_i F_{i,b}(q_i)\,,$$

where $F_{i,a}$ and $F_{i,b}$ are the elastic (tension) forces applied by the two muscles. The two forces of the pair of muscles depend on their internal pressures, $p_{i,a}$ and $p_{i,b}$. As in the work of Tonietti and Bicchi (2002), it can be assumed that the relations between elastic forces and pressures are expressed in the form

$$\begin{aligned} F_{i,a}(q_i) &= K^g_{i,a}\,\phi_{i,a}(q_i)\,p_{i,a}\,, \\ F_{i,b}(q_i) &= K^g_{i,b}\,\phi_{i,b}(q_i)\,p_{i,b}\,, \end{aligned}$$

where $K^g_{i,a}$ and $K^g_{i,b}$ are construction-dependent muscle parameters, and $\phi_{i,a}(q_i)$ and $\phi_{i,b}(q_i)$ are the elongations of the muscles, given by the relations

$$\begin{aligned} \phi_{i,a}(q_i) &= (l_{i,a,n} - q_i R_i)^2 - l^2_{i,a,m}\,, \\ \phi_{i,b}(q_i) &= (l_{i,b,n} + q_i R_i)^2 - l^2_{i,b,m}\,, \end{aligned}$$

where $l_{i,a,n}$ and $l_{i,b,n}$ are the muscles' nominal lengths and $l_{i,a,m}$ and $l_{i,b,m}$ their minimum ones. To achieve a more compact form, assume for simplicity that each antagonistic pair of muscles have identical construction constants, i.e. $K^g_{i,a} = K^g_{i,b} = K^g_i$, and define the constants $K_i = K^g_i R_i$. Denoting then the diagonal construction-dependent constant matrix $K = \mathrm{diag}(K_i)$, the muscle

elongation matrix $\Phi \in \mathbb{R}^{n\times 2n}$

$$\Phi(q) = \begin{pmatrix} \phi_{1,a}(q_1) & -\phi_{1,b}(q_1) & \dots & 0 & 0 \\ 0 & 0 & \ddots & \vdots & \vdots \\ 0 & 0 & \dots & \phi_{n,a}(q_n) & -\phi_{n,b}(q_n) \end{pmatrix},$$

and the pressure vector $p \in \mathbb{R}^{2n\times n}$ as

$$p = (p_{1,a}, p_{1,b}, p_{2,a}, p_{2,b}, \cdots, p_{n,a}, p_{n,b})^T,$$

the generalized elastic torque vector τ can be written as

$$\tau = K\,\Phi(q)\,p\,. \tag{2.2}$$

Eq 2.1 and 2.2 describe the dynamics of the joint position vector, under the actuation of the input pressure vector p.

Moving on now to the i-th joint's stiffness, by assuming that its pressure does not depend on its position, the stiffness itself can be obtained from its definition:

$$\begin{aligned} \sigma_i &= -\frac{\partial \tau_i}{\partial q_i} = \\ &= -K_i \left(\frac{\partial \phi_{i,a}}{\partial q_i}(q_i)\, p_{i,a} - \frac{\partial \phi_{i,b}}{\partial q_i}(q_i)\, p_{i,b} \right) = \\ &= -K_i \left(\phi_{q,i,a}(q_i)\, p_{i,a} - \phi_{q,i,b}(q_i)\, p_{i,b} \right). \end{aligned}$$

Defining a matrix $\Phi_q(q)$ as

$$\begin{pmatrix} \phi_{q,1,a}(q_1) & -\phi_{q,1,b}(q_1) & \dots & 0 & 0 \\ 0 & 0 & \ddots & \vdots & \vdots \\ 0 & 0 & \dots & \phi_{q,n,a}(q_n) & -\phi_{q,n,b}(q_n) \end{pmatrix},$$

the stiffness vector can be written more concisely as

$$\sigma = -K\,\Phi_q(q)\,p\,. \tag{2.3}$$

In order to obtain closed-loop control of the robot's stiffness σ, a dynamic model for this variable is also needed. Inspired by the approach of De Luca and Lucibello (1998), this can be obtained by considering the first time derivative of σ as in the following:

$$\dot{\sigma} = -K\,\dot{\Phi}_q(q)\,p - K\,\Phi_q(q)\,\dot{p}\,. \tag{2.4}$$

Therefore, a full model of a soft-robot with pneumatic muscles can be obtained from Eq. 2.1, 2.2, 2.4, and thus written as

$$\begin{aligned} B(q)\,\ddot{q} + C(q,\dot{q})\,\dot{q} + G(q) = K\,\Phi(q)\,p - \tau_{ext}\,, \\ \dot{\sigma} = -K\dot{\Phi}_q(q)\,p - K\Phi_q(q)\,\dot{p}\,, \end{aligned} \tag{2.5}$$

It will be assumed in the following that no interaction with the environment occurs, i.e. the external torque load is identically null ($\tau_{ext} = 0$ for all t), and that each pressure regulator is sufficiently fast to instantaneously control the corresponding pressure variable.

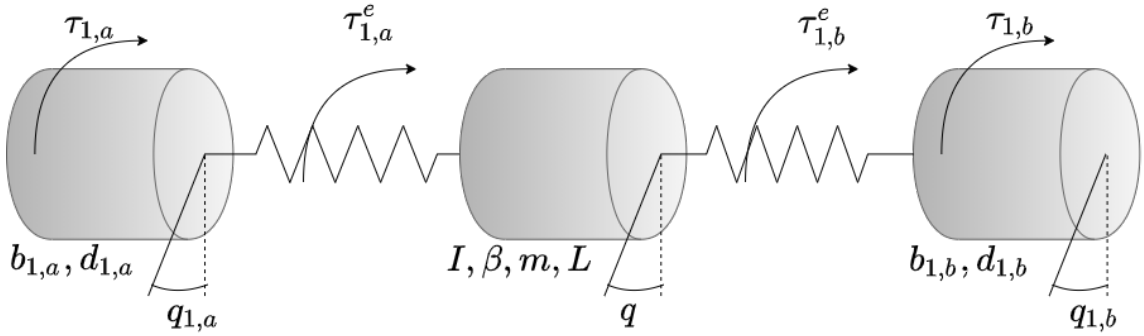

Figure 2.2: Depiction of a 1-DoF soft robotic arm actuated by DC motors in antagonistic configuration. The inertia, damping, mass, and length of the link are denoted with I, β, m, and L, respectively. Motor inertia and damping are $b_{1,a}$ and $d_{1,a}$ for the agonist drive, and $b_{1,b}$ and $d_{1,b}$ for the antagonist one. The commanded torques to motors are $\tau_{1,a}$ and $\tau_{1,b}$, while the generated flexibility torques are $\tau^e_{1,a}$ and $\tau^e_{1,b}$.

2.2 Electrically actuated soft articulated robots

Consider an n degree-of-freedom robot with flexible joints driven by electrical VSAs in agonist-antagonistic configurations. More precisely, each joint of the robot is actuated by a couple of DC motors, which are connected to the joint via tendons as in Fig. 2.2. By changing the internal motors positions, it is possible to vary both joints position (if motors rotate in the same direction) and stiffness (when motors rotate in opposite directions).

As described in Albu-Schäffer and Bicchi (2016), the robot dynamical model can be written as follows:

$$\begin{aligned} B(q)\,\ddot{q} + C(q,\dot{q})\dot{q} + G(q) &= -\tau_e(\phi_1,\phi_2) + \tau_{\text{ext}}\,, \\ B_a\,\ddot{q}_a + D_a\,\dot{q}_a - \tau^e_a(\phi_a) &= \tau_a\,, \\ B_b\,\ddot{q}_b + D_b\,\dot{q}_b - \tau^e_b(\phi_b) &= \tau_b\,, \end{aligned} \tag{2.6}$$

where $q \in \mathbb{R}^n$ is the link angle vector, τ^e_t is the total flexibility torque vector, and where $q_j \in \mathbb{R}^n$, τ^e_j, and τ_j are the motor position vectors, flexibility torque vectors, and commanded torque vectors, respectively, for the agonistic ($j = a$) and antagonistic ($j = b$) motor.

Moreover, $B(q)$ is the robot link inertia matrix, $C(\cdot)$ includes Coriolis, viscous friction, and centrifugal terms, and $G(\cdot)$ is a vector of gravity forces; matrices $B_j = \text{diag}(b_{i,j})$ and $D_j = \text{diag}(d_{i,j})$ contain motor's inertia and damping coefficients, respectively; finally, τ_{ext} is the external torque, assumed to be null in the remainder of the work.

It is worth remarking that the following property for motor dynamics holds:

Proposition 4. *The left-hand side of motor position dynamics can be expressed as a linear combination of regressor and parameters, i.e.*

$$\begin{aligned} B_a\,\ddot{q}_a + D_a\,\dot{q}_a &= Y_a(\dot{q}_a,\ddot{q}_a)\pi_a\,, \\ B_b\,\ddot{q}_b + D_b\,\dot{q}_b &= Y_b(\dot{q}_b,\ddot{q}_b)\pi_b\,. \end{aligned}$$

Furthermore, having denoted with $\phi_j = q - q_j$ the transmission deflection vectors of the agonistic and antagonistic motor's transmission, the total flexibility torque τ^e_t, in the first equation of the model, is given by

$$\tau^e = \tau^e_a(\phi_a) + \tau^e_b(\phi_b)\,. \tag{2.7}$$

The above element-wise dependency on the transmission deflection, i.e. the fact that for the

i-th joint $\tau^e_{i,j} = \tau^e_{i,j}(\phi_{i,j})$, along with the diagonal form of the motor's inertia and damping matrices, justifies a decentralized viewpoint of motor's dynamics.

Therefore, the components $\sigma_{i,j}$ of the stiffness vector σ_j of each transmission are by definition

$$\sigma_{i,j}(\phi_{i,j}) = \frac{\partial \tau^e_{i,j}}{\partial \phi_{i,j}} (\phi_{i,j}) \,, \tag{2.8}$$

leading to the total joint stiffness and its time derivative

$$\begin{aligned} \sigma_i &= \sigma_{i,a}(\phi_{i,a}) + \sigma_{i,b}(\phi_{i,b}) \,, \\ \dot{\sigma}_i &= \frac{\partial^2 \tau^e_{i,a}}{\partial \phi^2_{i,a}} \dot{\phi}_{i,a} + \frac{\partial^2 \tau^e_{i,b}}{\partial \phi^2_{i,b}} \dot{\phi}_{i,b} \,. \end{aligned} \tag{2.9}$$

Moreover, it can be assumed that the flexibility torque is an odd function, meaning that compression and extension have the same effect on transmission behavior:

$$\tau^e(0) = 0 \quad \text{and} \quad \tau^e_{i,j}(-\phi_{i,j}) = -\tau^e_{i,j}(\phi_{i,j}), \ \ \forall \phi \,.$$

Finally, the full model of an electric antagonistic VSA states:

$$\begin{aligned} B(q)\,\ddot{q} + C(q,\dot{q})\dot{q} + G(q) &= -\tau_e(\phi_1, \phi_2) + \tau_{\text{ext}} \,, \\ B_a\,\ddot{q}_a + D_a\,\dot{q}_a - \tau^e_a(\phi_a) &= \tau_a \,, \\ B_b\,\ddot{q}_b + D_b\,\dot{q}_b - \tau^e_b(\phi_b) &= \tau_b \,, \\ \dot{\sigma} &= \frac{\partial^2 \tau^e_a}{\partial \phi^2_a} \dot{\phi}_a + \frac{\partial^2 \tau^e_b}{\partial \phi^2_b} \dot{\phi}_b \,. \end{aligned} \tag{2.10}$$

In the remainder of the thesis, it will be assumed that the electrical dynamics of the motor system can be neglected due to its fast response.

Chapter 3

Soft-bodied robots

Being endowed with morphological flexibility and compliance, continuum soft robots promise to have a disruptive impact in several areas where safety, robustness, and adaptability are a main concern Rus and Tolley (2015). Yet, to fully exploit their potentialities, one has to face the challenge of dealing with systems characterized by states of theoretically infinite sizes. One possible strategy to deal with such systems is by using model-free machine learning techniques that regard a soft robot as a black box Thuruthel et al. (2018). On the other end of the spectrum, model-based techniques fully taking into account the infinite nature of the problem are still unfeasible Mironchenko and Prieur (2019).

These reasons have steered the research attention towards the development of approximated but finite-dimensional models Grazioso et al. (2019); Sadati et al. (2019), trading modeling accuracy with numerical efficiency, as well as reduced-order models, enabling an analytic design of model-based controllers Thieffry et al. (2018). Within this context, the Piecewise Constant Curvature (PCC) approximation-based paradigm is an effective attempt to leverage on the equivalence between a soft-bodied robot and a large enough rigid one, aiming at enabling a variety of classical control approaches already established in robotics. The planar case is discussed in Della Santina et al. (2020b) while the three dimensional case is addressed in Katzschmann et al. (2019). However, this latter work relies on the classic 3D representation of PCC robots Webster III and Jones (2010), which is subject to several singularities issues making the controller not well defined in several boundary conditions (e.g. straight configuration). In Della Santina et al. (2020a), it is discussed that these issues can be solved by using a different parameterization of the configuration manifold of a PCC robot, which is global and everywhere well defined. However, no connection to the augmented rigid robot formulation is provided in that work.

A contribution of the present work is therefore to extend the 3D augmented rigid representation of Katzschmann et al. (2019) to the improved parameterization proposed in Della Santina et al. (2020a). This allows the derivation of controllers which are numerically stable and well defined in the whole configuration space.

3.1 Modeling of soft robots under PCC hypothesis

3.1.1 Background

Consider a soft-bodied robot consisting of n Constant-Curvature (CC) segments. Let $\{S_0\}$ be the robot's base frame and $\{S_1\}, \dots, \{S_n\}$ the n local frames attached to the end of each segment. Under the PCC assumption, i.e. when each segment can be characterized by a unique CC segment in the space, the i-th segment's configuration is fully determined by the frames $\{S_{i-1}\}$ and $\{S_i\}$. Accordingly, it suffices to adopt the following variables per segment Katzschmann

et al. (2019): 1) the angle ϕ_i between the bending plane and the plane described by the unit vectors $\hat{n}_{i-1}$ and $\hat{o}_{i-1}$; 2) the relative rotation θ_i between the two frames in the curvature plane; 3) the segment's length change δL_i, whose minimum is physically bounded by $-L_{0,i}$, where $L_{0,i} \in \mathbb{R}$ is the rest value. However, singularity issues arise whenever $\theta_i = 0$ or $\phi_i = \pm\pi$, which leads to known description inaccuracies.

It has been recently established that a singularity-free representation can be obtained by considering, for each segment, the four arcs originating from the positive and negative directions of the x and y axes of $\{S_{i-1}\}$ and terminating into the corresponding ones of $\{S_i\}$ Della Santina et al. (2020a). Accordingly, the i-th segment configuration is $q_i = (\Delta_{x,i}, \Delta_{y,i}, \delta L_i)^T \in \mathbb{R}^3$ (see Fig. 3.1), where

$$\Delta_{x,i} = \tfrac{1}{2}(L_{2,i} - L_{1,i}), \quad \text{and} \quad \Delta_{y,i} = \tfrac{1}{2}(L_{4,i} - L_{3,i}),$$

with $L_{j,i}$ being the four arc lengths ($j = 1, \cdots, 4$). The two sets of coordinates are related by the invertible mapping

$$\begin{array}{rcl} \phi_i & = & \arccos\left(\frac{\Delta_{x,i}}{\Delta_i}\right) = \arcsin\left(\frac{\Delta_{y,i}}{\Delta_i}\right), \\ \theta_i & = & \Delta_i / d_i, \end{array} \tag{3.1}$$

where $\Delta_i = \sqrt{\Delta_{x,i}^2 + \Delta_{y,i}^2}$ and d_i is a free parameter, which can be chosen to match some specific location, e.g. where strain sensors are placed, so to have direct readings of the configuration. For the sake of readability, it is assumed $d_i = 1$ m in the remainder of the work.. In terms of the elements of the configuration vector q_i, the i-th homogeneous transformation mapping S_{i-1} into S_i is given by

$$T_{i-1}^i = \begin{pmatrix} R_{i-1}^i & t_{i-1}^i \\ 0_{1\times 3} & 1 \end{pmatrix},$$

where

$$R_{i-1}^i = \begin{pmatrix} 1 + \frac{\Delta_{x,i}^2}{\Delta_i^2}\alpha_i & \frac{\Delta_{x,i}\Delta_{y,i}}{\Delta_i^2}\alpha_i & -\frac{\Delta_{x,i}}{\Delta_i}s_{\Delta_i} \\ \frac{\Delta_{x,i}\Delta_{y,i}}{\Delta_i^2}\alpha_i & 1 + \frac{\Delta_{y,i}^2}{\Delta_i^2}\alpha_i & -\frac{\Delta_{y,i}}{\Delta_i}s_{\Delta_i} \\ \frac{\Delta_{x,i}}{\Delta_i}s_{\Delta_i} & \frac{\Delta_{y,i}}{\Delta_i}s_{\Delta_i} & c_{\Delta_i} \end{pmatrix},$$
$$t_{i-1}^i = \frac{L_{0,i}+\delta L_i}{\Delta_i}\left(\frac{\Delta_{x,i}}{\Delta_i}\alpha_i, \frac{\Delta_{y,i}}{\Delta_i}\alpha_i, s_{\Delta_i}\right)^T,$$

with $\alpha_i = c_{\Delta_i} - 1$, and finally $c_{\Delta_i} = \cos\Delta_i$ and $s_{\Delta_i} = \sin\Delta_i$. According to this notation, the configuration of a soft-bodied robot with n PCC segments is fully described by the vector $q = (q_1^T, \cdots, q_n^T)^T \in \mathbb{R}^{3n}$.

3.1.2 Augmented PCC representation with improved parameterization

One should first focus on finding a globally-valid augmented representation for the i-th CC segment. The idea is that of trying to match the segment's kinematics and dynamic map with those of a classical rigid robot with sufficient degrees of freedom. The matching is obtained when the two models are said to be *kinematically* and *dynamically equivalent*, that is if the reference frame attached to the end-effector of the segment's augmented model coincides with that of the rigid robot, and when their respective centers of mass coincide, respectively. It has been shown very recently in Katzschmann et al. (2019) that an equivalent augmented representation can be obtained with a ten degree-of-freedom rigid robot whose segment variables are ϕ_i, θ_i, and δL_i. This model is almost always valid, except at the above-mentioned singularity configurations.

However, by leveraging on the recently developed improved parameterization Della Santina et al. (2020a), it is proceeded herein to a rigid-robot equivalent representation, using the variables $\Delta_{x,i}$, $\Delta_{y,i}$, and δL_i to describe each segment, for $i = 1, \cdots, n$, which therefore has no singularity issues. In terms of the newly chosen configuration vector q_i, the augmented config-

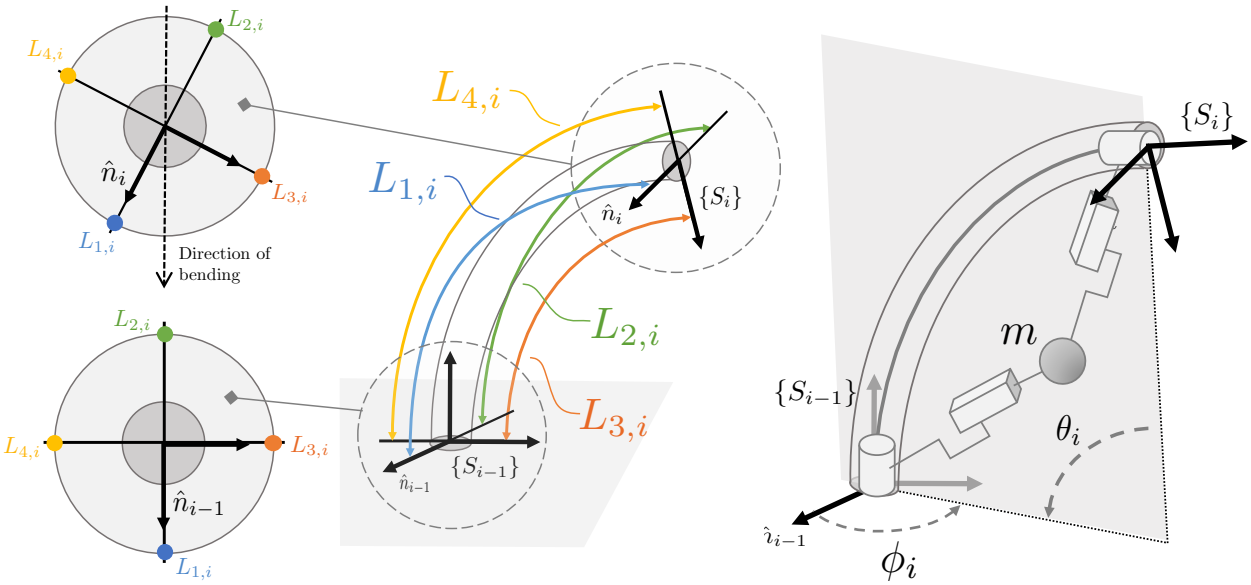

(a) Improved Parametrization (b) Aug. rigid model

Figure 3.1: Three dimensional description of a CC segment. Panel (a) shows the improved parameterization, which is free from singularities and discontinuities. Herein it is connected to augmented rigid model in Panel (b).

uration vector $\xi_i \in \mathbb{R}^{10}$ from Della Santina et al. (2020a) can be described by a nonlinear map of the form

$$\xi_i = m_i(q_i) = m_i(\Delta_{x,i}, \Delta_{y,i}, \delta L_i)\,,$$

which explicitly reads:

$$\begin{pmatrix} \xi_{10(i-1)+1} \\ \xi_{10(i-1)+2} \\ \xi_{10(i-1)+3} \\ \xi_{10(i-1)+4} \\ \xi_{10(i-1)+5} \\ \xi_{10(i-1)+6} \\ \xi_{10(i-1)+7} \\ \xi_{10(i-1)+8} \\ \xi_{10(i-1)+9} \\ \xi_{10(i-1)+10} \end{pmatrix} = \begin{pmatrix} \arccos \frac{\Delta_{x,i}}{\Delta_i} \\ \frac{\Delta_i}{2} - \eta_i^*(q_i) \\ b_i^*(q_i) \\ \eta_i^*(q_i) \\ -\arccos \frac{\Delta_{x,i}}{\Delta_i} \\ \arccos \frac{\Delta_{x,i}}{\Delta_i} \\ \eta_i^*(q_i) \\ b_i^*(q_i) \\ \frac{\Delta_i}{2} - \eta_i^*(q_i) \\ -\arccos \frac{\Delta_{x,i}}{\Delta_i} \end{pmatrix}, \tag{3.2}$$

where

$$b_i^*(q_i) = \frac{L_{0,i}+\delta L_i}{\Delta_i}\,\gamma_i(q_i)\,,\ \eta_i^*(q_i) = \arccos\left(\sin\left(\frac{\Delta_i}{2}\right)/\gamma_i(q_i)\right)\,,$$

with

$$\gamma_i(q_i) = \sqrt{1 + \operatorname{sinc}\left(\frac{\Delta_i}{2}\right)\left(\operatorname{sinc}\left(\frac{\Delta_i}{2}\right) - 2\cos\left(\frac{\Delta_i}{2}\right)\right)}\,.$$

and the asterisk is used to distinguish them from the analogous ones in the previous ϕ_i, θ_i and δL_i based formalization. Recall that $\operatorname{sinc}(x) = \sin(x)/x$ and its value in zero is 1. Mapping m_i is globally defined as it holds

$$\lim_{||q_i||\to 0} b_i^*(q_i) = \frac{L_{0,i}}{2}\,, \lim_{||q_i||\to 0} \eta_i^*(q_i) = 0\,,$$
$$\lim_{||q_i||\to 0} \arccos\left(\frac{\Delta_{x,i}}{\Delta_i}\right) = 0\,.$$

Following from the above reasoning, a globally-valid augmented representation of a soft-

bodied robot, under the PCC hypothesis, can be obtained by serially connecting its n CC segments. This leads to an augmented vector $\xi \in \mathbb{R}^{10n}$ that is related to the robot's configuration $q = (\Delta_{x,1}, \Delta_{y,1}, \delta L_1, \cdots, \Delta_{x,n}, \Delta_{y,n}, \delta L_n)^T$ via the decentralized mapping

$$\xi = m(q) = \begin{pmatrix} m_1(\Delta_{x,1}, \Delta_{y,1}, \delta L_1) \\ \vdots \\ m_n(\Delta_{x,n}, \Delta_{y,n}, \delta L_n) \end{pmatrix} . \tag{3.3}$$

Then, one can now move on to deriving the dynamic model corresponding to this new formalization. The rigid robot's dynamics described as a function of ξ reads

$$B_\xi(\xi)\,\ddot{\xi} + C_\xi(\xi, \dot{\xi})\,\dot{\xi} + G_\xi(\xi) = \tau_\xi + J_\xi^T f_{\text{ext}}\,, \tag{3.4}$$

where $B_\xi, C_\xi \in \mathbb{R}^{10n\times 10n}$, $G_\xi \in \mathbb{R}^{10n}$ are the inertia and Coriolis matrices and gravity vector, respectively, $J_\xi \in \mathbb{R}^{6\times 10n}$ the Jacobian of the direct kinematics, and τ_ξ and f_{ext} are the generalized forces along the ξ-coordinates and external wrench vector. Substituting in (3.4) the first two time derivatives of (3.3), i.e. the relations

$$\dot{\xi} = J_m(q)\,\dot{q}\,, \qquad \ddot{\xi} = \dot{J}_m(q, \dot{q})\,\dot{q} + J_m(q)\,\ddot{q}\,, \tag{3.5}$$

where $J_m(q) : \mathbb{R}^{3n} \to \mathbb{R}^{10n\times 3n}$ is the Jacobian of mapping $m(q)$ with respect to q, left-multiplying the resulting equation by J_m^T, and finally using (3.3) to replace ξ with q, the intermediate result is obtained:

$$B(q)\,\ddot{q} + C(q, \dot{q})\,\dot{q} + G(q) = \tau^* + J^T(q)\,f_{\text{ext}}\,,$$

where $B, C \in \mathbb{R}^{3n\times 3n}$, $G \in \mathbb{R}^{3n}$, $J(q) \in \mathbb{R}^{6\times 3n}$ is the Jacobian of the direct kinematics with respect to q, and $\tau^* = (\tau^*_{x,1}, \tau^*_{y,1}, \tau^*_{L,1}, \cdots, \tau^*_{x,n}, \tau^*_{y,n}, \tau^*_{L,n})^T$ is the generalized force along the q-coordinates. Specifically, it stands:

$$\begin{aligned} B(q) &= J_m^T\, B_\xi(m(q))\, J_m\,, \\ C(q, \dot{q}) &= J_m^T \left(B_\xi(m(q))\, \dot{J}_m + C_\xi\left(m(q), J_m\,\dot{q}\right) J_m \right)\,, \\ G(q) &= J_m^T\, G_\xi(m(q))\,, \\ J(q) &= J_\xi(m(q))\, J_m\,. \end{aligned}$$

As a further step, one can now add at segment level Della Santina et al. (2020a) the elastic and friction terms, which are proportional to q and $\dot{q}$, respectively, and thus can be described via a block-diagonal stiffness matrix $K = \text{diag}(K_1, \cdots, K_n)$, with $K_i = \text{diag}(k_{\Delta_{x,i}}, k_{\Delta_{y,i}}, k_{\delta L_i})$, and a block-diagonal damping matrix $D = \text{diag}(D_1, \cdots, D_n)$, with $D_i = \text{diag}(\beta_{\Delta_{x,i}}, \beta_{\Delta_{y,i}}, \beta_{\delta L_i})$. Finally, to complete the model, one can express the i-th segment's subset of inputs, $\tau^*_{x,i}$, $\tau^*_{y,i}$, and $\tau^*_{L,i}$, as linear combinations of the corresponding externally applicable inputs, $\tau_{x,i}$, $\tau_{y,i}$, and $\tau_{L,i}$, via the segment's actuation sub-matrix

$$A_i = \begin{pmatrix} \frac{\Delta_{x,i}\Delta_{y,i}}{\Delta_i^2}\,\nu_i & -\frac{\Delta_{x,i}^2\,\nu_i + \Delta_i^2 \sin\Delta_i}{\Delta_i^2} & \frac{\Delta_{x,i}\,\nu_i}{\Delta_i^2} L_i \\ \frac{\Delta_{y,i}^2\,\nu_i + \Delta_i^2 \sin\Delta_i}{\Delta_i^2} & -\frac{\Delta_{x,i}\Delta_{y,i}}{\Delta_i^2}\,\nu_i & \frac{\Delta_{y,i}\,\nu_i}{\Delta_i^2} L_i \\ 0 & 0 & \text{sinc}(\Delta_i) \end{pmatrix} .$$

with $\nu_i = 1 - \text{sinc}(\Delta_i)$ and $L_i = L_{0,i} + \delta L_i$.The robot's overall actuation matrix is therefore given by $A(q) = \text{diag}(A_1(q_1), \cdots, A_n(q_n))$. Since each A_i is globally well-defined and invertible (its determinant is $\text{sinc}^2(\Delta_i)$), the robot is fully actuated. In conclusion, the sought soft-bodied

robot's dynamics can be written as

$$B(q)\,\ddot{q} + C(q,\dot{q})\,\dot{q} + G(q) + K\,q + D\,\dot{q} = A\,\tau + J^T f_{\text{ext}}\,, \tag{3.6}$$

where $\tau = (\tau_{x,1}, \tau_{y,1}, \tau_{L,1}, \cdots, \tau_{x,n}, \tau_{y,n}, \tau_{L,n})^T$. Without loss of generality, the external wrench vector is assumed null, i.e. $f_{\text{ext}} = 0$, in the remainder of the paper.

Before concluding, it is worthy to point out that such a model yields properties facilitating the application of classical control approaches. Herein only their statements are reported since the proofs follow from steps as in Della Santina et al. (2020b).

Proposition 5. *The inertia matrix $B(q)$ is positive semi-definite and bounded, i.e.*

$$B(q) \succeq 0\,, \|B(q)\| < \infty\,, \forall q \in \mathbb{R}^n,$$

if $\|J_m\| < 1$ and $|m_i(q)| < \infty$ for all $q \in \mathbb{R}^n$ and $\forall i$ such that the i-th joint is prismatic. Moreover, under the above hypothesis on B, given any matrix $R(q) \in \mathbb{R}^{nh \times d_r}$ such that $\operatorname{rank}(B_\xi(m(q)) = d_r$ and $\operatorname{span}(R(q))$ is the range of $B_\xi(m(q))$, then $\operatorname{rank}(R^T J_m(q)) = n$ implies that $B(q) \succ 0$.

Proposition 6. *If $C_\xi(\xi;\dot{\xi})$ is obtained via Christoffel symbols, then matrix $\dot{B}(q) - 2C(q,\dot{q})$ is skew-symmetric. If C_ξ is not built through Christoffel symbols, then $\dot{q}^T \left(\dot{B}(q) - 2C(q,\dot{q})\right) \dot{q} = 0$.*

The importance of this formalization is the possibility to model soft-bodied robots as fully-actuated rigid ones, with no singularity issues, which allows capitalizing on classical robust control techniques, as is also done in the following.

Remark 1. *In case robot is constrained to planar motions, the following map for the i-th segment is used*

$$m_i(q_i) = \begin{pmatrix} \frac{q_i}{2} & L_i \frac{\sin(q_i/2)}{q_i} & L_i \frac{\sin(q_i/2)}{q_i} & \frac{q_i}{2} \end{pmatrix}^T\,,$$

and the form for the i-th segment Jacobian is

$$J_{m,i}(q) = \begin{pmatrix} \frac{1}{2} & L_{c,i} & L_{c,i} & \frac{1}{2} \end{pmatrix}^T\,. \tag{3.7}$$

3.2 Soft inverted pendulum with affine curvature

Consider now a continuum soft robot of length L with diameter D subject to the gravity pointing downwards in a way that the robot becomes a soft inverted pendulum, as displayed in Fig. 3.2. The positions along the main axis of a pendulum are parameterized by the coordinate $s \in [0,1]$, which means that point at s is sL far from the base and has an attached reference frame S_s. Therefore, one can denote base frame with S_0, and tip frame with S_1. Introducing another variable $d \in [-\frac{1}{2}, \frac{1}{2}]$ to describe points lying outside the main axis, Cartesian coordinates of a point (s,d) in a global frame become $(x_{s,d}, y_{s,d})$ while in the local frame they are $(d,0)$. Therefore, the shape of a robot can be entirely described by a main axis, characterized by the curvature $\kappa_s(t) : [0,1] \times \mathbb{R} \longrightarrow \mathbb{R}$ which is affine with respect to the coordinate s:

$$\kappa_s(t) = \theta_0(t) + \theta_1(t)s\,,$$

where θ_0 and θ_1 are constant and linear components of a curvature, and moreover, the configuration variables of the system $\theta = (\theta_0, \theta_1)$. The dynamics of the soft inverted pendulum is modeled as

$$B(\theta)\ddot{\theta} + C(\theta,\dot{\theta})\dot{\theta} + G(\theta) + kH\theta + bH\dot{\theta} = H \begin{pmatrix} 1 \\ 0 \end{pmatrix} \tau\,,$$

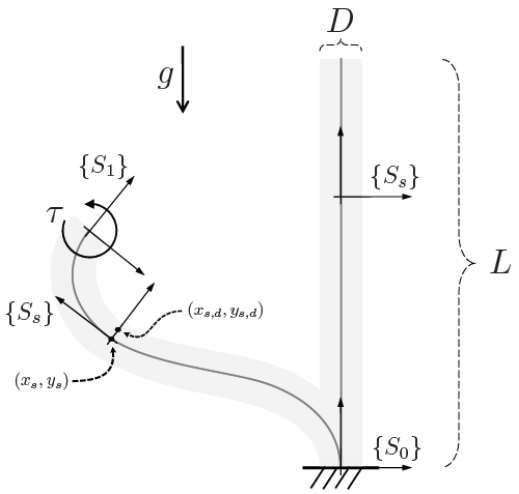

Figure 3.2: A soft inverted pendulum in two characteristic positions. Light gray color resembles the shape of the pendulum, while the dark gray line depicts the main line. The figure is taken from Della Santina (2020).

where $B(\theta)$, $C(\theta, \dot{\theta})$, and $G(\theta)$ are derived by summing up the infinitesimal mass elements Della Santina (2020), $H \in \mathbb{R}^{2\times 2}$ with $H_{i,j} = 1/(i + j - 1)$ is the Hankel matrix, $k \in \mathbb{R}$ is stiffness, and $b \in \mathbb{R}$ is damping of the pendulum. Finally, it is worth remarking that the affine curvature model is a generalization of the PCC model, for which it stands $\theta_0 \equiv 0$.

Part II

Stiffness Estimation

One of the principal objects of theoretical research in my department of knowledge is to find the point of view from which the subject appears in its greatest simplicity.

Josiah W. Gibbs

Chapter 4

Introduction

The main concept behind the stiffness estimation problem is that of finding the first derivative of the flexibility torque with respect to the flexible transmission. Pioneering results focused on estimating Cartesian stiffness Diolaiti et al. (2005), under the assumption that the robot's end-effector is in contact with the environment. On the other hand, joint stiffness estimation appears to be more convenient as it covers a general case when the contact between robot and environment can also happen sideways. Depending on the necessity of knowing the commanded torques to DC drives or commanded pressures in McKibben muscles, approaches can be divided into the invasive and non-invasive ones.

To this regard, the online, non-parametric, and non-invasive stiffness estimator presented by Grioli and Bicchi (2010) is able to identify stiffness from the link side, without needing any information of the actuating drive. Beyond the need to compute the time derivative of torque sensor from possibly noisy data, the practical applicability of such approaches remains challenging also because the state observability property is lost when the robot's link is in steady state.

A different perspective to the challenging problem of online stiffness estimation, which uses also measurements from the motor side, is the one offered by the promising research line of the work by Flacco and De Luca (2011). In the solution therein proposed, joint stiffness estimator is achieved via a two-phase process: first, an estimate of the flexibility torque applied to each motor is obtained by using residuals, and then a Recursive Least Square (RLS) algorithm is used to determine torque and stiffness approximations, which are parameterized with respect to the flexible transmission. The approach requires knowledge of the motor speed, which is estimated through a Modified Kinetic Kalman Filter (MKKF), whose parameters have to be properly tuned (Flacco et al. (2012a)). Another interesting method estimating instead stiffness in a direct way, and not requiring the computation of time derivatives, is the one proposed by Ménard et al. (2014), which uses so-called modulating functions. While the approach is advantageous as it provides a proof of the estimation error convergence, it requires an a-priori choice of the RLS algorithm parameters and of the integration window length, one of the modulating function parameter.

Within this setting, the solutions proposed in the following chapters tackle the challenge by leveraging on the theory of the delayed Unknown Input Observers (UIO) where either the flexibility torque or its time derivative are considered as an unknown input to the robot actuator system or the robot system itself. Then, an RLS algorithm is used to find the stiffness approximation. More precisely, Chapter 5 revises the theory of unknown input observers and recursive least square algorithm. Then, Chapter 6 describes an invasive approach of estimating stiffness in joints of pneumatically and electrically powered robots, followed by Chapter 7 that presents a non-invasive approach for electric soft-joint robots. It is worth remarking that, besides providing an elegant solution in a way that the observer is designed apriorly

and independently of the unknown-input signal model, the proposed method improves upon the above-mentioned approaches as no velocity information is necessary in case of the invasive approach, while force/torque sensor are needless for the non-invasive case.

Chapter 5

Background

Unknown Input Observers (UIO) are useful tools that have mainly been used for detecting system failures, by achieving correct state estimation independently of the unknown inputs. In this case, however, the research focuses on estimating the unknown input, which is a nonlinear time-variant function of our system variables. Among the input-observer categories studied in the literature, so-called "delayed" input-observers Sundaram and Hadjicostis (2007, 2008); Sundaram (2012) are preferable for our problem as they provide more information about the system. Indeed, thanks to the use of multiple output values, collected over consecutive sampling times, they are capable of estimating both the system's states and inputs, with a constant and predetermined delay, and they involve looser existence conditions for the realization of the input-observer. This leads to the appealing feature of being able to asymptotically reconstruct the unknown flexibility torque, without velocity sensor measurements, otherwise necessary with the observer obtained via the zero-delay approach Valcher (1999). Finally, compared to the approach in Saberi et al. (2000), the one in Sundaram and Hadjicostis (2007), which is used here, leads to a smaller state space of the observer.

Once flexibility torque is estimated via the UIO, the stiffness is straightforwardly determined by the RLS algorithm briefly presented in the subsequent section.

5.1 Delayed unknown input observers

The use of a so-called UIO filter has the advantage of simultaneously allowing state estimation and unknown input reconstruction. The main concept capitalizes on the equivalence between linear system's invertibility and unknown input observability, which has been explored in (Sain and Massey (1969);Hou and Patton (1998)). Thus, consider a linear, time-invariant, discrete-time system in a general form

$$\begin{aligned} X_{k+1} &= A\,X_k + B\,U_k\,, \\ Y_k &= C\,X_k + D\,U_k\,, \end{aligned} \tag{5.1}$$

where $X_k \in \mathbb{R}^n$ is a state vector, $U_k \in \mathbb{R}^m$ contains the unknown inputs, $Y_k \in \mathbb{R}^p$ is an output vector, A, B, C, and D are suitable matrices. Given a time delay $L \geq 0$, the history of the system's output, $\mathbb{Y}_k^L = (Y_k^T, \cdots, Y_{k+L}^T)^T$, can be expressed as

$$\mathbb{Y}_k^L = O^L X_k + \mathbb{H}^L\,U_k^L\,, \tag{5.2}$$

where $\mathbb{U}_k^L = (U_k^T, \cdots, U_{k+L}^T)^T$ is the system's input history, and O^L and $\mathbb{H}_k^L$ are the *L-step observability and invertibility matrices*, respectively. More precisely, for a zero delay, $L = 0$, the input and output histories reduce to $\mathbb{U}_k^0 = U_k$ and $\mathbb{Y}_k^0 = Y_k$, respectively, and the corresponding system's observability and invertibility matrices are $O^0 = C$ and $\mathbb{H}^0 = D$. For a positive time

delay, $L \geq 1$, it holds

$$\begin{aligned} O^L &= \left(C^T, (CA)^T, (CA^2)^T, \cdots, (CA^L)^T\right)^T = \\ &= \left(C^T, (O^{L-1}A)^T\right)^T , \end{aligned}$$

and

$$\mathbb{H}^L = \begin{pmatrix} D & 0 & 0 & 0 & \cdots & 0 \\ CB & D & 0 & 0 & \cdots & 0 \\ CAB & CB & D & 0 & \cdots & 0 \\ \vdots & \vdots & \vdots & \vdots & \ddots & \vdots \\ CA^{L-1}B & CA^{L-2}B & \cdots & \cdots & CB & D \end{pmatrix} .$$

As anticipated above, the system invertibility plays a crucial role in ensuring the observability of the unknown inputs. Therefore, first the condition for the system invertibility is presented:

Proposition 7 (System Invertibility)**.** *A linear dynamic system with state form as in Eq. 5.1, with state vector $X_k \in \mathbb{R}^n$ and $U_k \in \mathbb{R}^m$, is* invertible with delay L *if, and only if, the condition*

$$\operatorname{rank}\left(\mathbb{H}^L\right) = m + \operatorname{rank}\left(\mathbb{H}^{L-1}\right) \tag{5.3}$$

is satisfied for some $L \leqslant n$, where $\operatorname{rank}\left(\mathbb{H}^{-1}\right) = 0$ *by definition.*

Moreover, as the system output in Eq. 5.2 depends also on the initial state, whose knowledge can be approximate, it is useful to check also the system's strong observability according to the following:

Definition 1. *A discrete-time system as in Eq.5.1 is* strongly observable *if, for any initial state X_0 and any unknown input sequence $U_0, U_1, ...$, there exists a positive integer L such that X_0 can be recovered from the output sequence $Y_0, Y_1, ...$*

Proposition 8 (Strong Observability)**.** *A discrete-time system in Eq. 5.1 where $X_k \in \mathbb{R}^n$ is strongly observable if, and only if, for some $L \leqslant n$, it holds*

$$\operatorname{rank}\left(\left[O^L, \mathbb{H}^L\right]\right) = n + \operatorname{rank}\left(\mathbb{H}^L\right) .$$

A discrete-time linear delayed unknown input observer, introduced by Sundaram and Hadjicostis (2007), is described with

$$\begin{aligned} \hat{X}_{k+1} &= E\,\hat{X}_k + F\,\mathbb{Y}_k^L , \\ \hat{U}_k &= G \begin{pmatrix} \hat{X}_{k+1} - A\,\hat{X}_k \\ Y_k - C\,\hat{X}_k \end{pmatrix} , \end{aligned} \tag{5.4}$$

where E and F are observer matrices of suitable dimensions, being designed such that $\hat{X}_k \to X_k$ and $\hat{U}_k \to U_k$, and where $G = (B^T, D^T)^{T\,\dagger}$ is an input decoupling matrix, with full column rank, and $P^\dagger$ is the pseudo-inverse of a matrix P.

The existence conditions of a such UIO are the following:

Proposition 9 (Existence of delayed UIO)**.** *Given a linear dynamic system of the form in Eq. 5.1, an L-step delayed UIO described by Eq. 5.4 exists if, and only if, there exist two matrices E and F satisfying the conditions:*

1. *E is Schur, i.e. all its eigenvalues lay within the unit circle of the complex plane,*

2. $E = A - F\,O^L$, *and*

3. $F\,\mathbb{H}^L = (B, 0_{n\times Lm})$.

Proof. The conditions for the observer's stability are examined by driving the estimation error to zero, whose dynamics is:

$$\begin{aligned} e_{k+1} &= \hat{X}_{k+1} - X_{k+1} = \\ &= E\,\hat{X}_k + F\,\mathbb{Y}_k^L - A\,X_k - B\,U_k = \\ &= E\,e_k + F\,\mathbb{Y}_k^L + (E - A)\,X_k - B\,U_k = \\ &= E\,e_k + (E - A + F\,O^L)\,X_k + F\,\mathbb{H}^L\,\mathbb{U}_k^L - B\,U_k\,, \end{aligned}$$

where E and F are the observer's matrices to be suitably chosen. Under the theorem's assumptions, reduces to $e_{k+1} = E\,e_k$, thereby guaranteeing convergence for every unknown input signal U_k and every initial state e_0.

The condition for the existence of matrix F is equivalent to the one given in Prop. 7, while the matrix is obtained by following the design procedure described in Sundaram and Hadjicostis (2007); Sundaram (2012), shortly presented below.

First, consider the third condition $F\,\mathbb{H}^L = (B, 0_{n\times Lm})$ which is also called input-decoupling equation, as it decouples input from the estimation error. The matrix F can be expressed as

$$F = \hat{F}\,N = (\hat{F}_1, \hat{F}_2)\,N\,,$$

where N is chosen such that

$$N\,\mathbb{H}^L = \begin{pmatrix} 0 & 0 \\ I_m & 0 \end{pmatrix}.$$

This straightforwardly leads to the conclusion that $\hat{F}_2 = B$. Moving now on to the state-decoupling equation $E = A - F\,O^L$, named after property to decouple states and estimation error, the design degree-of-freedom of matrix $\hat{F}_1$ is used to suitably allocate eigenvalues of E, in order to keep it stable. If any desired eigenvalue position is given, robust pole placement procedures such as the one described in Kautsky et al. (1985) are recommended. □

5.2 Recursive Least Square algorithm

Consider a function f which can be approximated as a product of a regressor matrix Φ and a corresponding parameter vector $\Pi \in \mathbb{R}^\kappa$

$$f = \Phi\,\Pi\,.$$

Assuming that f and Φ are known, the RLS algorithm is used to estimate the parameter vector $\hat{\Pi}$ such that the estimation error $\epsilon = \hat{f} - \Phi\,\hat{\Pi}$ is minimized. Having denoted with $\hat{\Pi}[k] = (\hat{\pi}_1[k], \cdots, \hat{\pi}_\kappa[k])^T$ the parameter vector estimated at the k-th step, the following RLS algorithm proposed by Ljung (1999) can be used:

$$\begin{aligned} \epsilon[k] &= f[k] - \Phi[k]\,\hat{\Pi}[k]\,, \\ \rho[k] &= \Phi^T[k]\,P[k-1]\,\Phi[k]\,, \\ K[k] &= (1 + \rho[k])^{-1}\,(P[k-1]\,\Phi[k])\,, \\ \hat{\Pi}[k] &= \hat{\Pi}[k-1] + K[k]\,\epsilon[k]\,, \\ P[k] &= P[k-1] - K[k]\,\Phi^T[k]\,P[k-1]\,, \end{aligned} \tag{5.5}$$

where K indicates the gain vector, ρ presents a residual covariance, and P is the parameter covariance matrix. The algorithm is initialized with an a-priori assumption of parameters $\hat{\Pi}[0]$ and a positive definite covariance matrix $P[0]$.

Chapter 6

Invasive approach

This chapter proposes a technique for the estimation of stiffness and flexibility torque in robot joints assuming the availability of information about the commanded torques/pressures.

First, an online stiffness estimator is designed for a soft joint robot with the pneumatic actuation and, to the best of the author's knowledge, it presents a unique stiffness estimator for such robots. The challenge is attacked from the link side, hence, in order to design a linear observer, all robot nonlinearities are grouped with the flexibility torque and considered as an unknown input. It is worth noting that the only necessary information is that of commanded pressure in both McKibben muscles and link position. The disadvantage of the proposed method stems in the requirement of precise knowledge of robot dynamic parameters and nonlinearities. Moreover, the observability issue occurs when the robot is in zero position.

Regarding the electrically driven soft joint robots, a pivotal point of the strategy is the consideration of the flexibility torque signal as an unknown input of the linear motor model. Compared to the solution presented by Grioli and Bicchi (2010), approaching the problem from the link side, this approach avoids the known observability issue and does not require the installation of torque sensors, as it considers the problem from the motor side. Moreover, compared to the method presented by Flacco et al. (2012a), the present one requires no tuning of a Kalman Filter, thanks to the capacity of the UIO to simultaneously estimate velocity of motors and flexibility torque. However, similarly to Flacco et al. (2012a), the proposed approach estimates both joint stiffness and flexibility torque, which is useful for model-based control laws, but on the other hand it lacks the proof of stiffness convergence which is provided instead by Ménard et al. (2014).

Finally, while the approach by Ménard et al. (2014) requires a suitable tuning of the integration window length depending on the signal to be elaborated, the UIO-based approach involves matrices that are a-priori determined and thus independent of the signal rate. As a consequence, the UIO output alone tends to be more susceptible to noise, but the concurrently running RLS algorithm is capable of successfully compensating for it. It is also worth mentioning that, thanks to the decentralized structure of motor dynamic equations, this method can be applied for the stiffness estimation in flexible joints of electric robots with multiple degrees of freedom, joints driven by different VSA configurations, and, consequently, for Cartesian stiffness estimation based on joints' positions and stiffnesses.

6.1 Robots with pneumatic actuation

This section considers the estimation of flexibility torque and stiffness in the joint of a pneumatically actuated robot with one link, whose dynamic model is obtained from Eq. 2.5

and reads

$$I\ddot{q} + \beta\dot{q} + m\,g\,l\,\sin q = \tau_e \tag{6.1a}$$

$$\dot{\sigma} = \frac{d}{dt}\frac{\partial \tau_e}{\partial q}\,. \tag{6.1b}$$

It is a straightforward observation that in order to estimate stiffness, first a flexibility torque needs to be determined.

6.1.1 Flexibility torque estimator

The following result stands:

Theorem 1 (Flexibility torque estimator)**.** *Given a pneumatic soft robot system with one link, as in Eq. 6.1a, and a sampling time T, a delayed, discrete-time, input-state observer described by*

$$\begin{aligned} \hat{X}_{k+1} &= E\,\hat{X}_k + F\,\mathbb{Y}_k\,, \\ \hat{u}_k &= G\begin{pmatrix} \hat{X}_{k+1} - A\,\hat{X}_k \\ q_k - C\,\hat{X}_k \end{pmatrix}\,, \end{aligned}$$

where k is a discrete time step, allows the reconstruction of the flexibility torque τ_e. The state and output vector are

$$\hat{X}_k = \begin{pmatrix} \hat{q}_k \\ \hat{\dot{q}}_k \end{pmatrix},\ \mathbb{Y}_k = \begin{pmatrix} q_k \\ q_{k-1} \\ q_{k-2} \end{pmatrix},$$

and the matrices are

$$E = \begin{pmatrix} 1 & T \\ -1/T & -1 \end{pmatrix}\ F = \begin{pmatrix} 0 & 0 & 0 \\ 0 & 0 & 1/T \end{pmatrix}$$

$$G = \begin{pmatrix} 0 & b & 0 \end{pmatrix} \tag{6.2}$$

$$A = \begin{pmatrix} 1 & T \\ 0 & 1 - T\frac{d}{b} \end{pmatrix},\ C = \begin{pmatrix} 1 & 0 \end{pmatrix}$$

The estimated flexibility torque is obtained as

$$\hat{\tau}_{e,k} = \hat{u}_k - mgl\sin\hat{q}\,. \tag{6.3}$$

Proof. The input to the system, that will be considered as an unknown, collects all system nonlinearities such that

$$u = \tau_e - mgl\sin q$$

for the purpose of building a linear UIO estimator. Defining the state vector as $X = \left(q^T, \dot{q}^T\right)^T$ yields the linear state form

$$\dot{X} = A_c X + B_c u\,, \quad q = CX + Du\,,$$

with C defined in Eq. 6.2, while the other system matrices are given by

$$A_c = \begin{pmatrix} 0 & 1 \\ 0 & -\beta/I \end{pmatrix},\ B_c = \begin{pmatrix} 0 \\ 1/I \end{pmatrix},\ D = 0\,.$$

Now, to comply with the discrete-time form of an estimator, the system is transformed to its

discrete version by applying Euler's rule, such that $A = I_2 + TA_c$ and $B = TB_c$, and becomes

$$X_{k+1} = AX_k + Bu_k\,, q_k = CX_k + Du_k\,,$$

where A and B are given in Eq. 6.2. Moreover, matrices A, B, C, and D satisfy the invertibility and strong observability conditions for the delay $L = 2$, introduced in Prop. 7 and Prop. 8, which along the fact that the matrix E is stable for chosen $\hat{F}_1 = 0_{2\times 2}$ implies the existence of a UIO. Finally, the design procedure of the observer matrices, provided in Prop. 9, leads to the matrices E, F, and G as stated in Eq. 6.2.

Once the UIO has estimated the unknown input $\hat{U}_k$, the flexibility torque can be reconstructed by applying Eq. 6.3, which concludes the proof. □

6.1.2 Estimation of stiffness

With the aim of obtaining analytic expressions of flexibility torque and stiffness, an RLS algorithm is then used to identify the coefficients of a κ-th order parametric approximation of torque with respect to the commanded pressures and link position:

$$\hat{\tau}_e = \Phi\,\Pi\,,$$

where

$$\Phi = \left(p_a\left(1, q, \cdots, q^{\kappa}\right), p_b\left(1, q, \cdots, q^{\kappa}\right)\right)\,,$$
$$\Pi = \left(\pi_1, \pi_2, \cdots, \pi_{2\kappa}\right)^T\,,$$

are a regressor matrix, comprised of powers of a link position multiplied by pressures in agonist and antagonist McKibben muscle, and the corresponding vector of unknown parameters, respectively. The order κ is chosen so that the main features are captured and simultaneously the estimation is denoised. Afterward, stiffness is calculated as a first derivative of the flexibility torque approximation:

$$\hat{\sigma} = \frac{\partial \hat{\tau}_e}{\partial q} = \frac{\partial \Phi}{\partial q}\hat{\Pi}\,.$$

The block diagram of a stiffness estimator is presented in Fig. 6.1.

6.1.3 Simulation results

The proposed estimator is validated on a soft pneumatic robot actuated by two McKibben muscles arranged in the antagonistic setup. Nominal values for the parameters of robot dynamics are set to $I = 0.015$ kg m^2, $\beta = 10^{-5}$ Nm/s, $m = 0.4$ kg, $l = 0.3$ m, while the actuator parameters are $l_{a,n} = l_{b,n} = 0.36$ m, $l_{a,\min} = l_{b,\min} = 0.25$, $l_{b,n} = 0.36$ m, $K_g = 0.14$, and $R = 0.016$ m. Following the procedure presented in the previous section, a Taylor expansion of the flexibility torque and corresponding stiffness approximation can be derived as

$$\hat{\tau}_e = p_a \textstyle\sum_{n=0}^{2} q^n\,\pi_{a,n+1} + p_b \sum_{n=0}^{2} q^n\,\pi_{b,n+1}\,,$$

$$\hat{\sigma} = p_a \textstyle\sum_{n=0}^{2} nq^{n-1}\,\pi_{a,n+1} + p_b \sum_{n=0}^{2} nq^{b,n-1}\,\pi_{n+1}\,.$$

The RLS algorithm is initialized with the parameter vector equal to zero, meaning that parameters are completely unknown in the beginning, while the initial covariance matrix is set to $P[0] = 10^9 I_6$. Choosing the sampling time $T = 10^{-2}$ s, position and stiffness are commanded to follow the desired sinusoidal trajectory, i.e. $q_d = 0.3\sin\frac{\pi}{10}t$ m and $\sigma_d = 5 + \sin\frac{\pi}{6}t$ Nm/rad. Figure 6.2 presents the results of flexibility torque and stiffness estimation, as well as the relative errors. Apart from the initial time period, when the parameters of RLS algorithm are

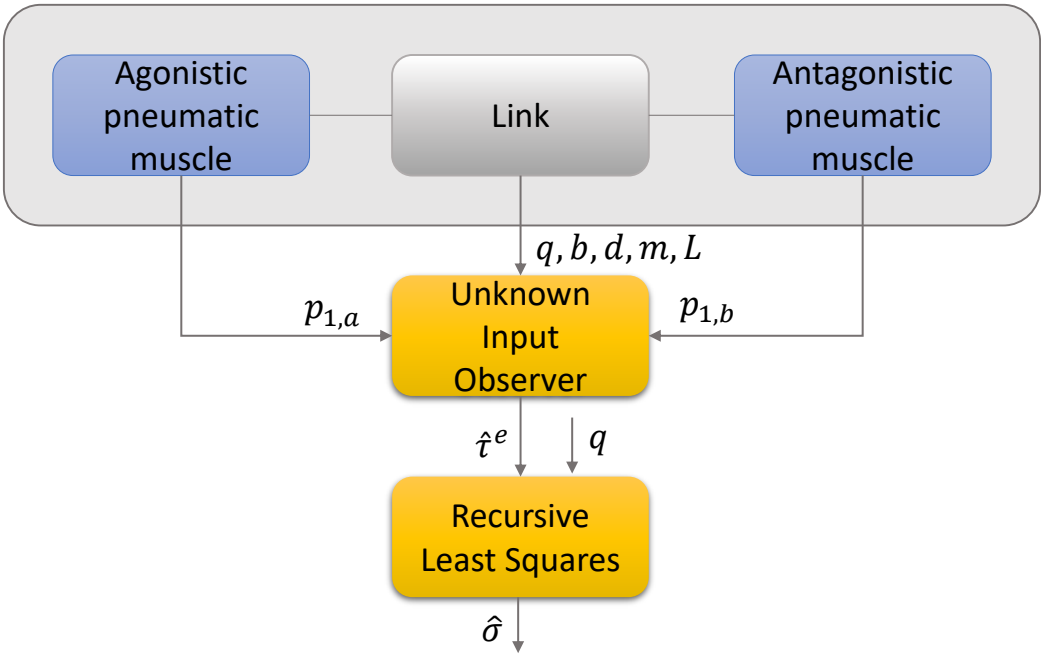

Figure 6.1: Block scheme of the algorithm for invasive estimation of stiffness in flexible robot joints, actuated by pneumatic antagonistic VSA.

being updated, both torque and stiffness values are estimated accurately. Moreover, the RLS parameters remain bounded and converge to the constant values, as shown in Fig. 6.3.

The estimation error can be quantitatively presented through the suitable indices such as Mean Square Error (MSE) and Mean Square Relative Error Percentage (MSREP). Given two sample sequences of a real signal χ and an estimated signal $\hat{\chi}$, those indices are defined as follows:

$$\text{MSE} = \frac{1}{n_2 - n_1 + 1} \sum_{n=n_1}^{n_2} (\chi(n) - \hat{\chi}(n))^2 \,,$$

$$\text{MSREP} = \frac{1}{n_2 - n_1 + 1} \sum_{n=n_1}^{n_2} \left(\chi(n) - \hat{\chi}(n)\right)^2 / \chi^2(n) \,,$$

where n_1 and n_2 indicate the initial and final time interval. The MSE for flexibility torque and stiffness estimation is 1.710^{-14} and 1.210^{-5} while the MSREP is equal to 1.610^{-8} and 0.45, respectively.

6.1.4 Conclusion

This section addressed stiffness estimation in robots with pneumatic drive. The method exploits delayed UIO to reconstruct the flexibility torque, tackling the challenge from the link side. Eventually, an RLS algorithm is applied to obtain an analytic expression of stiffness and flexibility torque. Simulation verification of the proposed estimator showed that both variables are well estimated, requiring just the knowledge of commanded pressures and link position. Moreover, the solution has observability issues only when the position of a robot is equal to zero. The main disadvantage is comprised of the necessity for the precise information about the link dynamic parameters and restriction to one segment only. Future work will consider the modification of a regressor matrix for the purpose of extending the method to multi link case.

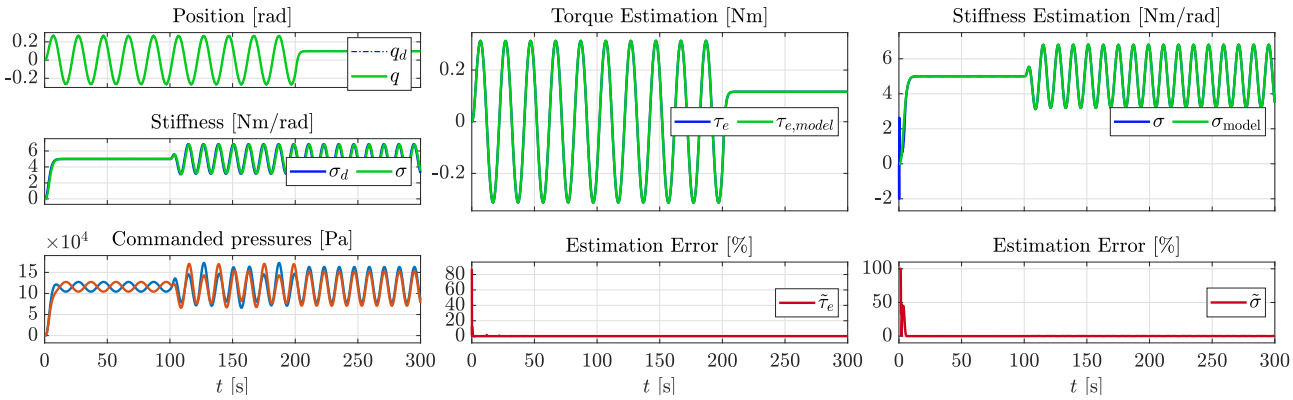

Figure 6.2: Simulation run of a one-DoF pneumatic robot driven by McKibben muscles in the antagonistic setup. In the leftmost figure, from top to bottom, desired and obtained position and stiffness, as well as commanded pressures are shown. The middle and rightmost figure depict results of flexibility torque and stiffness estimation.

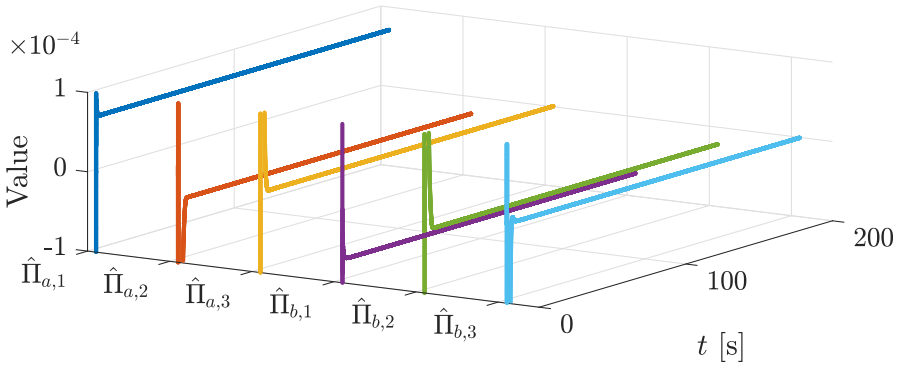

Figure 6.3: Temporal evolution of parameters estimated via RLS algorithm in Matlab Simulink. Parameters converge rapidly and remain constant.

6.2 Robots with electric actuation

Within the following, a methodology that tackles the challenge of stiffness estimation from a drive side has been presented. Therefore, since it is applied on robots with electric actuation, dynamics of each DC motor actuating the joint has to be considered in order to first reconstruct the local flexibility torque, and then leverage on Eq. 2.9 to determine stiffness.

Observing the j-th drive of an i-th joint in Eq. 2.10, the following dynamic relation for a motor stands

$$b_{i,j}\ddot{q}_{i,j} + d_{i,j}\dot{q}_{i,j} - \tau^{e}_{i,j}(\phi_{i,j}) = \tau_{i,j}\,, \tag{6.4}$$

and it will be addressed for the purpose of extracting the information of the local flexibility torque.

6.2.1 Local flexibility torque estimation

Theorem 2 (Local flexibility torque estimation)**.** *Given a system in Eq. 6.4, and a sampling time T, a delayed, linear, input-state observer can be designed of the following form*

$$\begin{aligned}\hat{X}_{i,j,k+1} &= E\,\hat{X}_{i,j,k} + F\,\mathbb{Y}_{i,j,k}\,,\\ \hat{U}_{i,j,k} &= G_{i,j}\begin{pmatrix}\hat{X}_{i,j,k+1} - A_{i,j}\,\hat{X}_{i,j,k}\\ \begin{pmatrix}q_{i,j,k}\\ \tau_{i,j,k}\end{pmatrix} - C\,\hat{X}_{i,j,k}\end{pmatrix}\,,\end{aligned}$$

with the aim of reconstructing the local flexibility torque $\tau^e_{i,j}$. The state, input, and output vector are

$$\hat{X}_{i,j,k} = \begin{pmatrix}\hat{q}_{i,j,k}\\ \hat{\dot{q}}_{i,j,k}\end{pmatrix},\ \hat{U}_{i,j,k} = \begin{pmatrix}\hat{\tau}^e_{i,j,k}\\ \tau_{i,j,k}\end{pmatrix},\ \mathbb{Y}_{i,j,k} = \Big(\big(q_{i,j,k}, q_{i,j,k-1}, q_{i,j,k-2}\big)^T, \big(\tau_{i,j,k}, \tau_{i,j,k-1}, \tau_{i,j,k-2}\big)^T\Big)^T,$$

while the matrices read

$$\begin{aligned}E &= \begin{pmatrix}1 & T\\ -\frac{1}{T} & -1\end{pmatrix},\ F = \begin{pmatrix}0 & 0 & 0 & 0 & 0 & 0\\ 0 & 0 & 0 & 0 & 1/T & 0\end{pmatrix},\\ G_{i,j} &= \begin{pmatrix}0 & -Tb_{i,j} & 0 & 1\\ 0 & 0 & 0 & 1\end{pmatrix} \qquad (6.5)\\ A_{i,j} &= \begin{pmatrix}1 & T\\ 0 & 1 - T\frac{d_{i,j}}{b_{i,j}}\end{pmatrix},\ C = \begin{pmatrix}1 & 0\\ 0 & 0\end{pmatrix}.\end{aligned}$$

The local flexibility torque is directly obtained from the unknown input vector.

Proof. Considering the state vector $X_{i,j} = (q_{i,j}, \dot{q}_{i,j})^T$, the input vector $U_{i,j} = (\tau^e_{i,j}, \tau_{i,j})^T$, and the output vector $Y_{i,j} = (q_{i,j}, \tau_{i,j})^T$, the state-space form of the system becomes

$$\dot{X}_{i,j} = A_{c_{i,j}}X_{i,j} + B_{c_{i,j}}U_{i,j}\,,\quad Y_{i,j} = CX_{i,j} + DU_{i,j}\,,$$

where C is given in Eq. 6.5 and the other matrices are

$$\begin{aligned}A_{c_{i,j}} &= \begin{pmatrix}0 & 1\\ 0 & -d_{i,j}/b_{i,j}\end{pmatrix},\ B_{c_{i,j}} = \begin{pmatrix}0 & 0\\ 1/b_{i,j} & 1/b_{i,j}\end{pmatrix},\\ D &= \begin{pmatrix}0 & 0\\ 0 & 1\end{pmatrix}.\end{aligned}$$

The discrete-time version of the system, necessary if one wants to derive the UIO, can be obtained by using the Euler's method. In this way, the system gains the form

$$X_{i,j,k+1} = A_{i,j}\,X_{i,j,k} + B_{i,j}\,U_{i,j,k}\,,\quad Y_{i,j,k} = C\,X_{i,j,k} + D\,U_{i,j,k}\,.$$

where $A_{i,j}$ and B are provided in Eq. 6.5. It is straightforward to conclude that the system is fully observable. However, regarding the existence conditions of a UIO, it is important to additionally examine the invertibility and strong observability of the system. According to Prop. 7, the sought delay, allowing the unknown input reconstruction, is $L = 2$. The strong observability condition is satisfied, again, for a delay $L = 2$ according to Prop. 8, which allows the conclusion that a two-sample delay is necessary and sufficient for observing unknown inputs.

Finally, the existence of UIO is ensured by choosing $\hat{F}_1 = 0_{2\times 2}$, so E becomes a stable matrix. The observer matrices E, F, and G, given in Eq. 6.5 are obtained by following the design procedure in Prop. 9. □

Remark 2. *It is worth remarking that although it might seem that both the commanded and the flexibility torque are considered as an unknown inputs in the UIO, the information about the commanded one is introduced by setting the corresponding element of D matrix to one. Therefore, the presented estimator is invasive.*

6.2.2 Estimation of stiffness

Once the flexibility torque has been estimated by the UIO, an RLS algorithm is used to determine the coefficients of a κ-th order parametric approximation of such torque with respect to flexible transmission, being $\hat{\tau}^e_{i,j} = \Phi_{i,j}\,\Pi_{i,j}$, where the quantities

$$\begin{aligned}\Phi_{i,j} &= \left(\phi_{i,j}, \phi^3_{i,j}, \cdots, \phi^{2\kappa+1}_{i,j}\right) ,\\ \Pi_{i,j} &= (\pi_{i,j,1}, \pi_{i,j,2}, \cdots, \pi_{i,j,\kappa})^T ,\end{aligned}$$

are a regressor matrix, comprising only odd powers of the transmission deflection since flexibility torque oddness is assumed, and the corresponding vector of unknown parameters, respectively. As in the case of pneumatic actuators, the order κ is set in a way that the main features are captured and simultaneously the estimation is denoised. Afterward, stiffness is calculated as a first derivative of the flexibility torque approximation:

$$\hat{\sigma}_{i,j} = \frac{\partial \hat{\tau}^e_{i,j}}{\partial \phi_{i,j}} = \frac{\partial \Phi_{i,j}}{\partial \phi_{i,j}} \hat{\Pi}_{i,j} .$$

The block diagram of a stiffness estimator is presented in Fig. 6.4.

6.2.3 Simulation results

The proposed technique has first been validated in simulations on a two degree-of-freedom soft robot, with rotary joints actuated by antagonistic VSAs, mounted in a vertical plane. The simulated actuators are *Qbmove Maker Pro* with servo DC motors provided by *qb-robotics*. According to the robot model in Eq. 2.10 and data-sheets qbmove Centro Piaggio (2011), the flexibility torque generated by each drive and the corresponding stiffness are

$$\begin{aligned}\tau^e_{i,j} &= k_i \sinh(a_i(q_i - q_{i,j})) ,\\ \sigma_{i,j} &= a_i\, k_i \cosh(a_i(q_i - q_{i,j})) ,\end{aligned} \tag{6.6}$$

where a_i and k_i denote VSA string characteristic, assumed to be same for each joint. The total flexibility torque and stiffness of the joint are straightforwardly determined in compliance with Eq. 2.7 and 2.9. Nominal values for the stated VSA are $b_{i,j} = 3 \cdot 10^{-6}$ kgm^2, $d_{i,j} = 10^{-6}$ Nms/rad, $a_1 = 6.7328$ Nm, $k_1 = 0.0227$ 1/rad, $a_2 = 6.9602$ Nm, and $k_2 = 0.0216$ 1/rad. Given the decentralized structure of motors' dynamics (cf. Ch. 2) and the fact that motors have the same characteristics by construction, the local flexibility torque at every motor i can be estimated by a copy of the very same UIO, which is designed only once, with a delay $L = 2$. Moreover, the following Taylor expansion of the flexibility torque and the corresponding stiffness approximation are used:

$$\begin{aligned}\hat{\tau}^e_{i,j} &= \textstyle\sum_{n=0}^{3} (q_i - q_{i,j})^{2n+1}\, \pi_{i,j,n+1} ,\\ \hat{\sigma}_{i,j} &= \textstyle\sum_{n=0}^{3} (2n+1)(q_i - q_{i,j})^{2n}\, \pi_{i,j,n+1} .\end{aligned}$$

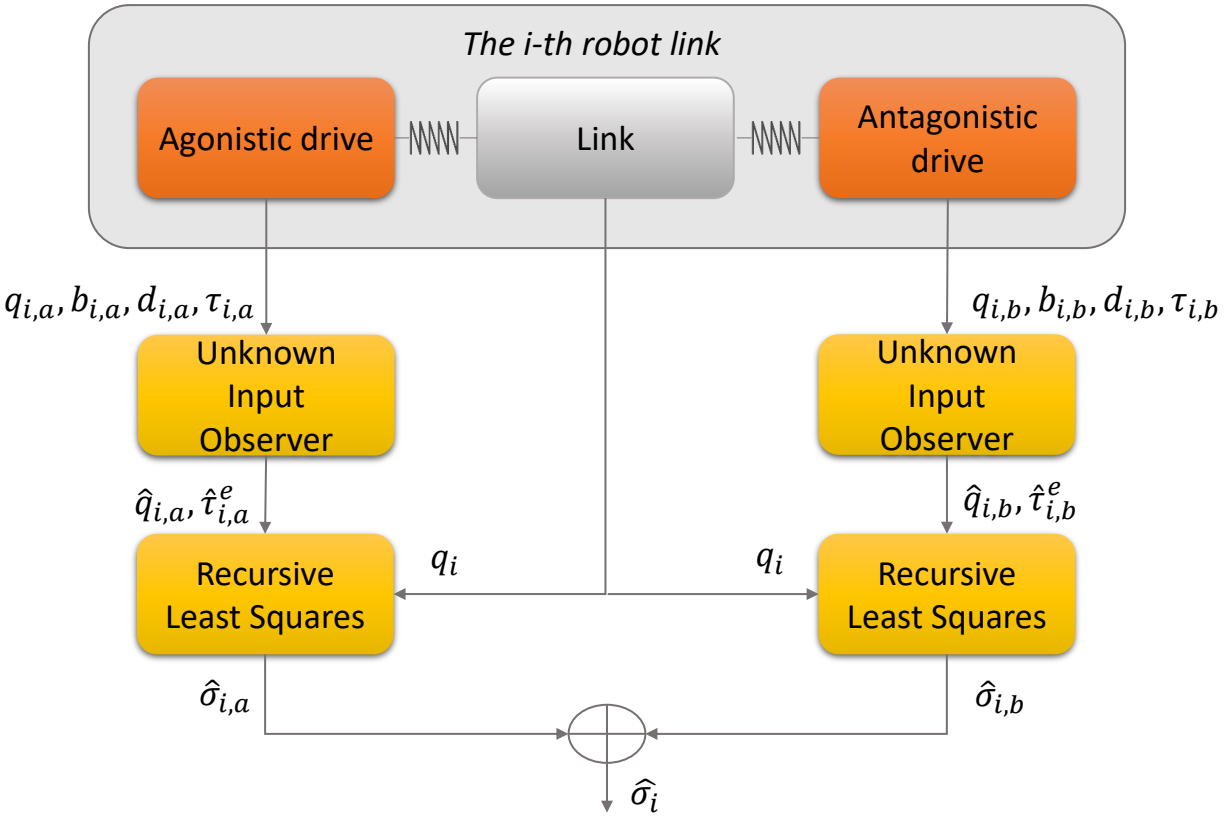

Figure 6.4: Block scheme of the algorithm for the invasive estimation of stiffness in flexible robot joints, actuated by electro-mechanical antagonistic VSA.

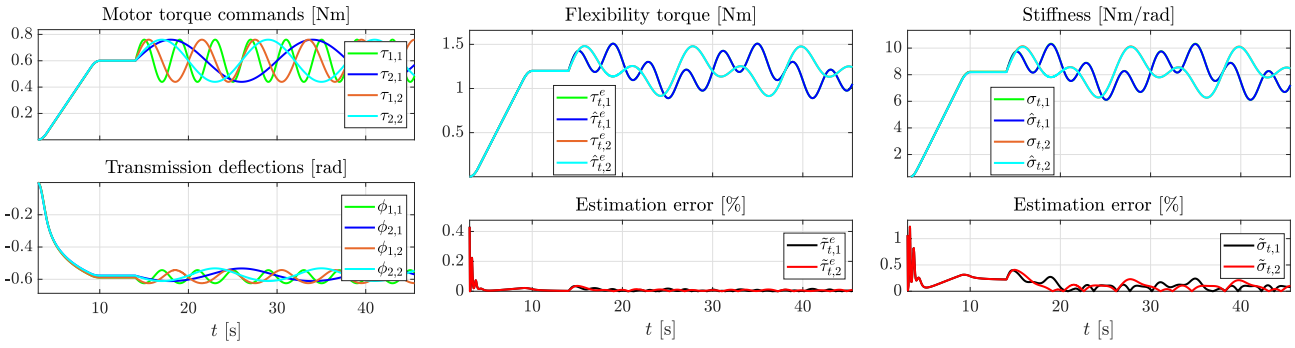

Figure 6.5: Simulation run of a two degree-of-freedom flexible joint robot driven by antagonistic VSA. From left to right, commanded torques $\tau_{i,j}$ applied to the motors and obtained transmission deflections $\phi_{i,j}$, estimated total flexibility torque $\hat{\tau}^e_{t,j}$ for each joint and corresponding error percentage $\tilde{\tau}^e_{t,j} = (\hat{\tau}^e_{t,j} - \tau^e_{t,j})/\tau^e_{t,j}$, and estimated stiffness $\hat{\sigma}_{t,j}$ in each joint and error percentage $\tilde{\sigma}_{t,j} = (\hat{\sigma}_{t,j} - \sigma_{t,j})/\sigma_{t,j}$. Both flexibility torques and stiffnesses are estimated effectively with quite small relative error.

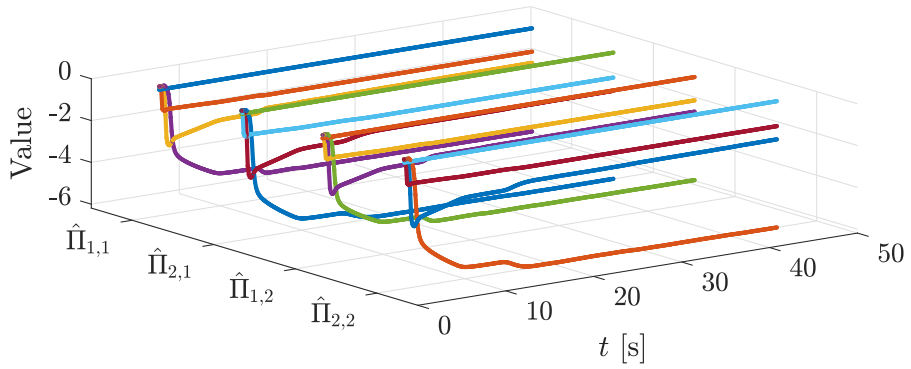

Figure 6.6: Temporal evolution of the parameter vectors estimated via the RLS algorithm in Matlab/Simulink. Parameters rapidly converge and remain constant.

Table 6.1: Evaluation criteria for simulated results

		MSE [N^2m^2/rad^2]	MSREP [%]
Stiffness estimation	1^{st} joint	$1.84 \cdot 10^{-7}$	$3.34 \cdot 10^{-7}$
	2^{nd} joint	$1.92 \cdot 10^{-7}$	$3.38 \cdot 10^{-7}$
Torque estimation	1^{st} joint	$1.49 \cdot 10^{-11}$	$2.85 \cdot 10^{-9}$
	2^{nd} joint	$1.62 \cdot 10^{-11}$	$2.84 \cdot 10^{-9}$

Starting the RLS algorithm with complete lack of knowledge of the parameter values, i.e. with a null $\hat{\Pi}_{i,j}[0]$, and an initial covariance matrix $P_{i,j}[0] = 10^8 I_4$, the simulation, run with a sampling period of $T = 10^{-3}$ s, gives the results reported in Fig. 6.5 and Fig. 6.6. More precisely, Fig. 6.5 shows the commanded torques to drives, which are chosen to be sinusoidal with the same amplitude of 0.15 Nm and with different frequencies of 0.25 Hz for $\tau_{1,1}$, 0.06 Hz for $\tau_{1,2}$, 0.17 Hz for $\tau_{2,1}$, and 0.08 Hz for $\tau_{2,2}$, and corresponding deflections. The figure also reports the total flexibility torque and stiffness estimation via UIO and RLS algorithm, as well as the relative error of the estimation with respect to the reference models. It is apparent that the UIO accurately estimates the flexibility torque with a negligible delay of 2 milliseconds. Estimation errors of flexibility torque and joint stiffness of few percents appear only during an initial phase, when the parameters' convergence has not been achieved yet.

Furthermore, it is worth noticing that the estimation performance is not affected by the joints' dynamic coupling, which is in accordance with the result in Flacco et al. (2012a), stating that the decentralized structure of motor dynamics allows the approach to be applied also to multiple degree-of-freedom robots. Moreover, Fig. 6.6 shows the estimated parameters' evolution over time. It is noticeable that, with rigid robot links as in this case, the robot's Cartesian stiffness can be straightforwardly calculated based on its well-known relation with joint stiffness Albu-Schäffer and Bicchi (2016). Finally, Tab. 6.1 reports a summary of the estimation performance for both torque and stiffness in each joint.

6.2.4 Experimental results

This section presents results of the experimental validation of the proposed approach for stiffness estimation, by using a real soft robot with flexible joints. Joints are actuated by *Qbmove Maker Pro* VSA devices qbmove Centro Piaggio (2011) shown in Fig. **??**, internally driven by two Hitec DC servo motor drives. For each VSA, three magnetic encoders with a resolution of 8192 pulses per revolution measure the position of the two VSA's motors and of the corresponding link, and two current sensors are used to measure motors currents, thereby

indirectly providing accurate information about the achieved motor torque. Reference flexibility torque and stiffness models are taken from the manufacturer's data-sheet and validated in Sec. 6.2.4.1. A sampling rate $T = 5 \cdot 10^{-3}$ s has been adopted. Then, the estimator performance is examined by using one and two DoF setups as shown in Sec. 6.2.4.2.

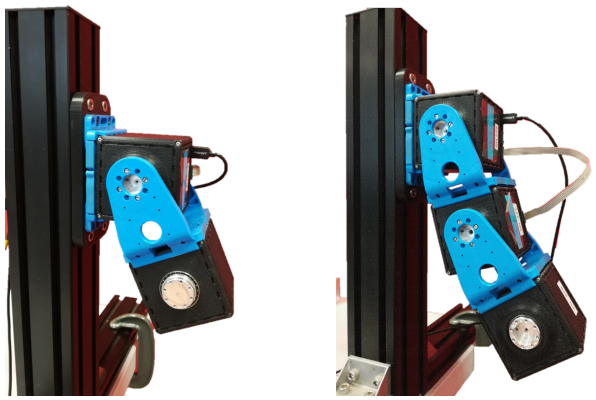

(a) (b)

Figure 6.7: The robotic setup with one (a) and two (b) degrees of freedom.

6.2.4.1 Stiffness characterization

The experiment for stiffness characterization of a qbmove VSA has been performed following the procedure described in Grioli et al. (2015). As a first step, the torque sensor ATI Axia80-M20 has been mounted on the shaft of the actuator in order to record the value of flexibility torque. Therefore, simultaneously both flexibility torque measurements and positions of the shaft and two motors are collected, for different stiffness presets ranging from 0% to 100%. Figure 6.8 shows results of the experiment applied on two different qbmove actuators from the same set, where the abscissa presents measured values of the flexibility torque and ordinate displays the deflection defined as $\delta = q - q_0$, where q_0 is the equilibrium position.

Leveraging on the collected data, one solution is that stiffness can be calculated as a numerical differentiation of a flexibility torque with respect to the deflection. Otherwise, an analytical model of a flexibility torque dependent on the deflection should first be determined, and stiffness obtained as an analytic derivative of flexibility torque model. Herein, the second approach

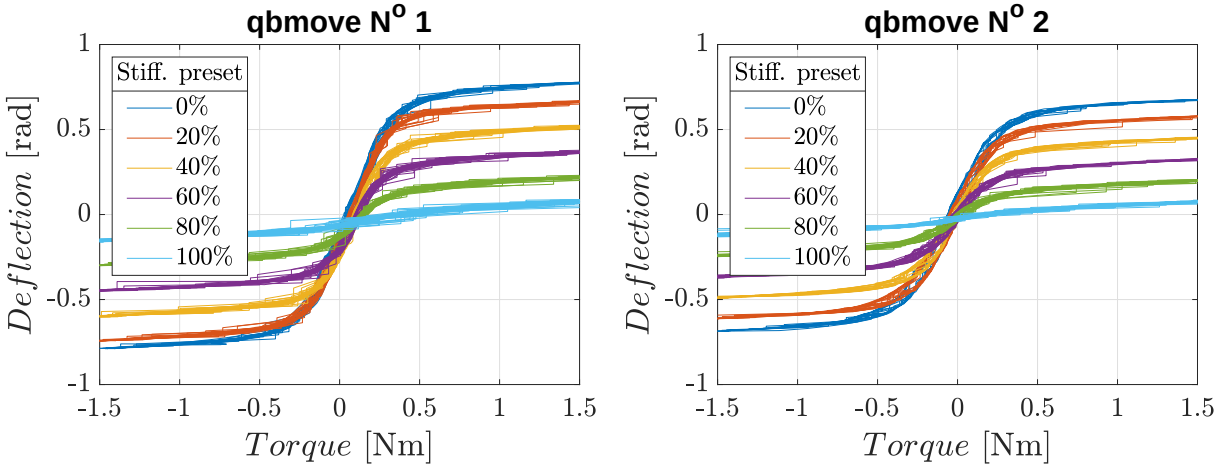

Figure 6.8: Torque-deflection relation obtained through the experiments on two different qbmove actuators

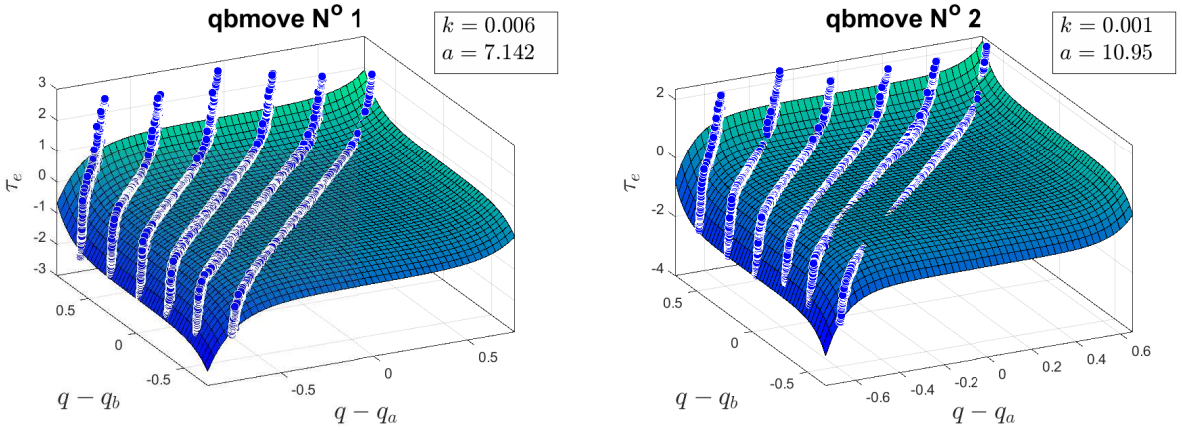

Figure 6.9: The result of fitting the torque and deflection data to the analytic $k\sinh(a(q-q_a))+k\sinh(a(q-q_b))$ function for 4 different qbmove actuators.

is chosen and for that reason proceed with finding the appropriate flexibility torque model by applying the trust region reflective fitting algorithm. This procedure is employed to fit the function equivalent to the one in the datasheet of qbmove actuators

$$\tau^e = k\sinh(a(q-q_a)) + k\sinh(a(q-q_b))\,.$$

where a and k are assumed to be coefficients, while q, q_a, and q_b are the independent variables. The results of fitting the data are shown in Figure 6.9.

It can be observed that the model does not fit properly the whole set of flexibility torque due to the existence of hysteresis and effects caused by the wear of springs. Therefore, the obtained model is valid only up to some error margin, which is calculated as a Root Mean Squared Relative Error (RMSRE):

$$RMSRE = \sqrt{\frac{1}{N}\sum_{i=1}^{N}\frac{X_{\text{sensor}} - X_{\text{model}}}{X_{\text{sensor}}}} \times 100 \;\; [\%]\,,$$

where X_{sensor} and X_{model} are the sensor and model data, respectively, while N is the number of samples.

When calculated, the value of RMSRE amounts to 19.96 % for qbmove N^o 1 and 21.06 % for qbmove N^o 2. In the remainder of the thesis, the unique value of 20% is adopted.

6.2.4.2 Validation of the estimator

In order to first prove the validity of this solution, two experiments of increasing complexity have been designed. Both of them include three consecutive test phases: 1) during the first phase (for $t \in [0, 200)$), both link positions and joint stiffnesses are chosen as sinusoids, 2) during the second phase ($t \in [200, 400)$), only link positions are varying and joint stiffnesses are constant, while 3) during the third phase ($t \in [400, 600]$) link positions are constant and joint stiffnesses are required to vary. One of the sought results from the experiments is indeed also the assessment of the method's effectiveness, during different operational conditions. Robots used for e.g. grasping tasks may be required to keep their link positions constant, while varying their joint stiffnesses, while when employed for manipulation they need to guarantee a constant stiffness for changing position. More precisely, the desired position and stiffness signals, during

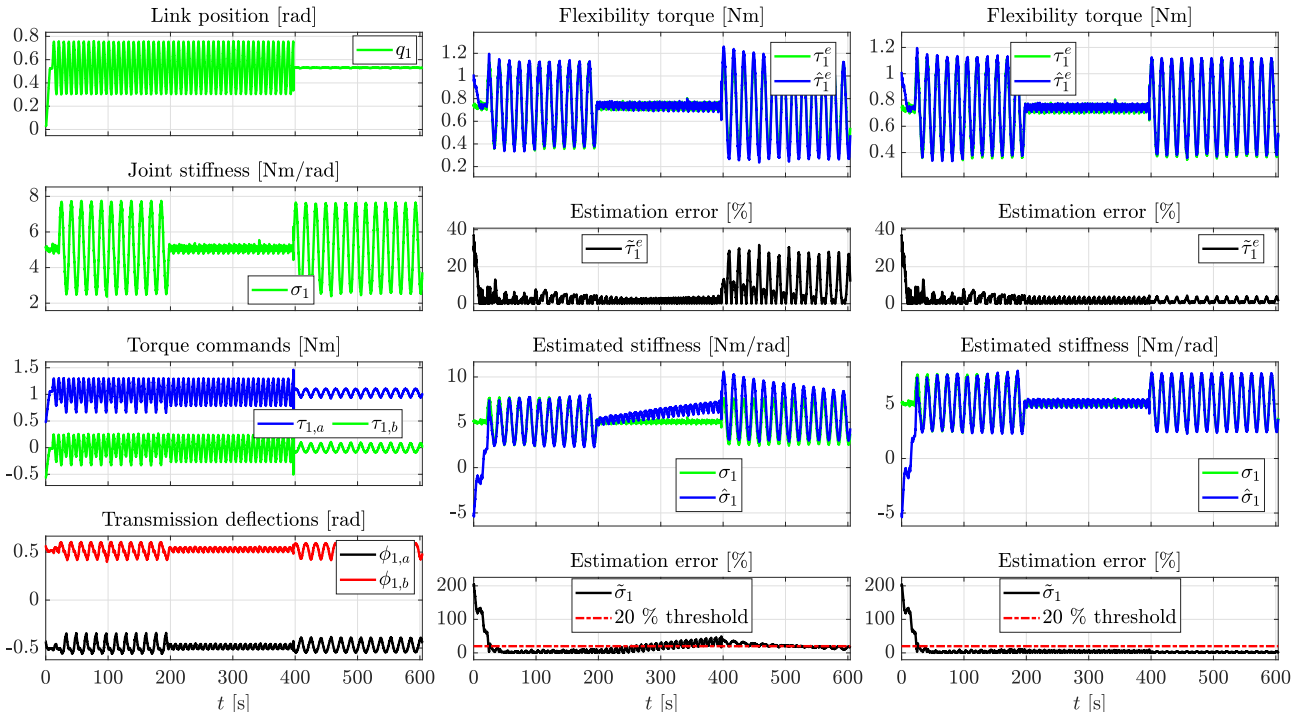

Figure 6.10: Experiment #1 (One degree-of-freedom setup) - The left-most column includes the desired link position and joint stiffness, motors' commanded torques and obtained deflections; the mid and right-most columns report the estimated and model-based computed flexibility torques and stiffnesses without and with parameter update termination, respectively.

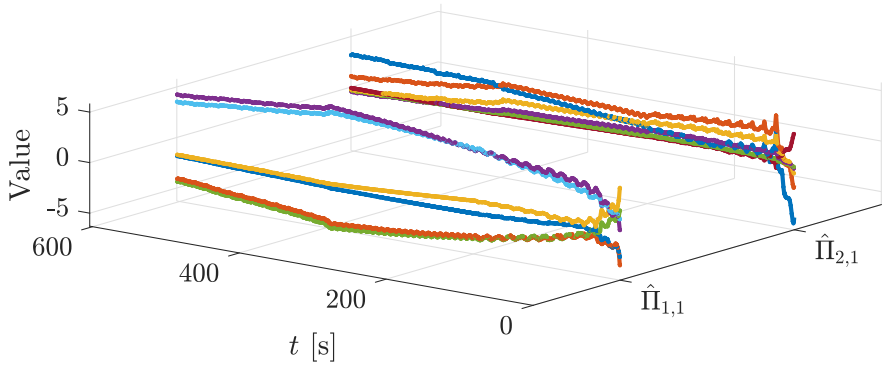

Figure 6.11: Experiment #1 (One degree-of-freedom setup) - Temporal evolution of the parameter vectors experimentally estimated via the RLS algorithm without update termination.

the three phases, are as follows:

$$\text{Phase 1:} \begin{cases} q(t) = 0.53 + 0.2\ \sin(\pi t/4)\ \text{rad}\,, \\ \sigma(t) = 5 + 2.5\ \sin(\pi t/8)\ \text{Nm/rad}\,; \end{cases}$$

$$\text{Phase 2:} \begin{cases} q(t) = 0.53 + 0.2\ \sin(\pi t/4)\ \text{rad}\,, \\ \sigma(t) = 5\ \text{Nm/rad}\,; \end{cases}$$

$$\text{Phase 3:} \begin{cases} q(t) = 0.53\ \text{rad}\,, \\ \sigma(t) = 5 + 2.5\ \sin(\pi t/8)\ \text{Nm/rad}\,. \end{cases}$$

The first experiment has been carried out by using a soft robot with only one degree of freedom, actuated by a single VSA device. Fig. 6.10 and Fig. 6.11 report the obtained results.

The test reveals that the proposed approach is capable of estimating both flexibility torque

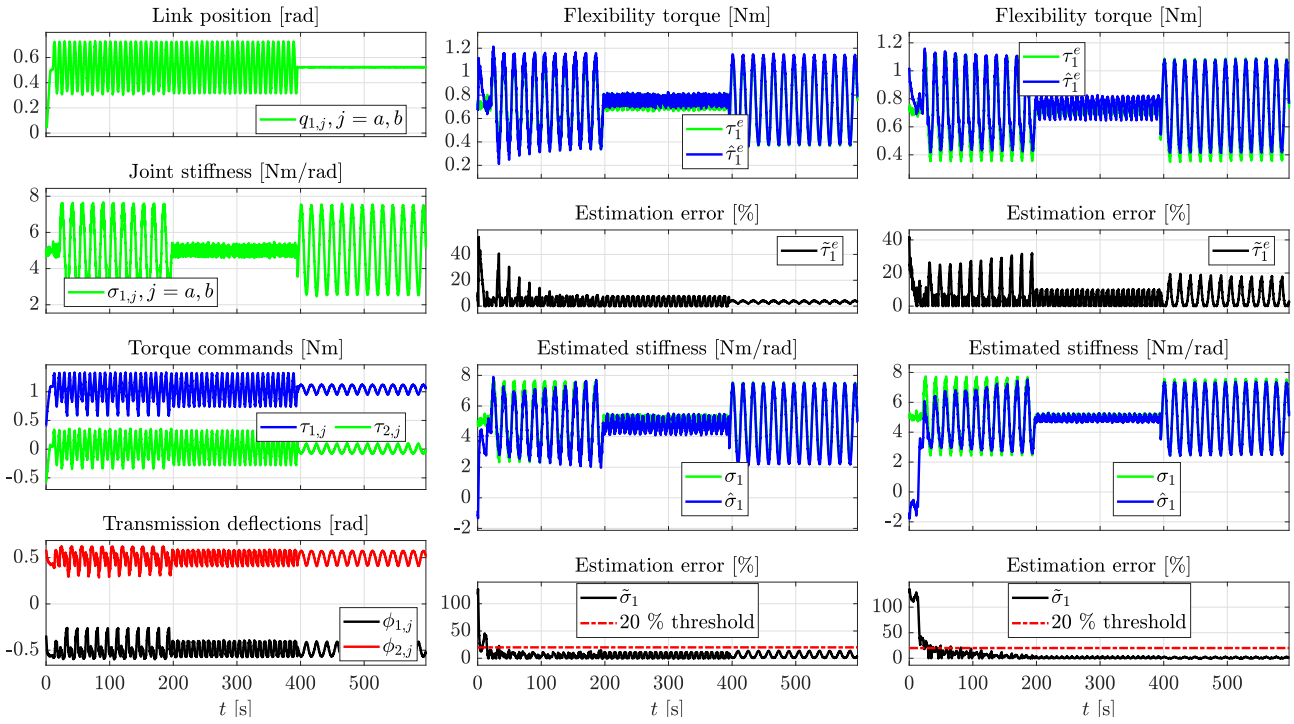

Figure 6.12: Experiment #2 (Two degree-of-freedom setup) - The left-most column illustrates desired and commanded quantities for all joints and motors; the mid and right-most column show estimation results for the first and second joint, respectively.

Table 6.2: Experiment #1 - Evaluation criteria

		MSE [N^2m^2/rad^2]	MSREP [%]
With drift	Stiffness	0.5304	0.0187
	Torque	$8.8 \cdot 10^{-6}$	$3.3 \cdot 10^{-5}$
Without drift	Stiffness	0.0258	0.001
	Torque	$1.1 \cdot 10^{-6}$	$2.7 \cdot 10^{-6}$

Table 6.3: Experiment #2 - Evaluation criteria

Without drift		MSE [N^2m^2/rad^2]	MSREP [%]
Stiffness estimation	1^{st} joint	0.048	0.002
	2^{nd} joint	0.033	0.001
Torque estimation	1^{st} joint	$9 \cdot 10^{-4}$	0.002
	2^{nd} joint	$1.1 \cdot 10^{-5}$	$4 \cdot 10^{-5}$

and stiffness. It is noticeable that simultaneous position and stiffness variations, which occur during the first phase, have a positive overall benefit to the estimation process. Indeed, apart from the initial estimation error of the RLS, due to the imprecise initialization of its parameters, the algorithm itself shows good performance, which only degrades when its input signals (including the transmission deflection ϕ_i) are poorly exciting. To be more precise, it is known from Flacco et al. (2012a) that, to better estimate the time-varying joint stiffness, it is necessary that the transmission deflection ϕ_i covers larger ranges, so that more information is provided to the estimation process. It is apparent that, during the second phase, the transmission deflection is instead almost constant (refer to the bottom-left plot in Fig. 6.10), which leads to worse RLS

performance, and, consequently, to the observed drift of the stiffness estimation.

Furthermore, the estimation performance is improved when the input signal has a richer spectral content. As a rule of thumb, according to Ljung (1999), given the κ parameters of the RLS, it is advisable to have κ spectral lines in the spectrum of the algorithm's input signal, meaning that the input signal is persistently exciting of order κ. To this respect, by observing frequency domain of the transmission deflection, the richest spectral content of the RLS input is present during the first phase, where indeed it shows its best accuracy. In line with this, if the transmission deflection is constant or it has poor frequency content with respect to the number of the RLS algorithm parameters, then it presents poor excitation to the RLS algorithm which becomes prone to instability and divergence.

Therefore, a strategy to avoid this limitation and prevent such negative side-effects (including the drift of stiffness estimation in the second phase), is to stop the parameters' update, whenever the poor excitation condition is detected. In this experiment, during the first phase, when the input signal is sufficiently exciting, parameters reach a combination of values allowing an accurate enough estimation of the flexibility torque function, and consequently of the stiffness. This in turn enables good estimation performance even afterward (for $t > 200$ s), when the parameter update is terminated (see the last column of Fig. 6.10). The corresponding MSE and MSREP criteria are presented in Tab. 6.2.

Capitalizing on the outcomes of the first experiment, a second test has been carried out by using a two degree-of-freedom setup, with the main purpose to experimentally validate the proposed method for multiple link robots with flexible joints. Specifically, results reported in Fig. 6.12 show that the dynamic coupling between joints does not impact the performance of the flexibility torque and stiffness estimation processes. As for the previous experiment, MSE and MSREP criteria have been calculated and listed in Tab. 6.3.

6.2.5 Conclusion

The problem of estimating stiffness in flexible robot joints driven by electrical VSAs was addressed in this section. The proposed solution included a delayed UIO, reconstructing flexibility torques at each electrical drive, and an RLS algorithm, subsequently obtaining stiffness from a parameterization of the torque expression with respect to the flexible transmission.

Validation via simulation showed that both flexibility torque and stiffness are well estimated, while experimental tests revealed a slow stiffness estimation drift in case of poor excitation. However, as shown, the problem can be overcome by stopping parameter vector update when such condition occurs. Moreover, the solution has shown several advantages. First, there are no observability issues, since the problem is tackled from the motor side. Secondly, torque and velocity sensors do not have to be mounted, as the UIO simultaneously estimates the motor speed and reconstructs the flexibility torque. Third, the observer matrices are a-priori calculated, making tuning of this method easier than that of state-of-the-art solutions. Fourth, thanks to the decentralized property of motor's dynamics, the proposed solution can be applied to multiple degree-of-freedom articulated soft robots. The main limitation of the method is the need for persistent excitation of the RLS algorithm. Future work will extend the research in order to also estimate other relevant impedance parameters.

Chapter 7

Noninvasive approach

The literature on non-invasive stiffness estimation approaches is not abundant. Considering the state-of-the-art solution by Grioli and Bicchi (2010), the proposed approach has several important advantages. First, it does not suffer from the observability issues when the position of robot is still. Moreover, the proposed estimator is extendable to multi-DoF robots due to its decentralized nature. Finally, there is no necessity of mounting force/torque sensors. The main motivation behind approaching this challenge in a non-inavise way stems from the fact that it is a promising step towards estimating human arm stiffness.

The strategy to reconstruct the current robot joint stiffness σ in a noninvasive way has two phases. The first consists in extracting information about the partial derivatives appearing in Eq 2.9, from the measured signals of the robot link position and speed, and then combining it with data about the VSA's internal transmission deflections, so as to obtain an estimate $\hat{\sigma}$ of the current joint stiffness σ. The first step is performed by using an Unknown Input Observer (Sundaram and Hadjicostis (2007)), while the second one is achieved by using an RLS algorithm (Ljung (1999)). Chapter initially describes the estimator for a one-link case, subsequently introducing the generalization of the proposed method. Simulation and experimental results are provided to verify the performance of the estimator.

7.1 Stiffness estimator for one-DoF soft robots

To find an approach of estimating stiffness in a non-invasive way without using force/torque sensors, first a scalar system is considered. Two central ideas are the consideration of the robot link system first time derivative and the collection of all nonlinearities into an unknown input for the purpose of obtaining a linear estimator.

As it is known from Flacco et al. (2012a), the first time derivative of the total flexibility torque τ_e contains the sought information about the partial derivatives appearing in the stiffness definition, as given by

$$\dot{\tau}_e = \frac{\partial \tau_e}{\partial \phi_a}\dot{\phi}_a + \frac{\partial \tau_e}{\partial \phi_b}\dot{\phi}_b = \frac{\partial \tau_{e,a}}{\partial \phi_a}\dot{\phi}_a + \frac{\partial \tau_{e,b}}{\partial \phi_b}\dot{\phi}_b = \sigma_a \phi_a + \sigma_b \phi_b \,, \tag{7.1}$$

where the structure in Eq. 2.7 has been used. This fact suggests considering a higher-order model of the robot's link dynamics, which can be obtained by time differentiating the robot link dynamics described with

$$I\ddot{q} + \beta\dot{q} + mgl\sin q = -\tau_e \,. \tag{7.2}$$

7.1.1 Flexible rotatum estimator

The subsequent theorem can be derived:

Theorem 3 (Flexibility Rotatum Estimator)**.** *Given a one-link soft robot system, as in Eq. 7.2, and a sampling time T, a delayed, discrete-time, input-state observer described by*

$$\begin{aligned} \hat{X}_{k+1} &= E\,\hat{X}_k + F\,\mathbb{Y}_k\,, \\ \hat{u}_k &= G\begin{pmatrix} \hat{X}_{k+1} - A\,\hat{X}_k \\ q_k - C\,\hat{X}_k \end{pmatrix}\,, \end{aligned}$$

where k is a discrete time step, enables the reconstruction of the flexibility rotatum p_e, i.e. the time derivative of the flexibility torque. The state and output vector are

$$\hat{X}_k = \begin{pmatrix} \hat{q}_k \\ \hat{\dot{q}}_k \\ \hat{\ddot{q}}_k \end{pmatrix},\ \mathbb{Y}_k = \begin{pmatrix} q_k \\ q_{k-1} \\ q_{k-2} \\ q_{k-3} \end{pmatrix},$$

and the observer matrices are

$$E = \begin{pmatrix} 1 & T & 0 \\ 0 & 1 & T \\ -\frac{1}{T^2} & -\frac{3}{T} & -2 \end{pmatrix},$$

$$F = \begin{pmatrix} 0_{2\times 3} & 0_{2\times 1} \\ 0_{1\times 3} & 1/T^2 \end{pmatrix},\ G = \begin{pmatrix} 0 & 0 & 1/T & 0 \end{pmatrix}, \tag{7.3}$$

$$A = \begin{pmatrix} 1 & T & 0 \\ 0 & 1 & T \\ 0 & 0 & 1 - T\frac{\beta}{I} \end{pmatrix},\ B = \begin{pmatrix} 0 \\ 0 \\ \frac{T}{I} \end{pmatrix}.$$

Finally, the estimated flexibility rotatum is obtained as

$$\hat{p}_{e,k} = -\hat{u}_k - mgl\dot{q}\cos q\,.$$

Proof. The information about the flexibility rotatum p_e can be extracted from the first time derivative of the link dynamics. More precisely, considering Eq. 7.2, it stands

$$p_e = \dot{\tau}_e = -(Iq^{(3)} + \beta\,\ddot{q} + mgl\,\dot{q}\,\cos q)\,,$$

where the $\star^{(i)}$ notation indicates the i-th time derivative. Now, all nonlinear terms can be grouped within the unknown input

$$u = -\dot{\tau}_e - mgl\,\dot{q}\cos q\,, \tag{7.4}$$

yielding the following linear system

$$Iq^{(3)} + \beta\,\ddot{q} = u\,,$$

whose state-space form becomes

$$\dot{X} = A_c\,X + B_c\,U\,,\quad q = C\,X + D\,u\,,$$

where C is defined as in Eq. 7.8 and the other matrices are

$$A_c = \begin{pmatrix} 0 & 1 & 0 \\ 0 & 0 & 1 \\ 0 & 0 & -\frac{\beta}{I} \end{pmatrix} \quad B_c = \begin{pmatrix} 0 \\ 0 \\ \frac{1}{I} \end{pmatrix}, \quad D = 0\,.$$

Since the estimator is designed in a discrete time, it is necessary to obtain its discrete-time form by applying Euler's rule, which eventually leads to

$$X_{k+1} = A\,X_k + B\,u_k\,, \quad q_k = C\,X_k + D\,u_k\,.$$

where A and B are as in Eq. 7.3.

It is now straightforward to determine that the considered system satisfies the invertibility and strong observability conditions of Prop. 7 and Prop. 8 for the delay of $L = 3$ time samples. Moreover, according to Prop. 9 the existence conditions of an UIO are satisfied, since matrix E is stable by setting $\hat{F}_1 = 0_{3\times 3}$.

Upon reconstructing the unknown input $\hat{U}_k$ and estimating link velocity $\dot{q}_k$ and acceleration $\ddot{q}_k$, the flexibility rotatum is retrieved by inverting Eq. 7.4. □

Remark 3. *It is worth noticing that the proposed observer requires only the use of the robot's link position, its inertia b, mass m, and the damping coefficient d, while no force/torque sensor is needed.*

7.1.2 Estimation of stiffness

As a second step, one can obtain an approximation of $\dot{\tau}_e$ by considering Taylor, Fourier or any other function-based expansions, truncated at some suitable order κ, of the partial derivatives appearing in Eq. 7.1, with respect to the two arguments, ϕ_a and ϕ_b, i.e.

$$\dot{\tau}_e \approx \left(\textstyle\sum_{j=0}^{\kappa} \pi_{a,j}\,\phi_a^j\right)\dot{\phi}_a + \left(\textstyle\sum_{j=0}^{\kappa} \pi_{b,j}\,\phi_b^j\right)\dot{\phi}_b\,,$$

where $\Pi_a = (\pi_{a,0}, \cdots, \pi_{a,\kappa})^T$ and $\Pi_b = (\pi_{b,0}, \cdots, \pi_{b,\kappa})^T$ are two unknown parameter vectors to be identified. Once such coefficients are estimated, one can derive, from Eq. 2.8, the sought joint's stiffness according to the following expression:

$$\sigma \approx \textstyle\sum_{j=0}^{\kappa} \pi_{a,j}\,\phi_a^j + \sum_{j=0}^{\kappa} \pi_{b,j}\,\phi_b^j\,. \tag{7.5}$$

According to what is stated above, the RLS algorithm can be used to determine the coefficients of a κ-th order parametric approximation of such torque with respect to the flexible transmissions, being $\dot{\tau}_e \approx \Phi\,\Pi$, where the quantities

$$\Phi = \left(\dot{\phi}_a\phi_a,\ \dot{\phi}_a\phi_a^2, \cdots,\ \dot{\phi}_a\phi_a^\kappa,\ \dot{\phi}_b\,\phi_b,\ \dot{\phi}_b\phi_b^2, \cdots,\ \dot{\phi}_b\phi_b^\kappa\right)^T,$$
$$\Pi = (\Pi_a^T, \Pi_b^T)^T\,,$$

are a regressor matrix and the corresponding vector of unknown parameters, respectively. The order κ is chosen so that the main features are captured and simultaneously the estimation is denoised. Therefore, having denoted with

$$\hat{\Pi}[k] = (\hat{\Pi}_a^T[k], \hat{\Pi}_b^T[k])^T$$

the parameter vector estimated at the k-th step, the RLS algorithm in Eq. 5.5 can be used where $\epsilon[k] = \dot{\hat{\tau}}_{e,k} - \Phi[k]\,\hat{\Pi}[k]$. Afterward, the stiffness can be calculated according to a best-effort

rule applied to Eq. 7.5, thereby obtaining

$$\hat{\sigma}[k] = (\phi_a, \phi_a^2, \cdots, \phi_a^\kappa, \phi_b, \phi_b^2, \cdots, \phi_b^\kappa)\, \hat{\Pi}[k]\,. \tag{7.6}$$

Remark 4. *It is worth noticing, referring to the system model in Eq. 2.10, that the only information used about the VSA's internal motors consists of their positions and speeds, q_a, q_b, $\dot{q}_a$, $\dot{q}_b$, which are needed to compute the two transmission deflections and their derivative. This kind of information is normally available on such devices, while data of the commanded motor torques τ_a and τ_b is not employed.*

7.2 Generalization of the Stiffness Estimator for Multi-DoF Soft Robots

This section extends the estimation approach, described for the scalar case in the previous section, by considering a complete multi-DoF soft robot. As it will be shown, a key feature of the derived solution is the decentralized form of both the UIO and the RLS algorithm, which scales with the number of robot joints. Indeed, the UIO consists of n copies of the estimator found for the scalar case, each of them using only information about the i-th joint position $q_{i,k}$ and its two first time-derivatives; analogously, the RLS algorithm is made of n copies of the scalar-case RLS using only transmission deflection data, $\phi_{i,a}$ and $\phi_{i,b}$.

7.2.1 Flexibility rotatum vector estimator

The following main result can be derived for the general case of a multi-DoF soft robot, which generalizes the one described in Sec. 7.1 for the scalar case:

Theorem 4 (Flexibility Rotatum Estimator)**.** *Given a soft robot described by Eq. 2.10 and a sampling time T_s, a delayed, discrete-time, input-state observer reconstructing the flexibility rotatum p_e, i.e. the time derivative of the flexibility torque τ_e, is described by the iterative system:*

$$\begin{aligned} \hat{X}_{k+1} &= E\,\hat{X}_k + F\,\mathbb{Y}_k\,, \\ \hat{U}_k &= G \begin{pmatrix} \hat{X}_{k+1} - A\,\hat{X}_k \\ q_k - C\,\hat{X}_k \end{pmatrix}, \end{aligned} \tag{7.7}$$

where k is a discrete step time, the state vector and the output history are

$$\hat{X}_k = \begin{pmatrix} \hat{q}_k \\ \hat{\dot{q}}_k \\ \hat{\ddot{q}}_k \end{pmatrix},\ \mathbb{Y}_k = \begin{pmatrix} q_k \\ q_{k-1} \\ q_{k-2} \end{pmatrix},$$

and the matrices are

$$E = \begin{pmatrix} \mathbb{I}_n & T\,\mathbb{I}_n & 0_n \\ 0_n & \mathbb{I}_n & T\,\mathbb{I}_n \\ -\dfrac{1}{T^2}\mathbb{I}_n & -\dfrac{3}{T}\mathbb{I}_n & -2\,\mathbb{I}_n \end{pmatrix},\ F = \begin{pmatrix} 0_{2n\times 3n} & 0_{2n\times n} \\ 0_{n\times 3n} & \dfrac{1}{T^2}\mathbb{I}_n \end{pmatrix},\ G = \begin{pmatrix} 0_{n\times 2n} & \dfrac{1}{T}\mathbb{I}_n & 0_n \end{pmatrix},$$

$$A = \begin{pmatrix} \mathbb{I}_n & T\,\mathbb{I}_n & 0_n \\ 0_n & \mathbb{I}_n & T\,\mathbb{I}_n \\ 0_n & 0_n & \mathbb{I}_n \end{pmatrix},\ B = \begin{pmatrix} 0 \\ 0 \\ T\mathbb{I}_n \end{pmatrix},\ C = \begin{pmatrix} \mathbb{I}_n & 0_{n\times 2n} \end{pmatrix}. \tag{7.8}$$

The estimated flexibility rotatum vector is obtained via the formula

$$\begin{aligned}\hat{p}_{e,k} = &-(B(\hat{q}_k)\,\hat{U}_k + \dot{B}(q_k,\hat{\dot{q}}_k)\,\hat{\ddot{q}}_k + \dot{C}(q_k,\hat{\dot{q}}_k)\,\hat{\dot{q}}_k + \\ &+ C(\hat{q}_k,\hat{\dot{q}}_k)\,\hat{\ddot{q}}_k + \dot{G}(q_k,\hat{\dot{q}}_k))\,.\end{aligned} \tag{7.9}$$

Proof. The expression for the instantaneous flexibility rotatum p_e can be obtained by differentiating with respect to time the link's dynamics, being described by the first relation in Eq. 2.10. This yields:

$$p_e = \dot{\tau}_e = -(B(q)\,q^{(3)} + \dot{B}(q)\,\ddot{q} + \dot{C}(q,\dot{q})\,\dot{q} + C(q,\dot{q})\,\ddot{q} + \dot{G}(q))\,.$$

By left-multiplying both members of the equation above by the inverse of $B(q)$ and collecting all nonlinear terms into an input vector U defined by the formula

$$U = B^{-1}(q)\left(p_e + \dot{B}(q)\,\ddot{q} + \dot{C}(q,\dot{q})\,\dot{q} + C(q,\dot{q})\,\ddot{q} + \dot{G}(q)\right)\,, \tag{7.10}$$

one obtains $q^{(3)} = U$. Defining the state vector choice as $X = (q^T, \dot{q}^T, \ddot{q}^T)^T$ leads to the linear the state form:

$$\dot{X} = A_c\,X + B_c\,U\,, \quad q = C\,X + D\,U\,,$$

where C is defined as in Eq. 7.8 and the other matrices are

$$A_c = \begin{pmatrix} 0_n & \mathbb{I}_n & 0_n \\ 0_n & 0_n & \mathbb{I}_n \\ 0_n & 0_n & 0_n \end{pmatrix}, \quad B_c = \begin{pmatrix} 0_n \\ 0_n \\ \mathbb{I}_n \end{pmatrix}, \quad D = 0_n\,.$$

In order to derive the sought rotatum estimator it is necessary to consider the corresponding discrete-time linear system, obtained via Euler's quantization rule, being given by:

$$X_{k+1} = A\,X_k + B\,U_k\,, \quad q_k = C\,X_k + D\,U_k\,, \tag{7.11}$$

where A and B are as in Eq. 7.8. Matrices A, B, C, and D satisfy the invertibility condition of Prop. 7 for $L = 3$, thus ensuring the existence of a UIO of the sought form using only three consecutive samples of the link position q_k. The procedure to derive the rotatum estimator consists of obtaining a dynamic equation for the state estimation error

$$e_k = \hat{X}_k - X_k$$

that is decoupled from the an unknown input u_k and then inverting the relation between the estimated state $\hat{X}_k$ and and the k-th sample u_k of the input u. These steps require the satisfaction of the conditions of Prop. 9, which can be carried out by following the reasoning described in its proof. It is noteworthy at this point that $\hat{F}_1$ is a null matrix, thus ensuring the stability of matrix E.

Once the UIO has reconstructed the unknown input $\hat{U}_k$, along with link velocity $\hat{\dot{q}}_k$ and acceleration $\hat{\ddot{q}}_k$ vectors, an estimate $\hat{p}_e$ of the flexibility rotatum p_e can be obtained by inverting Eq. 7.10. This leads to Eq. 7.9 and concludes the proof. □

Corollary 1. *The decentralized nature of the estimator allows expressing the i-th component $\hat{\dot{\tau}}_{e,i}$ of the total flexibility rotatum $\hat{\dot{\tau}}_e$ as a function of only i-th joint flexible transmissions $\phi_{i,a} = q_i - q_{i,a}$ and $\phi_{i,b} = q_i - q_{i,b}$ and their corresponding time derivatives.*

7.2.2 Estimation of stiffness

According to Corollary 1, stiffness in each joint can be estimated in a decoupled way. More precisely, by considering the following κ-th order approximation of the flexibility rotatum:

$$\hat{\dddot{\tau}}_{e,i} \approx \left(\sum_{j=0}^{\kappa} \pi_{i,a,j}\, \phi_{i,a}^{j}\right) \dddot{\phi}_{i,a} + \left(\sum_{j=0}^{\kappa} \pi_{i,b,j}\, \phi_{i,b}^{j}\right) \dddot{\phi}_{i,b}\,,$$

and, by using Eq. 2.8, one obtains

$$\sigma_i \approx \sum_{j=0}^{\kappa} \pi_{i,a,j}\, \phi_{i,a}^{j} + \sum_{j=0}^{\kappa} \pi_{i,b,j}\, \phi_{i,b}^{j}\,. \tag{7.12}$$

Similarly to the previous section, the RLS algorithm is used to find the coefficients of the flexibility rotatum approximation $\hat{\dddot{\tau}}_{e,i} = \Phi_i \Pi_i$ where

$$\begin{aligned}\Phi_i &= \left(\dddot{\phi}_{i,a}\phi_{i,a},\, \cdots,\, \dddot{\phi}_{i,a}\phi_{i,a}^{\kappa},\, \dddot{\phi}_{i,b}\,\phi_{i,b},\, \cdots,\, \dddot{\phi}_{i,b}\phi_{i,b}^{\kappa}\right)^T,\\ \Pi_i &= (\Pi_{i,a}^T, \Pi_{i,b}^T)^T = ((\pi_{i,a,0}, \cdots, \pi_{i,a,\kappa})^T, (\pi_{i,b,0}, \cdots, \pi_{i,b,\kappa})^T)^T\end{aligned}$$

Finally, the i-th joint stiffness estimate can be calculated as

$$\hat{\sigma}_i[k] = \left(\phi_{i,a}, \phi_{i,a}^2, \cdots, \phi_{i,a}^{\kappa}, \phi_{i,b}, \phi_{i,b}^2, \cdots, \phi_{i,b}^{\kappa}\right) \hat{\Pi}_i[k]\,. \tag{7.13}$$

Remark 5. *Note that the UIO uses only information about the robot's link positions and leans on the knowledge of the model including inertia matrix, Coriolis, centrifugal, viscous damping terms, and gravity vector, but no force/torque sensor is required. The RLS algorithm uses motors' positions and speeds to estimate stiffness.*

The block diagram of the proposed stiffness estimator is presented in Fig. 7.1.

7.3 Simulation results

This section evaluates the effectiveness of the presented estimation approach in simulation on a single- and two-DoF soft robot.

For this purpose, first the dynamical model of a 1-DoF robot with a soft joint actuated by a QB-move VSA device has been considered. The nominal values of the flexibility torque's and stiffness' are computed according to their models, which are available from the manufacturer qbmove Centro Piaggio (2011). More precisely, they are given by

$$\begin{aligned}\tau_e &= k_1 \sinh(a_1(q - q_a)) + k_2 \sinh(a_2(q - q_b))\,,\\ \sigma &= a_1 k_1 \cosh(a_1(q - q_a)) + a_2 k_2 \cosh(a_2(q - q_b))\,,\end{aligned} \tag{7.14}$$

where k_1, k_2, a_1, and a_2 are suitable constants. A fourth-order Taylor expansion of $\dddot{\tau}_e$ is chosen, namely

$$\dddot{\tau}_e \approx (\pi_{a,0} + \pi_{a,2}\,\phi_a^2 + \pi_{a,4}\,\phi_a^4)\,\dddot{\phi}_a + (\pi_{b,0} + \pi_{b,2}\,\phi_b^2 + \pi_{b,4}\,\phi_b^4)\,\dddot{\phi}_b\,,$$

which only includes even-order coefficients as time-derivatives of the functions in Eq. 7.14 with respect to the transmission deflections. Therefore, the parameter vectors to be identified online are

$$\Pi_a = (\pi_{a,0}, \pi_{a,2}, \pi_{a,4})^T \quad \Pi_b = (\pi_{b,0}, \pi_{b,2}, \pi_{b,4})^T\,.$$

By identifying such vector, it is subsequently possible to obtain the following approximation of the joint's stiffness

$$\sigma \approx \pi_{a,0} + \pi_{a,2}\,\phi_a^2 + \pi_{a,4}\,\phi_a^4 + \pi_{b,0} + \pi_{b,2}\,\phi_b^2 + \pi_{b,4}\,\phi_b^4\,.$$

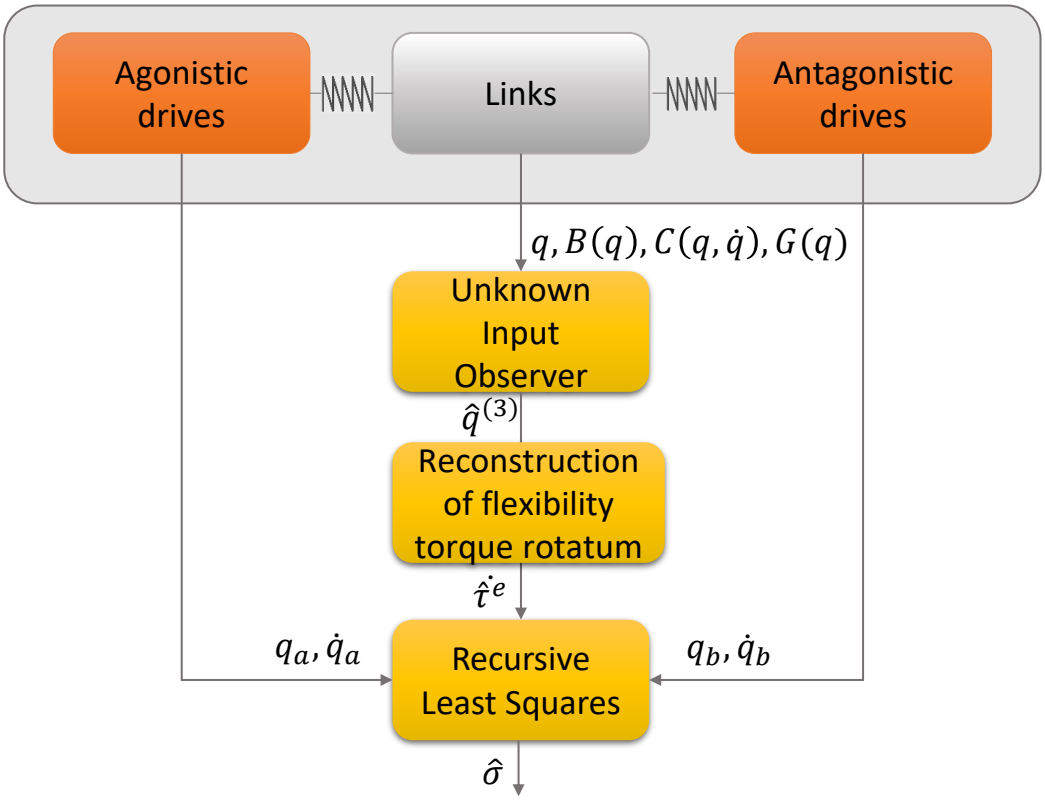

Figure 7.1: Block scheme of the algorithm for non-invasive estimation of stiffness in flexible robot joints, actuated by pneumatic antagonistic VSA.

A first simulation has been done by using the numerical values $m = 0.4\,\text{kg}, l = 0.3\,\text{m}, I = 0.015\,\text{kgm}^2, \beta = 10^{-7}\text{Nms/rad}, a_1 = 6.7328\,\text{rad}^{-1}, a_2 = 6.9602\,\text{rad}^{-1}, k_1 = 0.0227\,\text{Nm}, k_2 = 0.0216\,\text{Nm}$. Results of such simulation run are reported in Fig. 7.2 that shows that $\dot{\tau}_e$ and the sought stiffness σ are well estimated. The only initially appearing estimation error in the stiffness reconstruction occurs due to the worst-case hypothesis of complete lack of knowledge of two parameter vectors, Π_a and Π_b, which are chosen to be initially null, i.e. $\hat{\Pi}_a[0] = \hat{\Pi}_b[0] = 0$. After the initial transient, the time-derivative of the flexibility torque and the joint's stiffness are successfully tracked over time.

A simulation verification of results extendes to the two-DoF robotic setup which includes joints actuated by two QB-move VSAs. The robot's dynamics is of the form in Eq. 2.10, where the inertia matrix is

$$B(q) = \begin{pmatrix} b_{11}(q) & b_{12}(q) \\ b_{12}(q) & b_{22} \end{pmatrix},$$

with $b_{11}(q) = I_1 + m_1\frac{l_1^2}{4} + I_2 + m_2 l_1^2 + m_2\frac{l_2^2}{4} + m_2 l_1 l_2 c_2$, $b_{12}(q) = I_2 + m_2\frac{l_2^2}{4} + \frac{1}{2}m_2 l_1 l_2 c_2$, $b_{22} = \frac{1}{2}m_2 l_2^2 + I_2$, the matrix containing of Coriolis and centrifugal forces is

$$C(q,\dot{q}) = \frac{1}{2}\begin{pmatrix} -m_2 l_1 s_2 \dot{q}_2 & -m_2 l_1 s_2 (\dot{q}_1 + \dot{q}_2) \\ m_2 l_1 s_2 \dot{q}_1 & 0 \end{pmatrix},$$

and the gravity vector

$$G(q) = \frac{1}{2}\begin{pmatrix} (m_1 + m_2) l_1 g s_1 + m_2 l_2 g s_{12} \\ m_2 l_2 g s_{12} \end{pmatrix},$$

where s_i, c_i, and $s_{i,j}$ denote $\sin(q_i)$, $\cos(q_i)$, and $\sin(q_i + q_j)$, respectively. Numerical values

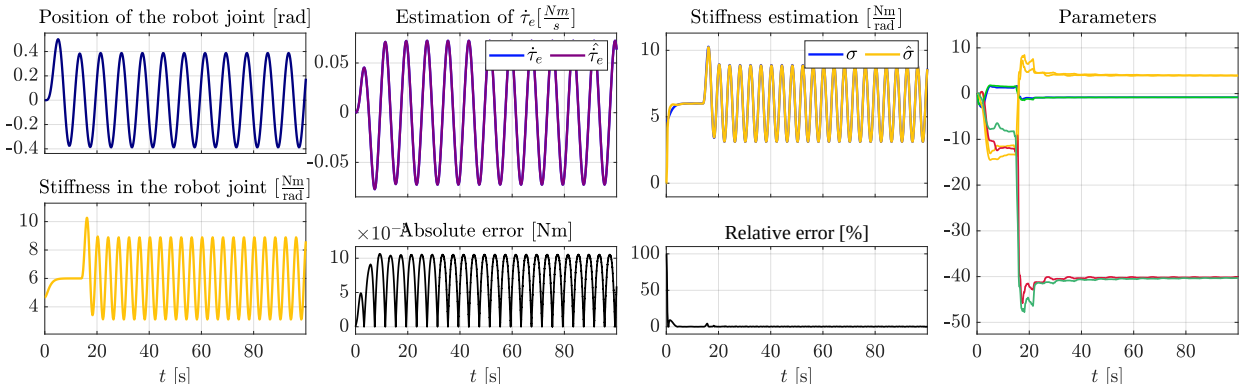

Figure 7.2: Simulation #1 (Single-DoF setup) - Reconstruction of the time-derivative of the flexibility torque $\hat{\dot{\tau}}_{e,k}$ by the UIO (above), and corresponding estimated stiffness $\hat{\sigma}_k$ obtained via the RLS algorithm (below), for a single joint soft-robot.

Table 7.1: Nominal values of geometric and inertial parameters of the two-link soft robot.

Param.	Value	Unit	Description
m_1	0.26	kg	First link mass
m_2	0.26	kg	Second link mass
l_1	0.09	m	First link length
l_2	0.09	m	Second link length
I_1	0.0021	kgm^2	First link inertia
I_2	0.0021	kgm^2	Second link inertia
g	9.81	$\mathrm{m/s}^2$	Gravity constant

of the robot's inertial and geometric parameters are listed in Table 7.1. As described in the theory, the first step is to obtain the corresponding state-space as in Eq. 7.11, which can be done by defining the state vector $x = (q_1, q_2, \dot{q}_1, \dot{q}_2, \ddot{q}_1, \ddot{q}_2)^T$ and the input vector

$$u = \begin{pmatrix} q_1^{(3)} \\ q_2^{(3)} \end{pmatrix} = B^{-1}(q)\left(\dot{\tau}_e - \dot{B}(q)\ddot{q} - \dot{C}(q,\dot{q})\dot{q} - C(q,\dot{q})\ddot{q} - \dot{G}(q)\right) \ .$$

The corresponding matrices are:

$$A_c = \begin{pmatrix} 0_{4\times 2} & \mathbb{I}_4 \\ 0_{2\times 2} & 0_{2\times 4} \end{pmatrix} , \ B_c = \begin{pmatrix} 0_{4\times 2} \\ \mathbb{I}_2 \end{pmatrix} ,$$

$$C = \begin{pmatrix} \mathbb{I}_2 & 0_{2\times 4} \end{pmatrix} , \quad D = \ 0_{2\times 1} \ .$$

According to Th. 4, the input-state observer is obtained with a delay $L = 3$ and consists of the

matrices

$$E = \begin{pmatrix} 1 & 0 & T_s & 0 & 0 & 0 \\ 0 & 1 & 0 & T_s & 0 & 0 \\ 0 & 0 & 1 & 0 & T_s & 0 \\ 0 & 0 & 0 & 1 & 0 & T_s \\ -\frac{1}{T_s^2} & 0 & -3/T_s & 0 & -2 & 0 \\ 0 & -\frac{1}{T_s^2} & 0 & -3/T_s & 0 & -2 \end{pmatrix},$$

$$F = \begin{pmatrix} \hat{F}_1 & B \end{pmatrix} \begin{pmatrix} \mathbb{I}_8 \\ 0_{2\times 6} \quad \frac{1}{T_s^3}\mathbb{I}_2 \end{pmatrix},$$

$$G = \begin{pmatrix} 0_{2\times 4} & \frac{1}{T_s}\mathbb{I}_2 & 0_{2\times 2} \end{pmatrix},$$

where $\hat{F}_1$ is a matrix to be suitably chosen in order to place E's eigenvalues at the desired positions.

Furthermore, the i-th entries of the total flexibility torque vector τ_e and joint stiffness vector σ are provided by the manufacturer qbmove Centro Piaggio (2011) via the following identified formulas:

$$\begin{aligned} \tau_{e,i} &= k_1 \sinh(a_1(q_i - q_{i,a})) + k_2 \sinh(a_2(q_i - q_{i,b})), \\ \sigma_i &= a_1 k_1 \cosh(a_1(q_i - q_{i,a})) + a_2 k_2 \cosh(a_2(q_i - q_{i,b})). \end{aligned}$$

Expanding the time differentiated quantity $\dot{\tau}_{e,i}$ as a Taylor series and approximating it to the fifth-order yields

$$\begin{aligned} \dot{\tau}_{e,i} \approx (\pi^a_{i,0} + \pi^a_{i,1}\,\phi_{i,a} + \pi^a_{i,2}\,\phi^2_{i,a} + \pi^a_{i,3}\,\phi_{i,a} + \pi^a_{i,4}\,\phi^4_{i,a})\,\dot{\phi}_{i,a} + \\ +(\pi^b_{i,0} + \pi^b_{i,1}\,\phi_{i,b} + \pi^b_{i,2}\,\phi^2_{i,b} + \pi^b_{i,3}\,\phi_{i,b} + \pi^b_{i,4}\,\phi^4_{i,b})\,\dot{\phi}_{i,b}, \end{aligned}$$

and correspondingly the i-th joint's stiffness can be approximated as

$$\begin{aligned} \sigma_i \approx \pi^a_{i,0} + \pi^a_{i,1}\,\phi_{i,a,1} + \pi^a_{i,2}\,\phi^2_{i,a} + \pi^a_{i,3}\,\phi_{i,a,3} + \pi^a_{i,4}\,\phi^4_{i,a} + \\ \pi^b_{i,0} + \pi^b_{i,1}\,\phi_{i,b,1} + \pi^b_{i,2}\,\phi^2_{i,b} + \pi^b_{i,3}\,\phi_{i,b,3} + \pi^b_{i,4}\,\phi^4_{i,b}. \end{aligned}$$

Two unknown parameter vectors are present for each joint, which are given by

$$\Pi_1 = (\Pi^T_{1,a}, \Pi^T_{1,b})^T, \quad \Pi_2 = (\Pi^T_{2,a}, \Pi^T_{2,b})^T,$$

with

$$\begin{aligned} \Pi_{1,a} &= (\pi^a_{1,0}, \pi^a_{1,1}, \pi^a_{1,2}, \pi^a_{1,3}, \pi^a_{1,4})^T, \\ \Pi_{1,b} &= (\pi^b_{1,0}, \pi^b_{1,1}, \pi^b_{1,2}, \pi^b_{1,3}, \pi^b_{1,4})^T, \\ \Pi_{2,a} &= (\pi^a_{2,0}, \pi^a_{2,1}, \pi^a_{2,2}, \pi^a_{2,3}, \pi^a_{2,4})^T, \\ \Pi_{2,b} &= (\pi^b_{2,0}, \pi^b_{2,1}, \pi^b_{2,2}, \pi^b_{2,3}, \pi^b_{2,4})^T. \end{aligned}$$

As in the case of a single degree-of-freedom setup, parameters $\Pi_{i,a}$ and $\Pi_{i,b}$ are assumed to be completely unknown initially, i.e. $\hat{\Pi}_{i,a}[0] = 0$ and $\hat{\Pi}_{i,b}[0] = 0$, for $i = 1, 2$. Fig. 7.3 reported the simulation results showing that the proposed UIO-RLS-based solution successfully reconstructs both components of the flexibility torque and the joint stiffness.

7.4 Experimental results

The proposed stiffness estimator is first validated on an one-DoF soft robotic setup with the electric variabel stiffness actuation (Fig. 7.4a) and then on a two-DoF setup (Fig. 7.4b). Regarding the former setup, a passive *Qbmove Maker Pro* actuator, subject to the gravity, is attached to the active one constituting the link with the moment of inertia $I = 0.0021$ kgm^2, mass $m = 0.26$ kg, and length $l = 0.09$ m. On the other hand, a two-DoF setup, built by

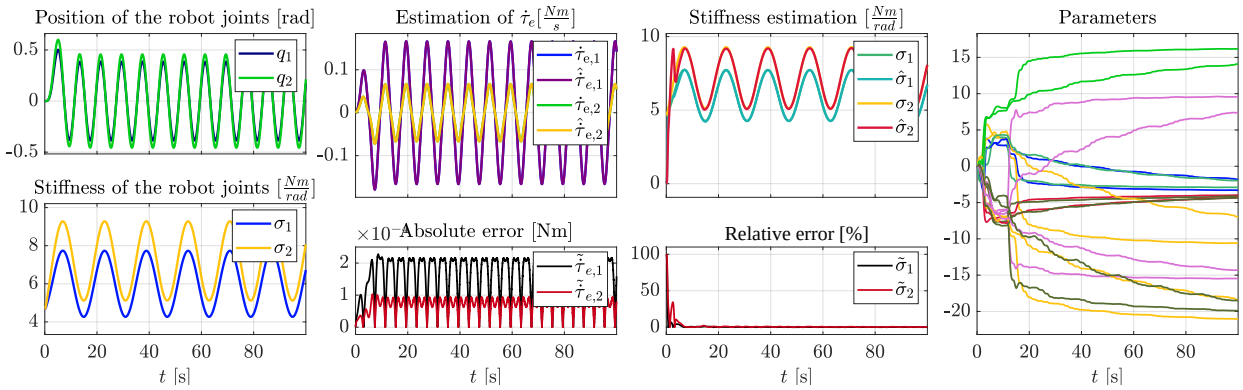

Figure 7.3: Simulation #2 (2-DoF setup) - Reconstruction of the time-derivative of the flexibility torque $\hat{\dot{\tau}}_{e,k}$ by the UIO (above), and corresponding estimated stiffness $\hat{\sigma}_k$ obtained via the RLS algorithm (below), for a single joint soft-robot.

adding another actuator, possess the equivalent inertia, mass and length parameters for both links with the same before-stated values. Again, a sampling rate $T = 5 \cdot 10^{-3}$ s has been used.

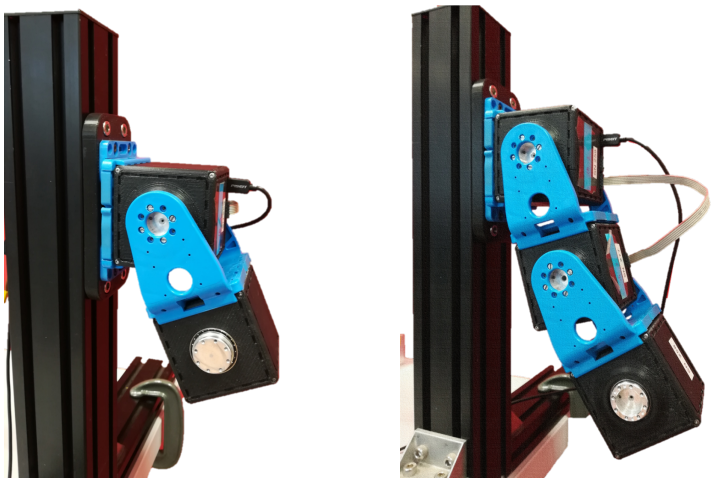

(a) (b)

Figure 7.4: The robotic setup with one (a) and two (b) degrees of freedom.

The experiment on a one-Dof setup is designed with a two-fold objective. First, both the position and stiffness change simultaneously during first 400 seconds, following the sinusoidal trajectories $q_d = 0.4{+}0.2\sin\frac{\pi}{4}t$ rad and $\sigma_d = 2{+}\sin\frac{\pi}{6}t$ Nm/rad. It is well-known that estimation of stiffness becomes challenging when the co-contraction is active, meaning that position is still while stiffness changes. In that regard, the second phase ($t \in (400, 800]$ s) consists of the constant position and varying stiffness desired evolution such that $\sigma_d = 2 + \sin\frac{\pi}{6}t$ Nm/rad.

The initial parameters of the RLS algorithm are assumed to be unknown $\hat{\Pi}[0] = 0_{8\times 1}$ while the covariance matrix at the first instance is set to $P[0] = \mathrm{diag}(1, 10^3, 10^5, 10^5, 1, 10^3, 10^5, 10^5)$. Assuming that the derivative of flexibility torque and stiffness are even functions, the regressor is constructed of the even powers of transmission deflections as follows

$$\Phi = \left(\dot{\phi}_a, \dot{\phi}_a\phi_a^2, \dot{\phi}_a\phi_a^4, \dot{\phi}_a\phi_a^6, \dot{\phi}_b, \dot{\phi}_b\phi_b^2, \dot{\phi}_b\phi_b^4, \dot{\phi}_b\phi_b^6\right) .$$

Figure 7.5 shows that after initial transient period, necessary for the RLS algorithm to update parameters, the estimation error goes below the calculated threshold. Moreover, it can also be observed that the estimated parameters of the RLS algorithm remain bounded. After

the parameters converge to the constant value, their update is stopped, thus ensuring that drift of estimated stiffness does not occur. It is worth remarking that the estimation is effective even with the switched off update of parameters, as can be observed from the fact that the relative error remains below threshold. The value of stiffness MSE and MSREP on the interval $t \in []200, 800]$ s are $3.8 \cdot 10^{-5}$ Nm/rad and 0.0012 %, respectively.

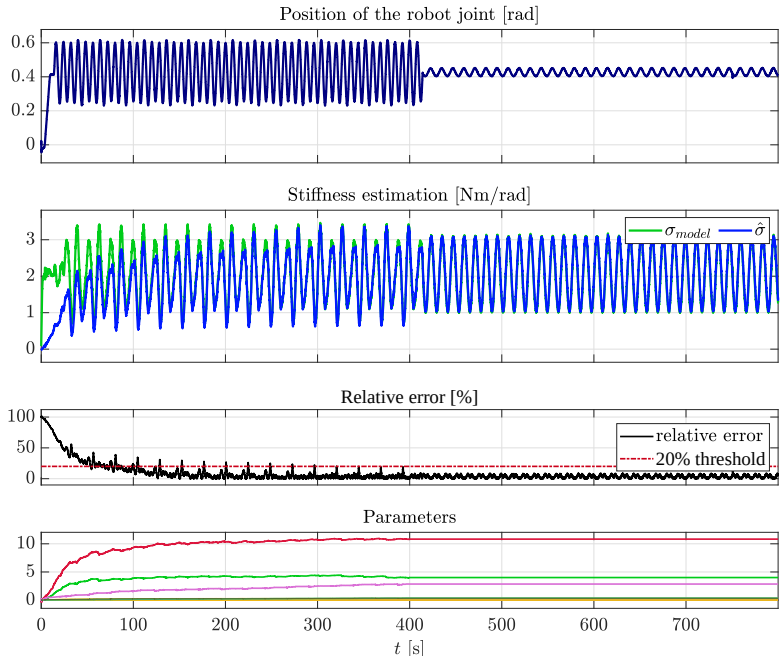

Figure 7.5: Experiment #1 (1-DoF setup) - The top figure shows the position of the first link, in the second row are depicted model and estimated value of stiffness, third row shows the obtained estimation error, and below are the estimated parameters of the RLS algorithm.

The experiment is then extended to estimate stiffness of the two-DoF soft robotic setup in a non-invasive way, which presents a greater challenge due to the existence of coupled terms. Again, position and stiffness are commanded to follow the sinusoidal trajectories, while the RLS algorithm is initialized with parameters equal to zero $\Pi[0] = 0_{8\times1}$ and covariance matrices that have the following values: $P_1 = \text{diag}(1, 10^2, 10^4, 10^5, 1, 10^2, 10^4, 10^5)$ and $P_2 = \text{diag}(1, 10, 10^5, 10^7, 1, 10, 10^5, 10^7)$.

Figures 7.6 and 7.7 show the estimation performance for both joints. It can be observed that the relative error is below the threshold after the initial period and that parameters remain bounded. Values of stiffness MSE and MSREP for the first joint are $1.9 \cdot 10^{-4}$ Nm/rad and $6.3 \cdot 10^{-4}$ %, respectively, while the second joint has $MSE = 3.8 \cdot 10^{-4}$ Nm/rad and $MSREP = 0.002$ %.

7.5 Conclusion

This chapter introduced a novel approach to estimate stiffness in flexible joint robot in a non-invasive way. Leveraging only on the information of link and drives positions, stiffness is effectively estimated without any apriori knowledge of its model. Validation is performed within both simulation environment and experimental setups, showing the accuracy of estimator even when the position is still and when multi-DoF setup is used. The future work will consider the robustification of the estimator with respect to the robot dynamic parameters.

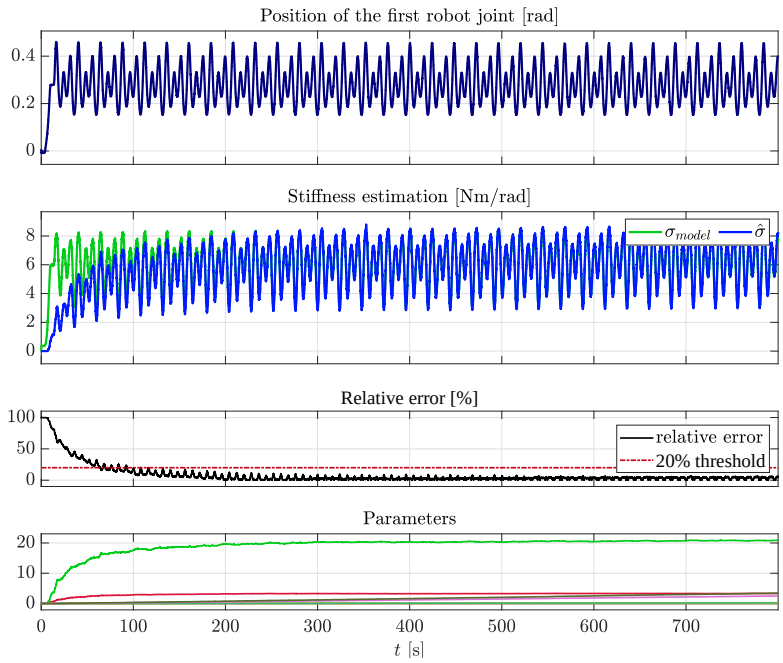

Figure 7.6: Experiment #2 (2-DoF setup - First joint) - The top figure shows the position of the second link, in the second row are depicted model and estimated value of stiffness, third row shows the obtained estimation error, and below are the estimated parameters of the RLS algorithm.

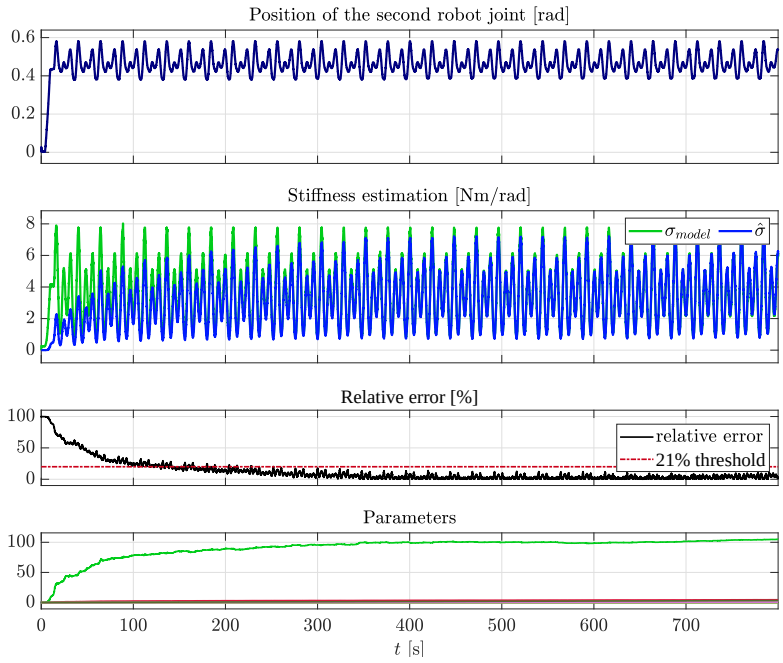

Figure 7.7: Experiment #2 (2-DoF setup, Second joint) - The top figure shows the position of qbmove actuator, in the second row are depicted model and estimated value of stiffness, third row shows the obtained estimation error, and below are the estimated parameters of the RLS algorithm.

Part III

Nonlinear Adaptive Control of Soft Robots

All stable processes we shall predict. All unstable processes we shall control.

John von Neumann

Chapter 8

Introduction

Several approaches have been proposed for joint stiffness and position control such as static and dynamic feedback linearization approach (De Luca and Lucibello (1998); Palli et al. (2008); Potkonjak et al. (2011)), backstepping control law (Petit et al. (2015)), and energy-shaping controllers Albu-Schäffer and Petit (2012). All the above-mentioned approaches assume that the dynamic model is precisely known, which complicates their practical implementations. Moreover, current results exposed by Della Santina et al. (2017) and Angelini et al. (2018) indicate the importance of compliance preserving and show, by means of learning algorithms, that this can be achieved by reducing the effect of the feedback action and, on the contrary, reinforcing the feedforward term. This has motivated the application of robust control based on adaptive technique, which can successfully cope with the model parametric uncertainties.

When it comes to soft articulated robots, their compliance is usually set in open loop, which means that the elastic characteristic of a soft robot has to be obtained in advance, either by using analytical calculation from the datasheet of the VSA as in the work of Angelini et al. (2018), or performing model identification as carried out in (Lukić et al. (2016); Lukic et al. (2019)). On the contrary, closed loop stiffness control has several benefits, as it provides position and stiffness feedback and information about the dynamical relation between actuation system and joints. Stiffness feedback approaches enable the soft robot manipulator to be reactive to external disturbances (Hogan (1985)), e.g. in the case when there is a contact between the environment and the robot. They are advantageous when the goal is to store energy (Garabini et al. (2011); Keppler et al. (2016)) or to perform task that requires delicate contact with the environment (Albu-Schaffer and Hirzinger (2002); Ott et al. (2008)). Furthermore, if decoupling position and stiffness control is obtained, soft articulated robots are able to achieve high position accuracy, while in the meantime realize a range of possible joint stiffness.

In this regard, Chapter 10 presents the decoupled adaptive control of position and stiffness for pneumatic soft robots, while Chapter 11 shows the method for achieving the similar results with electro-mechanically driven robots. In the end, Chapter 12 implements adaptive control of highly-deformable soft-bodied robots position.

Chapter 9

Background

Given a robot with dynamical model of the form as in Eq. 2.1, it is known by Proposition 3 that the left-hand side expression of such a model can be conveniently factorized as the product of a *regressor* matrix $Y \in \mathbb{R}^{n \times \kappa}$ and a κ-dimensional vector $\pi \in \mathbb{R}^{\kappa}$ of uncertain parameters, i.e.

$$B(q)\,\ddot{q} + C(q,\dot{q})\,\dot{q} + G(q) = Y(q,\dot{q},\ddot{q})\,\pi\,. \tag{9.1}$$

It is important to note that the property also allows determining other regressor forms, as done below, by linearly combining the matrices $B(q)$ and $C(q,\dot{q})$ and the vector $G(q)$ of the system's dynamics. By using this property, the following result can be proved (cf. the technique by Slotine and Li (1991)):

Proposition 10. *Given any desired joint trajectory $q_d : [0,\infty) \to \mathbb{R}^n$, with $q_d(t) \in \mathcal{C}^2$, a nonlinear adaptive controller ensuring asymptotic tracking of the joint evolution $q(t)$, for all initial parameter estimate $\hat{\pi}_0$, is described by the following dynamic system:*

$$\begin{aligned} \dot{\hat{\pi}} &= K_\pi\, Y^T(q,\dot{q},q_r,\dot{q}_r,\ddot{q}_r)\, s\,, \\ \tau &= Y(q,\dot{q},q_r,\dot{q}_r,\ddot{q}_r)\,\hat{\pi} + K_d\, s\,, \end{aligned} \tag{9.2}$$

where $\hat{\pi}$ and τ are the parameter estimate vector and the joint torque control, respectively, $\dot{q}_r = \dot{q}_d + \Lambda\,\tilde{q}$, $s = \dot{\tilde{q}} + \Lambda\,\tilde{q}$, $\tilde{q} = q_d - q$, K_d and Λ are two positive definite matrices determining the tracking error convergence speed, and K_π is a positive definite matrix specifying the parameter adaptation rate.

Moreover, when the input control torque τ is applied to the robot through a flexible actuation system as in Eq. 2.2, whose model also includes separable uncertain parameters, the above result can be modified as suggested in the work by Tonietti and Bicchi (2002):

Proposition 11. *Given a flexible joint robotic system with pneumatic actuation model as in Eq. 2.2, with K a positive diagonal matrix, the nonlinear adaptive controller in Eq. 9.2 can be generalized as*

$$\begin{aligned} \dot{\hat{\Pi}} &= K_\pi\, Y_*^T(q,\dot{q},\dot{q}_r,\ddot{q}_r)\,\sigma\,, \\ p &= \Phi(q)^\dagger \left(Y_*(q,\dot{q},\dot{q}_r,\ddot{q}_r)\,\hat{\Pi} + K_d\,\sigma \right)\,, \end{aligned}$$

where $\hat{\Pi} \in \mathbb{R}^{\kappa_*}$ is a modified parameter vector also including the actuator uncertainties, and $\Phi(q)^\dagger \in \mathbb{R}^{2n \times n}$ is the pseudo-inverse of the known part of the actuator model.

Proof. Given the regressor form in Eq. 9.1 and the actuator model in Eq. 2.2, it holds

$$K\,\Phi(q)\,p = Y(q,\dot{q},\dot{q}_r,\ddot{q}_r)\,\pi\,.$$

Premultiplication by K^{-1} yields

$$\Phi(q)\, p = K^{-1} Y(q, \dot{q}, \dot{q}_r, \ddot{q}_r)\, \pi = Y_*(q, \dot{q}, \dot{q}_r, \ddot{q}_r)\, \Pi\,,$$

where Y_* is a suitable matrix allowing the factorization on the right of all unknown quantities into the modified parameter vector Π. The remainder of the proof straightforwardly follows. $\square$

Note that although $K = K_g R$ is immersed into the parameter vector Π, the joint pulley radius R must still be known, as it is part of the nonlinear expression of the actuator matrix.

Chapter 10

Soft articulated robots with pneumatic drives

This section lays on the foundation of the works by Tonietti and Bicchi (2002); Bicchi and Tonietti (2002), Spong (1989), and Della Santina et al. (2017); Keppler et al. (2018). Compared to the work by Tonietti and Bicchi (2002), a first extension stems in the fact that the robot's stiffness is controlled in closed-loop, which benefits to the overall system safety.

The second appealing feature of the proposed method is the use of the control degrees of freedom, associated with the null-space of the actuator matrix, to decouple the tracking of position commands from stiffness ones. The actuator matrix maps here the relation between muscle pressures and joint elastic torque. While the idea of using the null-space projections is not new in robotics — it has been applied to the Jacobian matrix of a redundant manipulator to achieve force (Khatib (1987)) and torque (Dietrich et al. (2015)) control — the presented approach enables the above-mentioned decoupling, without the necessity of higher order derivatives (cf. Palli et al. (2008); Keppler et al. (2018)), even when the system model is not perfectly known.

The third contribution of this work is the experimental validation of the method on a real two-DoF soft robot arm with rigid links and flexible rotary joints, driven by pneumatically powered VSAs in an antagonistic setup. In the setup, artificial McKibben muscles are used as a flexible part of the pneumatic actuator system (Chou and Hannaford (1996); Gavrilović and Marić (1969)), behaving as springs with nonlinear characteristics due to the air compressibility.

10.1 Design of the control law

A novel nonlinear adaptive decoupled stiffness and position control is presented in this section. First, Proposition 10 briefly introduces the nonlinear adaptive control framework (Slotine and Li (1991)) underlying the proposed one. Afterwards, Proposition 11 provides the opportunity to assume uncertainty of both model and actuator parameters. This leads to the main result of the paper presented in Theorem 5, where decoupling of position and stiffness control is achieved by an additional control degree-of-freedom, that exploits the actuator matrix's null-space. Finally, the stability of the proposed approach is analyzed and proved.

When both desired stiffness and position signals have to be simultaneously tracked, a full model that also includes stiffness dynamics is more appropriate. Under the hypothesis that all system parameters are exactly known, this objective can be effectively achieved for flexible robots with electrically driven actuators, by using a dynamic feedback linearization approach of De Luca and Lucibello (1998). As it is known, the solution therein proposed obtains exact stiffness and position decoupling by exploiting information contained in higher-order derivatives of such variables.

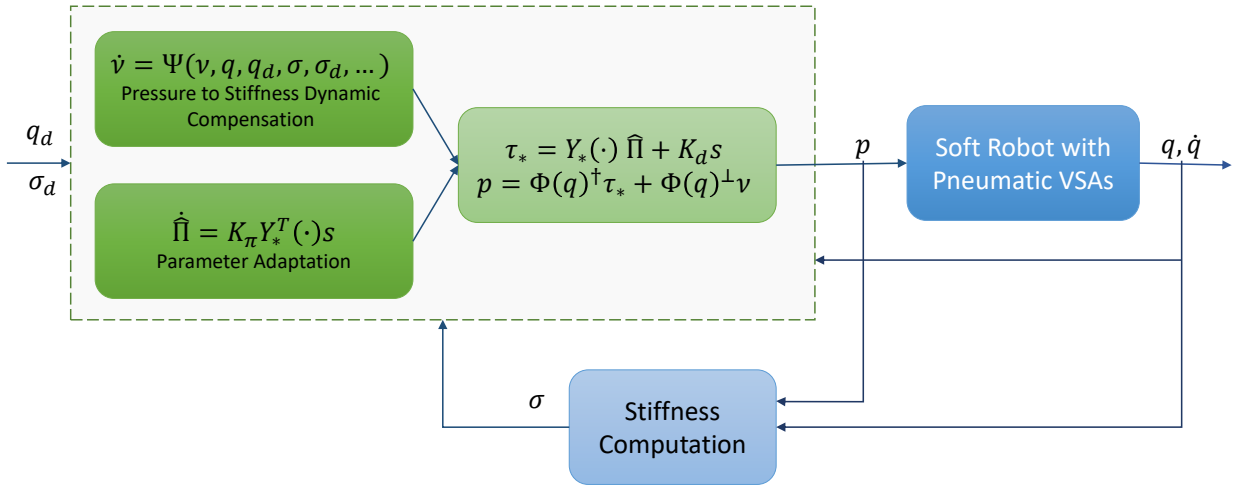

Figure 10.1: Depiction of the proposed decoupled nonlinear adaptive and decoupling control approach.

On the contrary, when some system parameters are uncertain or even completely unknown, accurate and decoupled control can be achieved by endowing the controlled system with adaptivity capacity in different ways. One possible solution to achieve this is described in the following theorem, which leverages on the control degree of freedom obtained by projection to the actuator matrix's null-space. A depiction of the proposed nonlinear adaptive control is in Fig. 10.1.

Theorem 5. *Given a soft robot with dynamics as in Eq. 2.5, if matrix $K^{-1}B(q)$ is positive definite for all q, an adaptive and decoupling controller generating a pressure command signal $p(t)$, which allows simultaneous asymptotic tracking of any desired position and stiffness reference signals, $q_d : [0, \infty) \to \mathbb{R}^n$, with $q_d(t) \in \mathcal{C}^2$ and $\sigma_d : [0, \infty) \to \mathbb{R}^n$, with $\sigma_d(t) \in \mathcal{C}^1$, is described by the following system with dynamics given by*

$$\begin{aligned} \dot{\nu} \;=\; & \left(\Phi_q(q)\Phi(q)^\perp\right)^\dagger \Big(K_\sigma(\sigma - \sigma_d) - K^{-1}\dot{\sigma}_d \\ & - \Phi_q(q)\tfrac{d}{dt}\left(\Phi(q)^\dagger \tau_*\right) - \Phi_q(q)\Phi(q)^\dagger \tau_* \\ & - \left(\Phi_q(q)\Phi(q)^\perp + \dot{\Phi}(q)^\perp\right)\nu \Big), \end{aligned} \tag{10.1}$$

$$\dot{\hat{\Pi}} = K_\pi\, Y_*^T(q, \dot{q}, q_r, \dot{q}_r, \ddot{q}_r)\, s\,, \tag{10.2}$$

and output signal given by

$$p = \Phi(q)^\dagger \tau_* + \Phi(q)^\perp \nu\,, \tag{10.3}$$

with

$$\tau_* = Y_*(q, \dot{q}, \dot{q}_r, \ddot{q}_r)\,\hat{\Pi} + K_d\, s\,, \tag{10.4}$$

where $\nu \in \mathbb{R}^n$ is an internal controller state, $\hat{\Pi} \in \mathbb{R}^\kappa$ is the estimated parameter vector, $\tau_* \in \mathbb{R}^n$ is a control signal directly affecting the applied torque, K_d, K_σ, and K_π are positive definite matrices determining the convergence speed of the position tracking error, the stiffness tracking error, and the parameter estimation error, respectively, Y_* is a regressor matrix for the robot's position dynamics, $\Phi(q)^\dagger$ is the pseudo-inverse of $\Phi(q)$, $\Phi(q)^\perp$ is a matrix in the null column-space of $\Phi(q)$, and $\Phi_q(q) = \frac{\partial \Phi}{\partial q}(q)$.

Note: *The theorem describes the state form of a dynamic controller whose internal variables, ν and $\hat{\Pi}$, are updated according to Eq. 10.1 and 10.2, and whose output p, can be algebraically computed by means of Eq. 10.3 and Eq. 10.4.*

Proof. The proof of the theorem is two stage. First, it can be proved that the full dynamic model of the robot can be rewritten in suitable regressor form, and thus that adaptive control laws for stiffness and position regulation can be found; then, it can be shown that such control laws can be converted to feasible pressure commands.

To begin with, from the property of Eq. 9.1, consider rewriting in regressor form the following expression, obtained from the first equation of the robot's dynamics:

$$\begin{aligned} & K^{-1}\left(B(q)\,\dot{s} + \tfrac{1}{2}\dot{B}(q)\,s\right) = \\ & = K^{-1}\left(B(q)\,(\ddot{q}_r - \ddot{q}) + \tfrac{1}{2}\dot{B}(q)\,s\right) = \\ & = K^{-1}\left(B(q)\ddot{q}_r + C(\cdot)\,\dot{q} + G(q) + \tfrac{1}{2}\dot{B}(q)s\right) - \Phi(q)\,p = \\ & = Y_*(q,\dot{q},\dot{q}_r,\ddot{q}_r)\,\Pi - \Phi(q)\,p\,, \end{aligned}$$

where Y_* is a suitable regressor matrix and Π is the corresponding parameter vector. Left-multiplying the second equation of the robot's dynamic model by K^{-1} yields

$$K^{-1}\dot{\sigma} = -\dot{\Phi}_q(q)\,p - \Phi_q(q)\,\dot{p}\,.$$

Furthermore, having defined a new control torque vector τ_* and a *stiffness control* vector u_σ as

$$\begin{array}{rcl} \tau_* & = & \Phi(q)\,p\,, \\ u_\sigma & = & -\dot{\Phi}_q(q)\,p - \Phi_q(q)\,\dot{p}\,, \end{array} \tag{10.5}$$

respectively, one obtains the following dynamic equations:

$$\begin{array}{rcl} K^{-1}\left(B(q)\,\dot{s} + \tfrac{1}{2}\dot{B}(q)\,s\right) & = & Y_*(q,\dot{q},\dot{q}_r,\ddot{q}_r)\,\Pi - \tau_*\,, \\ K^{-1}\dot{\sigma} & = & u_\sigma\,. \end{array}$$

Then, under the hypothesis that $K^{-1}B(q)$ is positive definite for all q, one can adopt a similar approach as in Prop. 10 and find adaptive control laws for the new inputs, by also including, this time, a positive definite term depending on stiffness. To this aim, one can choose the candidate Lyapunov function

$$V = \tfrac{1}{2}s^T K^{-1}B(q)s + \tfrac{1}{2}\tilde{\Pi}^T K_\pi^{-1}\tilde{\Pi} + \tfrac{1}{2}(\sigma-\sigma_d)^T\Gamma(q)(\sigma-\sigma_d)\,,$$

where $\tilde{\Pi} = \Pi - \hat{\Pi}$, $\hat{\Pi}$ is the parameter estimate vector, and $\Gamma(q)$ is a positive definite matrix to be properly chosen. The Lie derivative of V is

$$\begin{array}{rcl} \dot{V} & = & \dot{V}_1 + \tfrac{1}{2}(\sigma-\sigma_d)^T\dot{\Gamma}(q)(\sigma-\sigma_d) + \\ & & +(\sigma-\sigma_d)^T\Gamma(q)(\dot{\sigma}-\dot{\sigma}_d)\,, \end{array}$$

where

$$\begin{array}{rcl} \dot{V}_1 & = & s^T K^{-1}\left(B(q)\,\dot{s} + \tfrac{1}{2}\dot{B}(q)\,s\right) - \tilde{\Pi}^T\,K_\pi^{-1}\dot{\hat{\Pi}} = \\ & = & s^T\left(Y_*(q,\dot{q},\dot{q}_r,\ddot{q}_r)\,\Pi - \tau_*\right) - \tilde{\Pi}^T\,K_\pi^{-1}\dot{\hat{\Pi}}\,. \end{array}$$

Choosing τ_* as in Eq. 10.4 leads to

$$\dot{V}_1 = -s^T K_d\,s + s^T Y_*(q,\dot{q},\dot{q}_r,\ddot{q}_r)\,\tilde{\Pi} - \tilde{\Pi}^T\,K_\pi^{-1}\dot{\hat{\Pi}}\,.$$

The transposition of the second addend on the right-hand side of the above equation, which

can be done since it is a scalar, allows factorizing the expression of $\dot{V}_1$ as

$$\dot{V}_1 = -s^T K_d\, s + \tilde{\Pi}^T \left(Y_*^T(q, \dot{q}, \dot{q}_r, \ddot{q}_r)\, s - K_\pi^{-1} \dot{\hat{\Pi}} \right) .$$

Adopting the update rule in Eq. 10.2 for $\dot{\hat{\Pi}}$ makes the second addend to vanish and finally allows reducing $\dot{V}$ to

$$\begin{aligned} \dot{V} &= -s^T K_d\, s + \tfrac{1}{2}(\sigma - \sigma_d)^T \dot{\Gamma}(q)(\sigma - \sigma_d) + \\ &\quad + (\sigma - \sigma_d)^T \Gamma(q)(\dot{\sigma} - \dot{\sigma}_d) . \end{aligned}$$

Moreover, the choice $\Gamma(q) = K^{-1}$ allows using the stiffness dynamics equation and is compliant with the positive definiteness of V. It also ensures $\dot{\Gamma}(q) = 0$, thereby making the time derivative $\dot{V}$ equal to

$$\begin{aligned} \dot{V} &= -s^T K_d\, s + (\sigma - \sigma_d)^T K^{-1}(\dot{\sigma} - \dot{\sigma}_d) = \\ &= -s^T K_d\, s + (\sigma - \sigma_d)^T u_\sigma . \end{aligned}$$

Finally, by choosing the stiffness control input as

$$u_\sigma = K^{-1}\dot{\sigma}_d - K_\sigma(\sigma - \sigma_d) , \tag{10.6}$$

one obtains

$$\dot{V} = -s^T K_d\, s - (\sigma - \sigma_d)^T K_\sigma(\sigma - \sigma_d) .$$

which establishes the negative definiteness with respect to stiffness and position tracking errors. It is worth noticing that the parameter estimation convergence is not guaranteed, but their error remains bounded as it can be found from the study of the second time derivative and from Barbalat's Lemma.

One can now move on to converting these controls into feasible pressure commands. To achieve this, first assume that the sought commanded pressure vector has the form

$$p = A_1(q)\, \tau_* + A_2(q)\, \nu ,$$

where ν is another new control vector, and $A_1(q)$ and $A_2(q)$ are two position-dependent matrices to be conveniently chosen. From the first relation of Eq. 10.5, $\Phi(q)\, p = \tau_*$, one finds that it must be

$$\Phi(q) A_1(q)\, \tau_* + \Phi(q) A_2(q)\, \nu = \tau_* ,$$

which can be satisfied if $\Phi(q)A_1(q) = I_n$ and $\Phi(q)A_2(q) = 0_n$, where I_n and 0_n are the identity and the zero matrix of dimension n. The first of the two conditions requires that $A_1(q) = \Phi(q)^T \left(\Phi(q)\, \Phi(q)^T \right)^{-1} = \Phi(q)^\dagger$, which is the pseudo-inverse of $\Phi(q)$, while the second one implies that $A_2(q) = \Phi(q)^\perp$, in which $\Phi(q)^\perp$ is any matrix in the column null-space of $\Phi(q)$. Therefore, the commanded pressure vector p can be determined as in the form

$$p = \Phi(q)^\dagger\, \tau_* + \Phi(q)^\perp\, \nu ,$$

where ν is still to be determined. Moreover, after computing the time derivative of p, given by

$$\dot{p} = \frac{d}{dt} \left(\Phi(q)^\dagger\, \tau_* \right) + \dot{\Phi}(q)^\perp\, \nu + \Phi(q)^\perp\, \dot{\nu} ,$$

one can write from Eq. 10.5 that it must hold

$$\begin{aligned} u_\sigma &= -\dot{\Phi}_q(q)\,\Phi(q)^\dagger \tau_* - \dot{\Phi}_q(q)\Phi(q)^\perp\,\nu + \\ &\quad -\Phi_q(q)\left(\tfrac{d}{dt}\left(\Phi(q)^\dagger\,\tau_*\right) + \tfrac{d}{dt}\left(\Phi(q)^\perp\right)\,\nu + \right. \\ &\quad \left. +\Phi(q)^\perp\,\dot{\nu}\right)\,. \end{aligned}$$

Substituting in the above equation u_σ with its expression from Eq. 10.6 and then solving it for $\dot{\nu}$ allows deriving the differential relation for the controller internal state ν described in Eq. 10.1. To this purpose, first multiply both sides of the equation by the pseudo-inverse of $\Phi_q(q)\,\Phi(q)^\perp$, as in

$$\begin{aligned} \left(\Phi_q(q)\,\Phi(q)^\perp\right)^\dagger \left(K_\sigma(\sigma-\sigma_d) - K^{-1}\dot{\sigma}_d\right) = \\ = \left(\Phi_q(q)\,\Phi(q)^\perp\right)^\dagger \beta(q) + \dot{\nu}\,, \end{aligned}$$

with

$$\begin{aligned} \beta(q) &= \Phi_q(q)\tfrac{d}{dt}\left(\Phi(q)^\dagger\tau_*\right) + \dot{\Phi}_q(q)\Phi(q)^\dagger\tau_* + \\ &+ \left(\dot{\Phi}_q(q)\Phi(q)^\perp + \Phi_q(q)\,\tfrac{d}{dt}\left(\Phi(q)^\perp\right)\right)\nu\,, \end{aligned}$$

and then find the expression for $\dot{\nu}$. This concludes the search for a feasible and stabilizing pressure command vector and the theorem's proof. □

Remark 6. *As it is known, while the adaptive control approach always allows tracking of position and stiffness references, even with inexact parameter knowledge, no guarantees can be provided about the convergence of such parameters (Slotine and Li (1991)). Indeed, once the position tracking error e has converged to zero, the variable s becomes null, and the parameter adaptation stops (see Eq. 10.2).*

An explicit characterization of the achieved parameter estimation error is not simple and it is also reference-dependent. Once the position tracking error $\tilde{q}$ has converged, the following holds. By first writing the robot's dynamics in regressor form, on the left hand side, and applying the adaptive torque, on the right hand side, it stands:

$$Y_*(\cdot)\,\Pi = \Phi(q)\left(\Phi(q)^\dagger Y_*(\cdot)\,\hat{\Pi} + \Phi(q)^\perp\nu\right)\,,$$

where the variable dependency of matrix Y_* has been omitted for space reasons. The orthogonality construction gives independence on variable ν, which may in principle still evolve, thus leading to

$$Y_*(q,\dot{q},q_r,\dot{q}_r,\ddot{q}_r)\,\Pi = \Phi(q)\Phi(q)^\dagger Y_*(q,\dot{q},q_r,\dot{q}_r,\ddot{q}_r)\,\hat{\Pi}\,,$$

and consequently to

$$Y_*(q,\dot{q},q_r,\dot{q}_r,\ddot{q}_r)\left(\Pi-\hat{\Pi}\right) = 0\,,$$

which finally describes the surface on which the reached parameter estimation error must lie.

Apparently, when the desired stiffness σ_d is time-varying, the controller depends also on the actuator parameters K. However, for applications in which σ_d is slowly varying or piecewise constant, the following corollary to Theorem 5 provides a solution independent of the actuator parameters:

Corollary 2. *Under the hypotheses of Theorem 5, if the desired stiffness σ_d is slowly varying or piecewise constant, the nonlinear decoupling and adaptive controller is described by Eq. 10.2, Eq. 10.3, Eq. 10.4 and*

$$\begin{aligned} \dot{\nu} = \left(\Phi_q(q)\Phi(q)^\perp\right)^\dagger \left(K_\sigma(\sigma-\sigma_d) - \Phi_q(q)\tfrac{d}{dt}\left(\Phi(q)^\dagger\tau_*\right) + \right. \\ \left. - \Phi_q(q)\Phi(q)^\dagger\tau_* - \left(\Phi_q(q)\Phi(q)^\perp + \dot{\Phi}(q)^\perp\right)\nu\right)\,, \end{aligned} \tag{10.7}$$

and thus it is independent of the actuator parameters K.

Proof. The proof straightforwardly follows from Theorem 5 by assuming that $\dot{\sigma}_d = 0$. □

Remark 7. *By a first interpretation of the formula in Eq. 10.3, describing the expression of the stabilizing pressure command, it can be understood that the two signals τ_* and ν independently control the robot's position and stiffness. While τ_* directly affects the applied torque, the differential form of ν takes into account for the term depending on $\dot{p}$, which is present in the stiffness dynamics.*

Remark 8. *It is also worth noticing that the time derivatives of the terms $\Phi^\dagger(q)\tau_*$ and $\Phi(q)^\perp$, involved in Eq. 10.1 of Th. 5 and in Eq. 10.7 of Corollary 2, can be either numerically computed or, more accurately computed in an analytical way by using the chain rule for differentiation. Indeed it holds:*

$$\frac{d}{dt}\left(\Phi^\dagger(q)\,\tau_*\right) = \Phi^\dagger_q(q)\,\dot{q}\,\tau_* + \Phi^\dagger(q)\frac{\partial \tau_*}{\partial q}\,\dot{q}\,.$$

The explicit calculation of the Jacobian of τ_* with respect to q are reported, for the reader convenience, in the experimental section. An analogous situation occurs when applying backstepping techniques.

10.2 Simulation results

This section presents a first step towards the validation of the proposed control approach. To this purpose, a two-degree-of-freedom, planar soft robot arm, actuated via antagonistic McKibben artificial muscles, has been considered. The aim of this section is to show how the proposed method effectively works, when exact knowledge of matrix $\Phi(q)$ is available. Under such ideal hypothesis, the only difference between the regressor form and the system's model in Eq. 9.1 is in the values of unknown parameters Π. The reported simulations show indeed how the controller continuously adjusts the estimated parameter vector $\hat{\Pi}$, as the robot's position q and stiffness σ, are *exactly* steered to the desired values.

Having defined the robot's configuration vector as $q = (q_1, q_2)^T$, with q_1 the arm's shoulder angle and with q_2 its elbow angle, the robot's dynamic model can be written in the form of Eq. 2.5. As for the position's dynamic equation, the well-known expressions of the inertia and Coriolis matrices and of the gravity vector are standard and can be found e.g. in the text by Siciliano and Khatib (2008). More precisely, referring to the system's parameters reported in Table 7.1, the inertia matrix is:

$$B(q) = \begin{pmatrix} B_{11}(q) & B_{12}(q) \\ B_{12}(q) & B_{22}(q) \end{pmatrix},$$

with

$$\begin{gathered} B_{11}(q) = I_1 + m_1\left(\tfrac{l_1}{2}\right)^2 + I_2 + m_2 l_1^2\,, \\ +m_2\left(\tfrac{l_2}{2}\right)^2 + m_2 l_1 l_2 \cos q_2\,, \\ B_{12}(q) = I_2 + m_2\left(\tfrac{l_2}{2}\right)^2 + \tfrac{1}{2} m_2 l_1 l_2 \cos q_2\,, \\ B_{22}(q) = \tfrac{1}{2} m_2 l_2^2 + I_2\,, \end{gathered}$$

the matrix of Coriolis and centrifugal forces is

$$C(q,\dot{q}) = \begin{pmatrix} -\frac{1}{2} m_2 l_1 \sin q_2 \dot{q}_2 & -\frac{1}{2} m_2 l_1 \sin q_2\,(\dot{q}_1 + \dot{q}_2) \\ \frac{1}{2} m_2 l_1 \sin q_2 \dot{q}_1 & 0 \end{pmatrix},$$

Table 10.1: Definition of the actuator model's parameters.

Param.	Value	Unit	Description
R	0.03	m	Pulley radius
K_g	0.16	-	Actuator param.
l_{nom}	0.17	m	Nom. muscle length
l_{min}	0.14	m	Min. muscle length

and the vector containing gravitation components is

$$G(q) = \begin{pmatrix} (\frac{1}{2}m_1 l_1 + m_2 l_1) g \sin q_1 + \frac{1}{2} m_2 l_2 g \sin q_1 + q_2 \\ \frac{1}{2} m_2 l_2 g \sin q_1 + q_2 \end{pmatrix} .$$

Furthermore, as for the right-hand-side of Eq. 2.5, under the assumption of equal muscle parameters, i.e. $K = \mathrm{diag}(K_1, K_1)$, having denoted with $p_{i,a}$ and $p_{i,b}$ the pressures of the two artificial muscles of the i-th link, for $i \in \{1, 2\}$, and also referring to Table 10.1, the actuator model is given by the formula:

$$\tau_* = \Phi(q)\, p \,, \tag{10.8}$$

where

$$\begin{aligned} \tau_* &= (\tau_{*,1}, \tau_{*,2})^T = \tau / K_1 \,, \\ p &= (p_{1,a}, p_{1,b}, p_{2,a}, p_{2,b})^T \,, \end{aligned}$$

and

$$\Phi(q) = \begin{pmatrix} \phi_1(q) & -\phi_1(q) & 0 & 0 \\ 0 & 0 & \phi_2(q) & -\phi_2(q) \end{pmatrix} ,$$

with

$$\phi_i(q) = (l_{nom} - q_i R)^2 - l_{min}^2 \,.$$

One can now move on to deriving the equations of the adaptive and decoupling controller of Th 5. First, it can be verified that the condition $K^{-1}B(q)$ to be positive definite is satisfied, thereby allowing the proposed control approach to be applied. The regressor matrix reads

$$Y_* = \begin{pmatrix} \ddot{q}_{1,r} & \ddot{q}_{2,r} & Y_{13} & \sin q_1 & \sin(q_1 + q_2) \\ 0 & \ddot{q}_{1,r} + \ddot{q}_{2,r} & Y_{23} & 0 & \sin(q_1 + q_2) \end{pmatrix} , \tag{10.9}$$

with

$$\begin{aligned} Y_{13} &= (2\ddot{q}_{1,r} + \ddot{q}_{2,r}) \cos q_2 - \dot{q}_2 \left(\dot{q}_1 + \tfrac{1}{2}\dot{q}_2 + \dot{q}_{1,r} + \tfrac{1}{2}\dot{q}_{2,r} \right) \sin q_2 \,, \\ Y_{23} &= \ddot{q}_{1,r} \cos q_2 + \left(\dot{q}_1^2 + \tfrac{1}{2}\dot{q}_1 \dot{q}_2 - \tfrac{1}{2}\dot{q}_{1,r}\dot{q}_2 \right) \sin q_2 \,, \end{aligned}$$

and the parameter vector is

$$\begin{aligned} \Pi &= (\Pi_1, \Pi_2, \Pi_3, \Pi_4, \Pi_5)^T \\ &= \tfrac{1}{K_1} \begin{pmatrix} I_1 + m_1 \left(\frac{l_1}{2}\right)^2 + I_2 + m_2 (\frac{l_2}{2})^2 + m_2 l_1^2 \\ I_2 + m_2 \left(\frac{l_2}{2}\right)^2 \\ \frac{1}{2} m_2 l_1 l_2 \\ \left(\frac{1}{2} m_1 + m_2\right) l_1 g \\ \frac{1}{2} m_2 l_2 g \end{pmatrix} . \end{aligned}$$

The term $\Phi(q)^\dagger$ is the standard Moore-Penrose pseudo-inverse, which is omitted here for

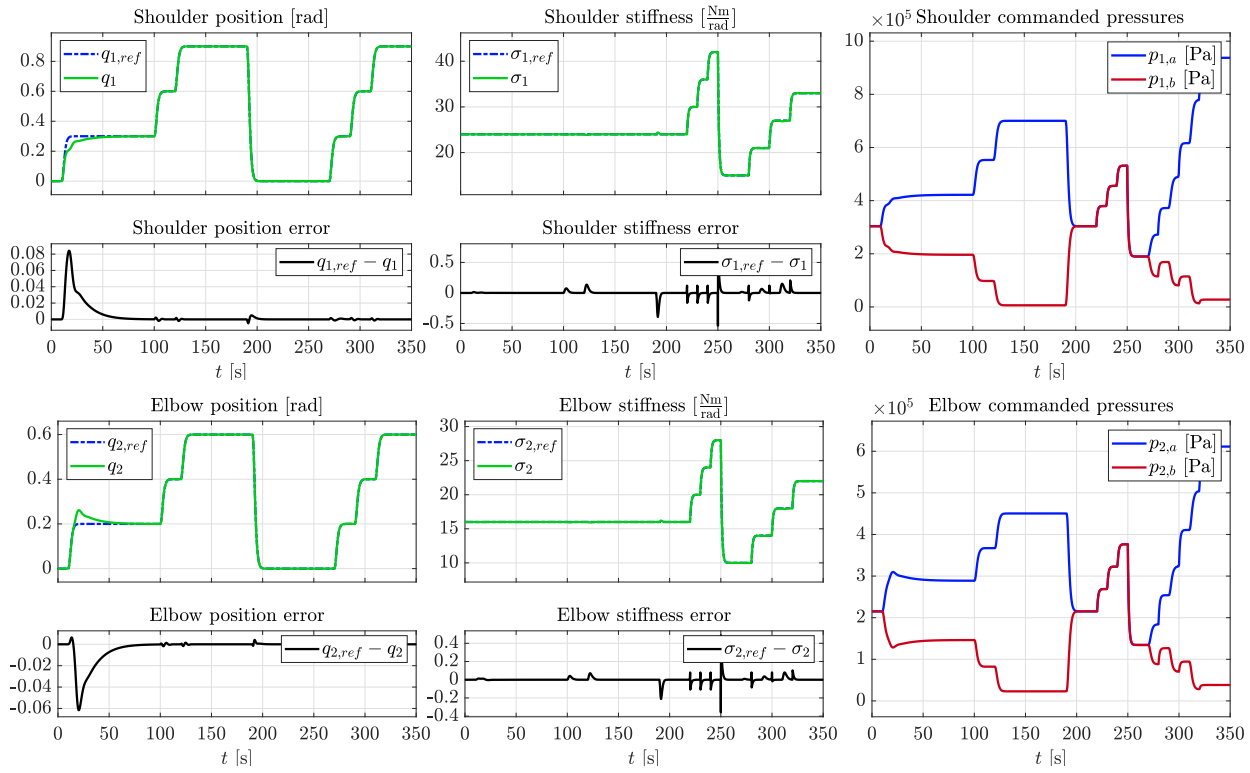

Figure 10.2: Simulation run of a 2-DoF pneumatic soft robot with initial parameter estimation error of 10% of the real values. Shoulder and elbow references for position and stiffness are specified first alternately (for $t \in [0, 250)$) and then simultaneously (for $t \in [250, 350)$). All commands are asymptotically tracked with feasible pressure commands.

the sake of space, while the null-space projector $\Phi(q)^{\perp}$ is given by

$$\Phi(q)^{\perp} = \begin{pmatrix} \phi_1(q) & 0 \\ \phi_1(q) & 0 \\ 0 & \phi_2(q) \\ 0 & \phi_2(q) \end{pmatrix}.$$

The internal state of the controller is the two-dimensional vector $\nu = (\nu_1, \nu_2)^T$. Therefore, the sought adaptive and decoupling controller can be obtained by implementing the internal state vector dynamics for ν in Eq. 10.1 and the parameter adaptation law in Eq. 10.2 for $\hat{\Pi}$, and then computing the adaptive control τ_* as in Eq 10.4 and, finally, the output command pressure p as in Eq. 10.3.

In order to show the effectiveness of the proposed approach, results from a typical simulation run are presented in the following. In the simulation, the robot's artificial muscles are initially inflated, so as to reach a *preset* stiffness σ of 2 Nm/rad. During this initial setup phase, no parameter adaptation is executed by setting the matrix gain K_π to zero, while as soon as the parameter adaptation is activated, K_π is set to 35. It is worth noticing that larger values of K_π allow achieving faster parameter adaptation response, but, depending on how large is the initial estimation error, attention should be drawn, in order not to drive system to instability during the very first instants. As for the position tracking error dynamics, the controller constants are chosen as $K_d = 18$ and $\lambda = 15$. It is important to recall from work of Della Santina et al. (2017) that it is preferable to keep their values low so that natural compliance of the robot is sustained, by reducing static feedback impact on the joints' stiffness. The estimated robot's parameters $\hat{\Pi}$ have been chosen to be 10% less than their real values Π.

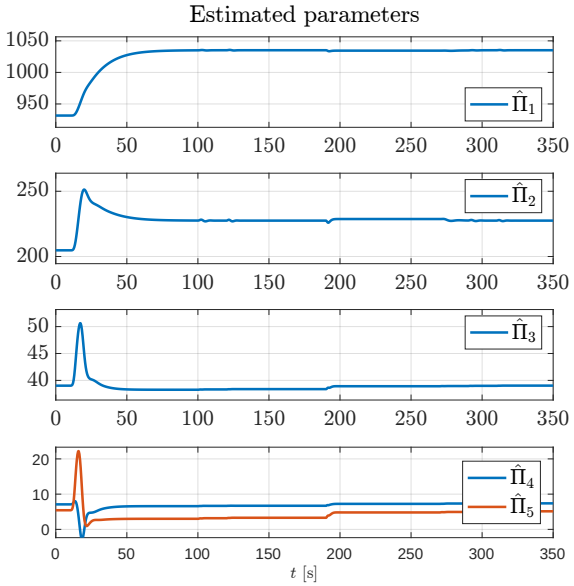

Figure 10.3: Evolution of the estimated parameter vector for the simulation scenario of Fig. 10.2. Parameter estimates are rapidly adjusted at the beginning of the simulation and then remain bounded.

Furthermore, desired position and stiffness trajectories, q_d and σ_d, have been designed, so as to include in the simulation three phases relating to three possible use-cases: 1) stepwise increasing position commands while stiffness is kept constant, 2) stepwise increasing stiffness commands while position is kept constant, 3) simultaneous stepwise commands for position and stiffness. Referring to Fig. 10.2 and 10.3, the three phases are for $t \in [0, 190)$, $t \in [190, 250)$, and $t \in [250, 350)$, respectively. Fig. 10.2 shows that, as soon as a suitable set of values for the estimated parameters is *learnt*, all position and stiffness commands are effectively tracked. Most importantly, it is shown that position commands are followed with almost null influence on the robot's joint stiffness and viceversa, thus proving that the sought decoupling is achieved. Very short transients of the stiffness can occur, only at the instantaneous changes of positions commands, but no steady state error remains. Such transients can be easily avoided by designing smoother reference signals. The figure also reports the corresponding commanded muscle pressures. Fig. 10.3 shows the adaptation of the components of the estimated parameter vector, which, as it is known, do not converge to the actual values, but remain bounded.

10.3 Experimental results

This section presents a final validation of the proposed control approach, using a pneumatic soft-robot system, *GioSte* (Fig. 10.4), which was developed at the University of Pisa by Tonietti and Bicchi (2002).

10.3.1 Hardware and Software Setup

The robotic system consists of an articulated arm with two rotary joints, each driven by a pair of McKibben muscles in antagonistic configuration. All muscles receive pressurized air from a common air compressor source at 8 bars. Inflation and deflation of each muscle is regulated by a dedicated SMC ITV-2050 electro-pneumatic valve, which receives voltage commands in the range of $[0, 6]$ Volts. Such voltage commands are obtained by suitably converting the pressure

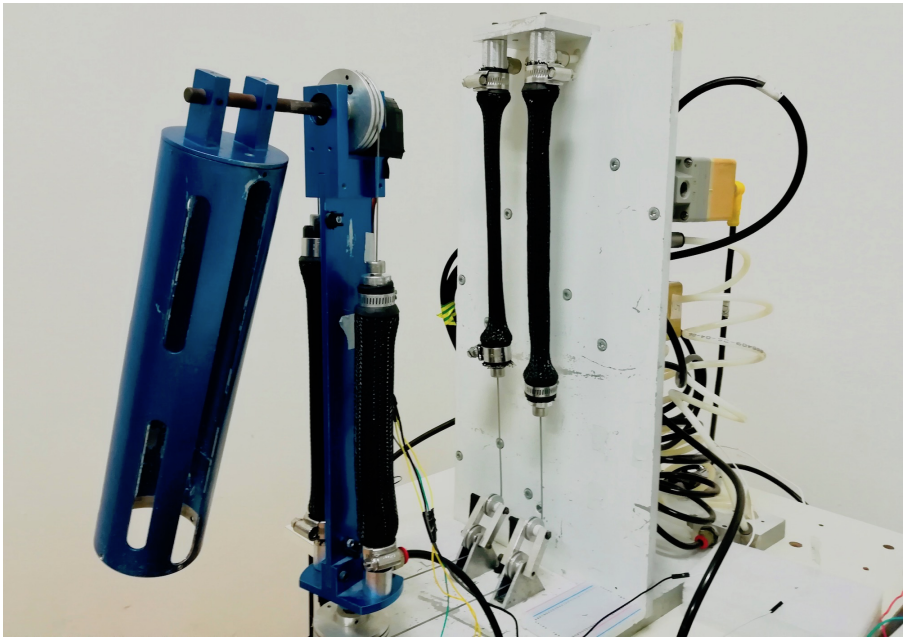

Figure 10.4: GioSte - Pneumatic soft robot arm designed and developed at the University of Pisa.

signals, as shown later, specified by the proposed controller according to Eq. 10.3. An ad-hoc valve pre-configuration phase has been carried out, in order to prevent valve chattering, by adjusting the pressure response time so as to suit the current application.

The angular positions of the rotary joints are measured through two optical and incremental encoders, HEDS 5500 A12, each attached to the shaft of the corresponding joint pulley. The encoders generate 500 counts per revolution, thus allowing to reach a resolution of $1.6 \cdot 10^{-3}$ rad if read in quadrature mode. A National Instruments PCIe6323 acquisition board is used with its screw terminal, so as to collect encoder data and send voltage-based pressure commands to the valves. Real-time control of the system through implementation of the proposed control algorithm has been done, by using Matlab/Simulink 2014a software, which is connected to the NI acquisition card via input-output drivers.

As for this validation, a single-degree-of-freedom version of the GioSte robotic system is first considered, followed by the results of the two-degree-of-freedom setup.

10.3.2 Actuator Model Identification for the one-link GioSte

A preliminary identification phase has been carried out in order to acquire accurate knowledge of the actuator model, as required by the hypotheses of Th. 5. Given the adopted one-link GioSte robot arm, the identification process has aimed at finding the following four mappings: 1) pressure-to-voltage for muscle a, 1) pressure-to-voltage for muscle b, 3) voltage-to-torque, and 4) voltage-to-stiffness.

The first two mappings have been obtained by applying specific voltage commands, covering the entire operation range, to each of the two antagonistic muscles, a and b, and measuring the corresponding achieved pressures, $p_{1,a}$ and $p_{1,b}$. A linear least squares criterium has been used to determine the following second-order polynomial approximation (also depicted in Fig. 10.5):

$$\begin{aligned} p_{1,a} &= \left(0.0025\, V_{1,a}^2 + 0.8611\, V_{1,a} - 0.4543\right) \cdot 10^5\,, \\ p_{1,b} &= \left(-0.0036\, V_{1,b}^2 + 0.9024\, V_{1,b} - 0.5382\right) \cdot 10^5\,. \end{aligned} \tag{10.10}$$

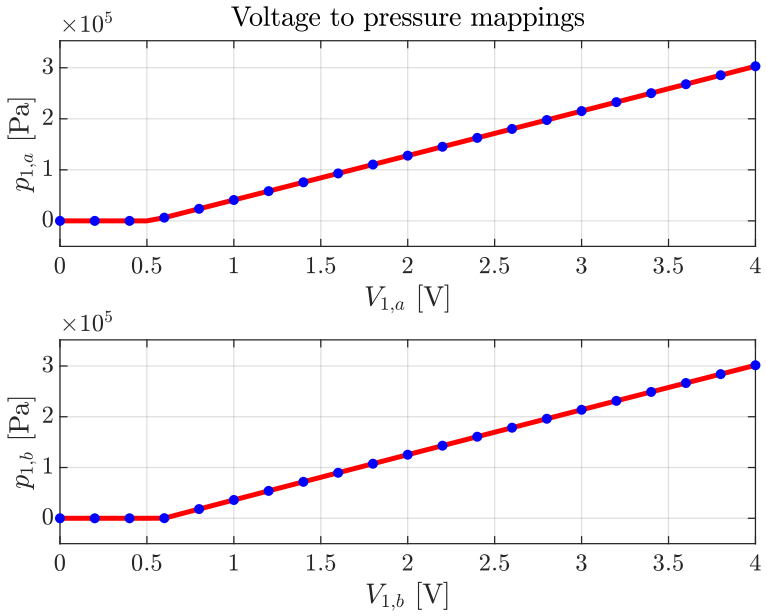

Figure 10.5: Estimated voltage to pressure mappings for two antagonistic McKibben muscles, actuating the one-link version of the GioSte robot.

The obtained mappings have been validated with a different set of voltage values and proved to be sufficiently precise, which is also due to the high accuracy of the internal controllers of each electro-valve.

As for the third and fourth mappings, the two muscles have been actuated by suitably varying the input voltages of their valves, and then measuring the finally attained steady-state joint position q_1 when subject to gravity. More precisely, experiments consisted of probing the entire voltage to torque and stiffness relation, by applying, *completely in open-loop*, constant voltages to one muscle and varying the one of the other muscle. It is important to state that, during this phase, no form of feedback has been used, so as to measure only the system's stiffness, and not the one induced by a control action. The elastic torque τ_1 has therefore been estimated by exploiting the fact that, when the joint is in the steady state, rotational equilibrium exists and thus, from Eq. 2.1 and 2.2, it holds

$$\tau_a - \tau_b - \tau_g = 0\,, \quad \text{with } \tau_g = m_1 g \tfrac{l_1}{2} \sin(q)\,,$$

where τ_a and τ_b are the two torques applied by the two muscles, and τ_g is the gravitational force.

The joint stiffness σ, achieved for a given pair of muscle voltages, has been derived by using the model of Eq. 2.3. By using an analogous least squares fitting algorithm, the following polynomial approximations have been simultaneously found:

$$\begin{aligned} \tau_1 &= (6.96 - 2.34\,q_1 - 0.71\,q_1^2)\; V_{1,a} + \\ &\quad -(7.03 + 2.07\,q_1 - 0.58\,q_1^2)\, V_{1,b}\,, \\ \sigma_1 &= (2.34 - 0.57\,q_1)\; V_{1,a} + (2.07 + 0.57\,q_1)\; V_{1,b}\,. \end{aligned} \tag{10.11}$$

The two mappings provide, for every actual angular position q_1, the torque τ_1 and the stiffness σ_1, obtained by applying some specific pair of voltage values, $V_{1,a}$ and $V_{1,b}$.

Finally, the validity of the last mapping, relating the stiffness model, has been experimentally verified, by measuring, for different positions q_1, the change of joint angle Δq_1 induced by a known variation of the gravity force $\Delta\tau_g$, produced by weights at the link tip of the link.

Experiments showed that the assumed model is reliable enough for the application. While it is possible to reconstruct more accurate mappings, by using e.g. force sensors mounted on tendons, or even torque sensor mounted on the joint's shaft, it is true that stiffness is a variable that in real applications does not require such high precision. Then, it has been chosen to use the model obtained by Tonietti and Bicchi (2002) for the experiments in this paper.

10.3.3 Experimental Results for the one-link GioSte

To evaluate and show the effectiveness of the proposed decoupling nonlinear adaptive control approach, a set of experiments realizing use-cases similar to the ones considered for the simulation validation have been carried out. Again, the purpose here is to show the ability of the controlled shoulder joint to simultaneously and independently track reference position and stiffness commands. The implemented use-cases are: 1) smoothed stepwise position commands with constant stiffness, 2) smoothed stepwise stiffness commands with constant position, and 3) simultaneous change of position and stiffness. Within all the experiments, the following dynamic model of the one-link GioSte soft-robot has been used:

$$\begin{aligned}\left(I_1 + m_1 \tfrac{l_1}{2}\right) \ddot{q}_1 + m_1 g \tfrac{l_1}{2} \sin(q_1) = \\ = K_1 \left(\phi_{1,a}(q_1), -\phi_{1,b}(q_1)\right) \begin{pmatrix} p_{1,a} \\ p_{1,b} \end{pmatrix},\end{aligned}$$

$$\begin{aligned}\dot{\sigma}_1 &= -K_1 \left(\dot{\phi}_{q,1,a}(q_1), -\dot{\phi}_{q,1,a}(q_1)\right) \begin{pmatrix} p_{1,a} \\ p_{1,b} \end{pmatrix} + \\ &+ -K_1 \left(\phi_{q,1,a}(q_1), -\phi_{q,1,a}(q_1)\right) \begin{pmatrix} \dot{p}_{1,a} \\ \dot{p}_{1,b} \end{pmatrix},\end{aligned}$$

where the viscous friction term has been neglected. Then, the regressor matrix from Theorem 5 is

$$Y_* = \left(\ddot{q}_{1,r}, \sin(q_1)\right),$$

and the unknown parameter vector is

$$\Pi = (\Pi_1, \Pi_2)^T = \left((I_1 + m_1 \left(\tfrac{l_1}{2}\right)^2)/K_1, m_1 g \tfrac{l_1}{2}/K_1\right)^T.$$

Moreover, before proceeding to presenting the experimental results, referring to Remark 8, it can be shown that the numerical time differentiation of the term $\Phi^\dagger(q_1)\tau_*$, involved in Eq. 10.1 of Th. 5 can be avoided by applying the chain rule. Indeed it holds:

$$\frac{d}{dt}\left(\Phi^\dagger(q_1)\,\tau_*\right) = \Phi^\dagger_q(q_1)\,\dot{q}_1\,\tau_* + \Phi^\dagger(q_1)\frac{\partial \tau_*}{\partial q_1}\dot{q}_1,$$

where

$$\begin{aligned}\frac{\partial \tau_*}{\partial q_1} &= \frac{\partial}{\partial q_1}\left(Y_*(q_1, \dot{q}_1, \dot{q}_{1,r}, \ddot{q}_{1,r})\,\hat{\Pi} + K_d\, s\right) = \\ &= \frac{\partial}{\partial q_1}\left(\left(\ddot{q}_{1,r}, \sin(q_1)\right)(\hat{\Pi}_1, \hat{\Pi}_2)^T\right) + \\ &+ \frac{\partial}{\partial q_1}\left(K_d\left(\dot{q}_{1,d} - \dot{q}_1 + \Lambda\left(q_{1,d} - q_1\right)\right)\right) = \\ &= \cos(q_1)\,\hat{\Pi}_2 - K_d\Lambda,\end{aligned}$$

which shows that no information regarding the acceleration $\ddot{q}_1$ is in fact necessary. As it is known, this fact allows avoiding noise amplification effects that would occur in numerical

differentiation.

Moving now on to the experiments, desired position and stiffness values are chosen in a way that they are compliant with the hardware. Some of the factors playing a role in such choice are the nominal and minimal muscle lengths and the maximal muscle pressure (cf. also by Medrano-Cerda et al. (1995)). Three tests have been carried out where the following gain values of the adaptive and decoupling controller have been chosen: $K_d = 2$, $\Lambda = 10$, and $K_\pi = 45$. Despite the slower tracking error obtained, such values have been chosen in order to be able to present some important features in the following plots.

During the first experiment, whose results are presented in Fig. 10.6, a stepwise reference signal $q_{1,d}(t)$ for the joint position, ranging from 0 to 0.3 radians, is given, with a constant desired stiffness $\sigma_d(t) = 10$ Nm/rad. The figure shows that, despite an initial tracking delay, mostly due to the imprecise value of the parameters, all position commands are asymptotically followed, while stiffness is maintained practically constant. The controlled system is able to cope with both the uncertainties of the left hand side of the model, and with the one of the construction-dependent constant K_1 of the pneumatic actuator. Moreover it also recovers from the residual error of the identification process, due to an inevitably not exact estimation of the nominal and minimum lengths of the two muscles. Another important feature to observe is how the controller's internal state ν evolves, nicely adjusting its value, in order to assure the sought decoupling. The commanded voltages $V_{1,a}$ and $V_{1,b}$ remain always within the feasible range. It can also be observed that the amplitude of the steady-state tracking error is of the same order of encoder resolution, and thus it could be reduced through the use of encoders with more pulses per revolution.

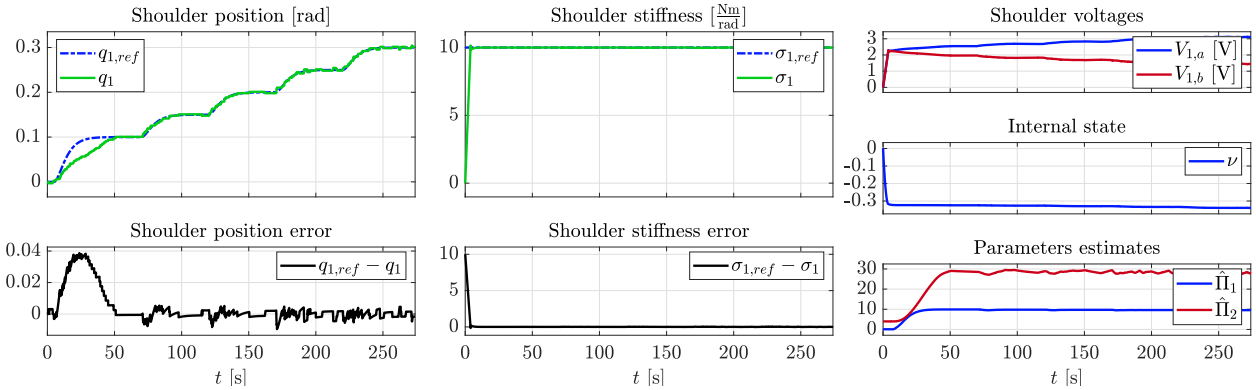

Figure 10.6: Experiment #1 - Smoothed stepwise position commands with constant stiffness. The position tracking error gradually decays as parameter adaptation advances. After adaptation, the tracking error is mostly affected by the noise of pressure regulators and has the same order of amplitude of the encoder resolution. The impact of position changes on the joint stiffness is negligible as desired. Estimated parameters, internal control state, and commanded voltages are bounded and smooth.

As a complementary second experiment, shown in Fig. 10.7, the desired stiffness is changed stepwise from 7 to 10 Nm/rad, while the desired position is kept constant at 0.2 rad. Similarly to the previous experiment, the largest tracking error of both stiffness and position occurs during an initial phase, when the adaptive control is still trying to *learn* a suitable combination of parameter values.

The last of the three experiments combines the two previous scenarios, including commanded position and stiffness signals that change simultaneously. It can be seen from Fig. 10.8 that the adaptive and decoupling controller allows tracking such references, with practically no interference with each other. As shown by De Luca and Lucibello (1998), dynamic feedback linearization is able to achieve perfect decoupling, in the absence of measurement noise and

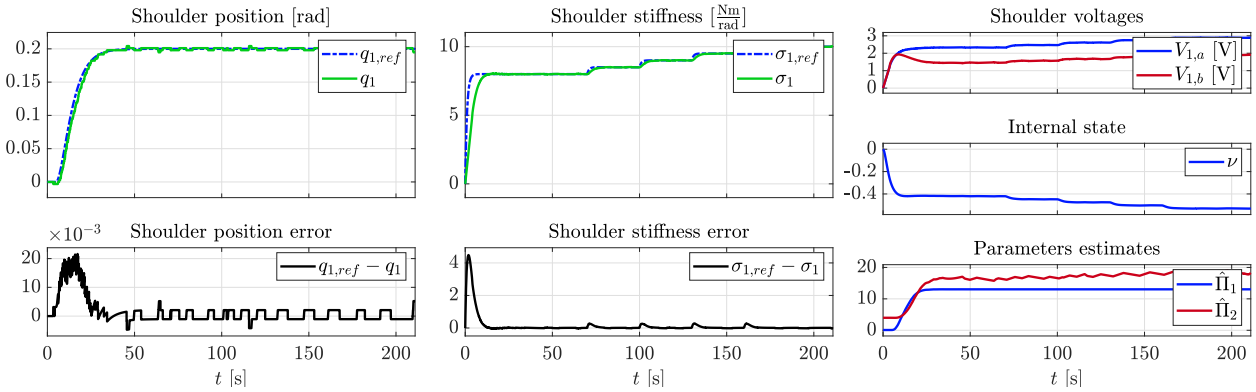

Figure 10.7: Experiment #2 - Smoothed stepwise stiffness commands with constant position. Dually to the previous experiment, the stiffness tracking error asymptotically converges. The position tracking error is not affected by the stiffness commands. Estimated parameters, internal control state and commanded voltages are bounded and smooth.

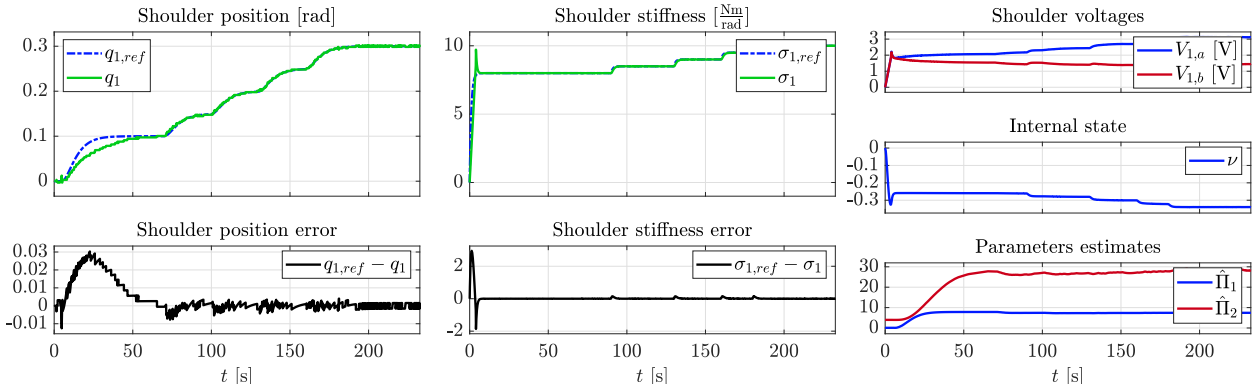

Figure 10.8: Experiment #3 - Simultaneous position and stiffness commands. All references are successfully tracked with no apparent mutual interference as desired.

model uncertainties. As said in the introduction, leveraging on the idea therein proposed of introducing a stiffness dynamics has allowed deriving the present adaptive approach, which has shown to be an effective solution.

10.3.4 Comparison Between Open- and Closed-loop Adaptive Stiffness Control

One could now proceed to further analyze the performance of the proposed control approach, by showing the different behavior of the adaptive open-loop control algorithm described in Tonietti and Bicchi (2002) and the above proposed closed-loop stiffness control.

To this purpose, a first set of experiments has been designed in order to investigate how the two systems respond to stepwise position commands with different rise times T_r, while the desired stiffness remains constant, i.e. $\sigma_d = \bar{\sigma}_d$. The comparison has been done by choosing the controller gain values $K_d = 12$, $\Lambda = 1.8$, and $K_\pi = 45$. First, Fig. 10.9 reports the behavior of the controlled GioSte robot with desired position rise time set to $T_r = 6.7158$ seconds. Smoothed position reference steps are applied at $t = 0$ and $t = 36$ seconds. It can be observed that, during the initial interval, the open-loop approach is able to faster track the desired position command; in fact, the requirement to adapt also to the stiffness dynamics provides the algorithm with some more conservative and slower behavior. After this first adaptation phase, the closed-loop approach has a similar response time as the open-loop one, as for what it concerns the position, but with the additional advantage that a smoother position tracking is achieved; however, due to the imposed stiffness dynamics, one can notice a transient in the stiffness tracking. It can also be seen that estimated parameters, the commanded voltages, and the internal control state ν well-behave from a numerical standpoint and remain bounded.

Furthermore, Fig. 10.10 summarizes the two approaches for three decreasing position rise times, namely $T_r = 4.39$, $T_r = 2.20$ and $T_r = 1.65$ seconds. Smoothed position reference steps are applied at $t = 0$, $t = 36$, and 46 seconds; they are not reported in the figures for the sake of clarity. The stiffness in open-loop is constantly maintained to 7 Nm/rad as in the previous experiment of Fig. 10.9. The leftmost plot of the figure shows that the system controlled via the open-loop stiffness method starts to experience an oscillatory behavior, more apparent as T_r decreases, and eventually goes to instability. The two other plots of the figure, the middle and rightmost, shows that, with the same setup, after some initial oscillations, the closed-loop stiffness control can preserve the system's stability. Indeed, the residual inaccuracy in the actuator model identification process may lead to such an oscillatory evolution, while the introduction of stiffness dynamics has the further benefit of providing the resulting system additional inertia. It is, thus, the faster rise time request in the position command $q_d(t)$ mostly responsible for the increase of the oscillatory and finally unstable behavior of the system controlled via the open-loop stiffness approach.

Proceeding to a second type of experiments, the intention has been to investigate the effect of stepwise stiffness commands on the joint position. To this aim, the desired position is kept constant and the stiffness reference is stepwise changing. Fig. 10.11 reveals that both controlled systems remain stable, but the impact of stiffness reference change on the position is larger in the case of the open-loop solution, which ultimately also show how this approach can embed the controlled system with better capacity of stiffness to position decoupling.

Broadly speaking, the fundamental difference between these two approaches lays in the general principles of open and closed-loop control frameworks. The advantage of stiffness regulation has been foreseen by Medrano-Cerda et al. (1995) and the vision of model-based independent joint position and stiffness control of electrically driven VSAs has been theoretically proposed by Palli et al. (2007) and Palli et al. (2008). The closure of stiffness loop is supposed to lead to the better performance when the desired reference profile of stiffness is time varying.

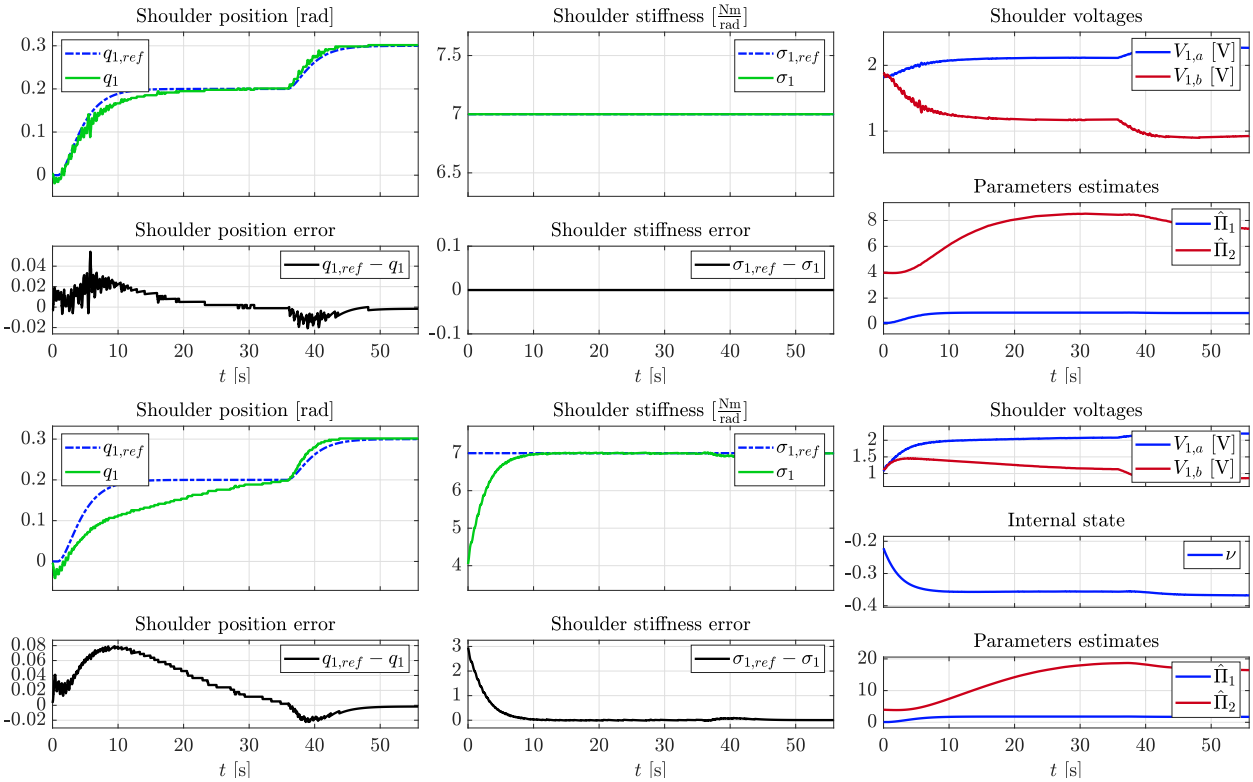

Figure 10.9: Experiment #4 - Comparison of the adaptive open-loop (first row) and closed-loop (second row) stiffness control with position references with rise time $T_r = 6.7158$ seconds. During the first interval, for $t < 40$ seconds, the open-loop approach is able to track faster the desired position command; indeed, the requirement to adapt also to the stiffness dynamics provides the algorithm with some more conservative and slower behavior, leading to the observed initial lag in the closed-loop response. After this first adaptation phase, the closed-loop approach has a similar response time as the open-loop one, as for what it concerns the position, but with the additional advantage that a smoother position tracking is achieved; however, due to the imposed stiffness dynamics, one can notice a transient in the stiffness tracking.

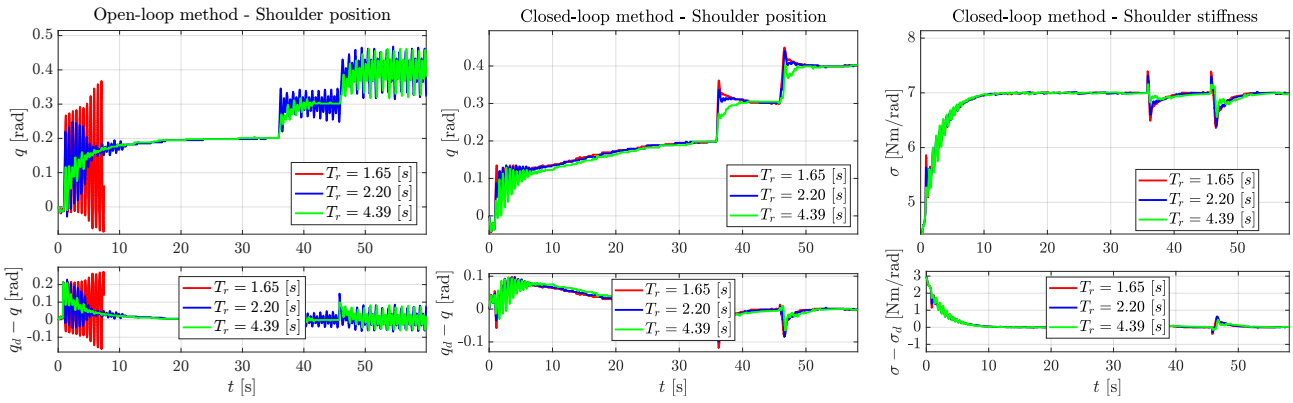

Figure 10.10: Experiment #5 - Comparison of open-loop (leftmost) and closed-loop (middle and rightmost) stiffness control for position references with decreasing rise times. Smoothed position reference steps are applied at $t = 0$, $t = 36$, and 46 seconds. While the open-loop solution starts to experience an oscillatory behavior, more apparent as T_r decreases, and eventually goes to instability, the closed-loop one, after some initial oscillations, is capable of preserving the system's stability.

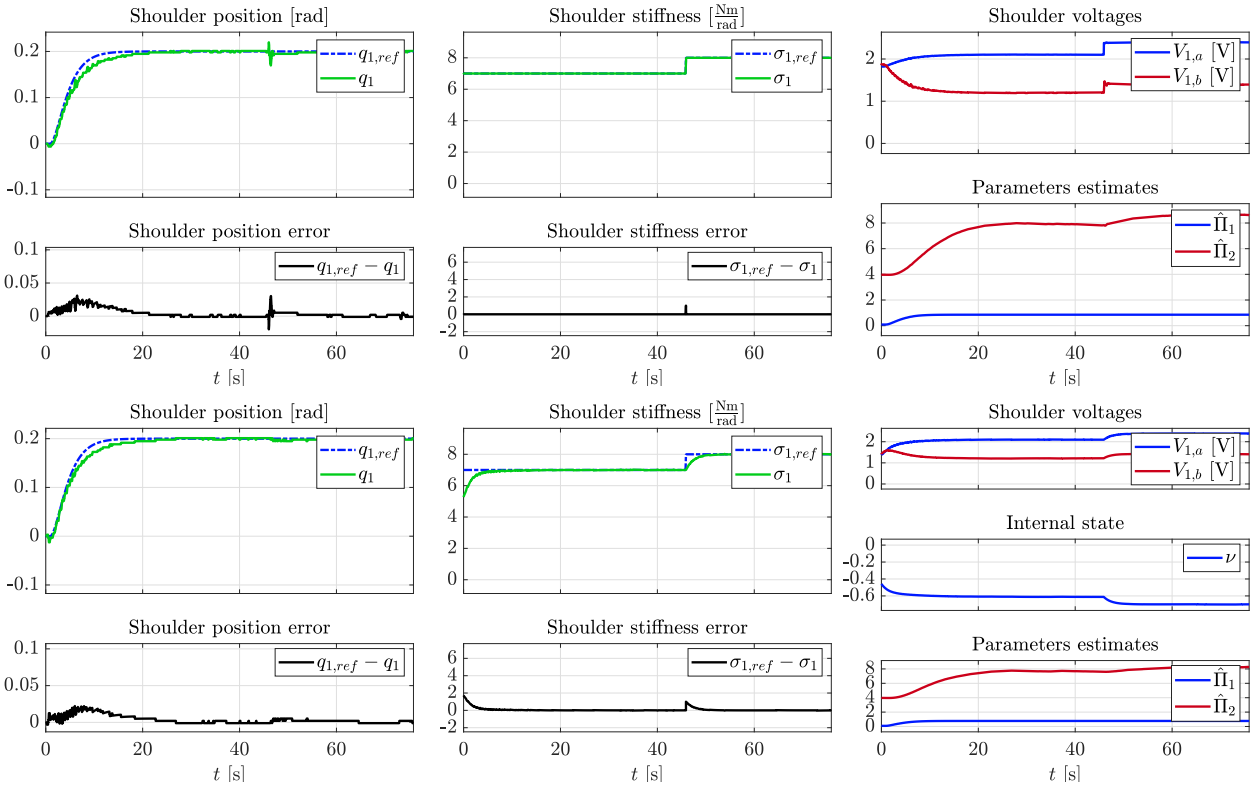

Figure 10.11: Experiment #6 - Adaptive open-loop (first row) and closed-loop (second row) control of stiffness for stepwise stiffness reference. The controlled system under open-loop stiffness regulation experiences position disturbance during the transient of stiffness reference. On the contrary, the closed-loop control of stiffness can suppress the oscillation of joint position.

Indeed, the inclusion of dynamics (i.e. an integrator) in the stiffness control allows the closed-loop system to better cope with the non-modeled dynamics of the mechanical system. On the other side, the implementation of the open-loop control by Tonietti and Bicchi (2002) is easier, which finally drives to the conclusion that specific use-cases will determine the choice of proper control approach.

10.3.5 Experimental Validation for the two-link GioSte

This subsection presents results of the validation and performance evaluation of the proposed control law the full two degree-of-freedom robot arm of Fig. 10.4. In this setup, the first link q_1 will act as the robot's *shoulder* and the second one q_2 will represent its *elbow*. Similarly to the procedure previously described for the one-DoF robot, the identification process for the two-link GioSte leads to the following mappings:

$$\begin{aligned}
\tau_1 &= (2.28 - 2.87\,q_1 + 2.16\,q_1^2)\; V_{1,a} + \\
&\quad -(2.54 + 2.28\,q_1 + 6.09\,q_1^2)\; V_{1,b}\,, \\
\tau_2 &= (6.96 - 2.34\,q_2 - 0.71\,q_2^2)\; V_{2,a} + \\
&\quad -(7.03 + 2.07\,q_2 - 0.58\,q_2^2)\; V_{2,b}\,, \\
\sigma_1 &= (2.87 + 0.83\,q_1)\; V_{1,a} + (2.28 - 0.83\,q_1)\; V_{1,b}\,, \\
\sigma_2 &= (2.34 - 0.57\,q_2)\; V_{2,a} + (2.07 + 0.57\,q_2)\; V_{2,b}\,.
\end{aligned}$$

The same mapping as in Eq. 10.10 has been used for the second link to relate the pressure $p_{2,a}$ and $p_{2,b}$ with the voltages $V_{2,a}$ and $V_{2,b}$. Moreover, the controller's gains are $K_d = \mathrm{diag}(K_{1,d}, K_{2,d}) = \mathrm{diag}(15, 2)$, $\Lambda = \mathrm{diag}(\Lambda_1, \Lambda_2) = \mathrm{diag}(8, 8)$, and $K_\pi = 45\, I_{5\times 5}$. Before moving to the experiments, it is worthwhile to observe, referring to Remark 3, that the Jacobian matrix

$$\frac{\partial \tau_*}{\partial q} = \left\{ \frac{\partial \tau_{*,i}}{\partial q_j} \right\}\,,\ \mathrm{i,j}\ \in \{1, 2\}\,,$$

includes the following terms:

$$\begin{aligned}
\frac{\partial \tau_{*,1}}{\partial q_1} &= \frac{\partial}{\partial q_1}\Big(Y_{*,1}(\cdot)\,\hat{\Pi} + K_{1,d}\,s_1\Big) = \\
&= \frac{\partial}{\partial q_1}\Big((\ddot{q}_{1,r}, \ddot{q}_{2,r}, Y_{13}(\cdot), \sin q_1, \sin q_1 + q_2)\,\hat{\Pi}\Big) + \\
&+ \frac{\partial}{\partial q_1}\left(K_{1,d}\left(\dot{q}_{1,d} - \dot{q}_1 + \Lambda_1\left(q_{1,d} - q_1\right)\right)\right) = \\
&= \Lambda_1\, \sin q_2\, \dot{q}_2\, \hat{\Pi}_3 + \cos q_1 \hat{\Pi}_4 + \cos q_1 + q_2 \hat{\Pi}_5 - K_{1,d}\Lambda_1\,,
\end{aligned}$$

$$\begin{aligned}
\frac{\partial \tau_{*,1}}{\partial q_2} &= \frac{\partial}{\partial q_2}\Big(Y_{*,1}(\cdot)\,\hat{\Pi} + K_{1,d}\,s_1\Big) = \\
&= -\Big(\Big(2\ddot{q}_{1,r} + \ddot{q}_{2,r} + \tfrac{1}{2}\Lambda_2\dot{q}_2\Big)\sin q_2 + \\
&\quad + \Big(\dot{q}_1 + \tfrac{1}{2}\dot{q}_2 + \dot{q}_{1,r} + \tfrac{1}{2}\dot{q}_{2,r}\Big)\,\dot{q}_2 \cos q_2\Big)\,\hat{\Pi}_3 + \cos q_1 + q_2\,\hat{\Pi}_5\,,
\end{aligned}$$

$$\begin{aligned}
\frac{\partial \tau_{*,2}}{\partial q_1} &= \frac{\partial}{\partial q_1}\Big(Y_{*,2}(\cdot)\hat{\Pi} + K_{2,d}\,s_2\Big) = \\
&= \frac{\partial}{\partial q_1}\Big((0, \ddot{q}_{1,r} + \ddot{q}_{2,r}, Y_{23}(\cdot), 0, \sin q_1 + q_2)\,\hat{\Pi}\Big) + \\
&+ \frac{\partial}{\partial q_1}\left(K_{2,d}\left(\dot{q}_{2,d} - \dot{q}_2\right) + \Lambda_2\left(q_{2,d} - q_2\right)\right) = \\
&= \tfrac{1}{2}\Lambda_1\dot{q}_2\, \sin q_2\, \hat{\Pi}_3 + \cos q_1 + q_2\, \hat{\Pi}_5\,,
\end{aligned}$$

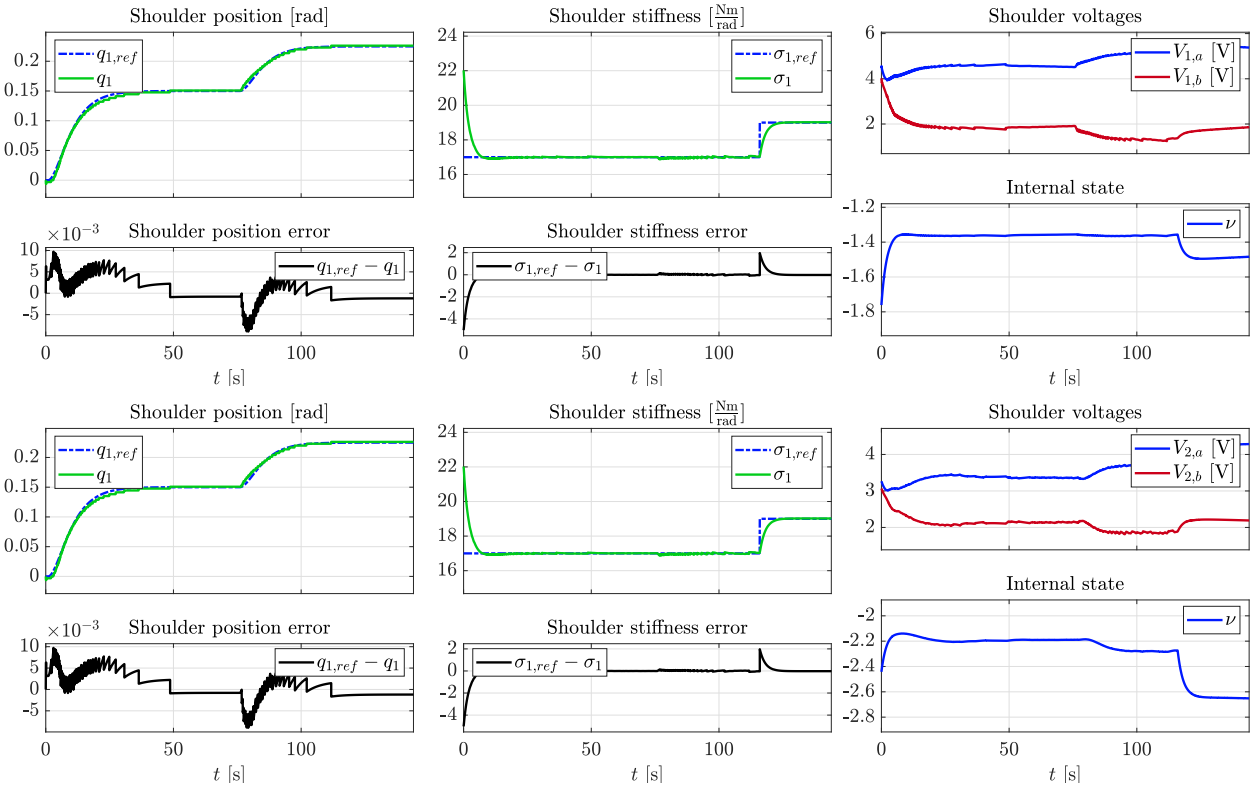

Figure 10.12: Experiment #7 - Experimental run of a 2-DoF pneumatic soft robot with smoothed stepwise references for position and stiffness of shoulder and elbow. Tracking errors converge to zero and there is no significant mutual impact between position and stiffness control. During the transients, a small position tracking error is induced due to the residual coupling between the joints.

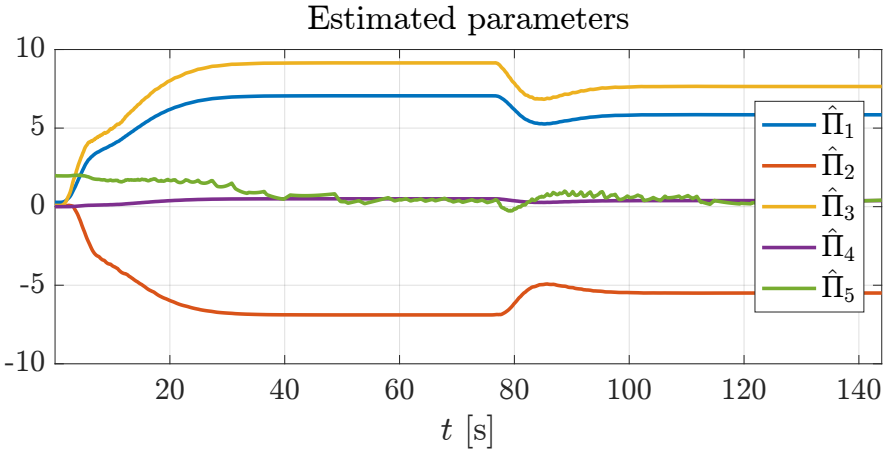

Figure 10.13: Evolution of the estimated parameter vector for the experiment shown in Fig. 10.12. Parameter estimates are adjusted at the beginning of the experiment and then remain bounded.

$$\begin{aligned}\frac{\partial \tau_{*,2}}{\partial q_2} &= \left(\left(\dot{q}_1^2 + \tfrac{1}{2}\dot{q}_1\dot{q}_2 - \tfrac{1}{2}\dot{q}_{1,r}\dot{q}_2\right)\cos q_2 - \ddot{q}_{1,r}\,\sin q_2\right)\hat{\Pi}_3 + \\ &+ \cos q_1 + q_2\,\hat{\Pi}_5 - K_{2,d}\,\Lambda_2\,.\end{aligned}$$

Accordingly, no joint acceleration and jerk are also needed for the two-DoF case.

The shoulder joint is commanded to simultaneously follow smoothed stepwise trajectories ranging from 0 to 0.25 radians for the positions, and 17 to 19 Nm/rad for the stiffness; the elbow joint is required to track smoothed stepwise trajectories ranging from 0 to 0.15 radians for the positions, and 12 to 14 Nm/rad for the stiffness. The obtained results in Fig. 10.12 show that independent and simultaneous tracking capabilities for both position and stiffness desired evolution are achieved, while the estimated parameters converge as depicted in Fig. 10.13. As anticipated, the largest tracking error is observed during the adaptation phase, which is due to the parameter uncertainty, and during the position transients, caused by the residual coupling between joints. The change of stiffness reference has a negligible impact on the position. Thus, the effectiveness of proposed method has been confirmed also for multi-DoF setups.

10.4 Comparison with feedback linearization

The groundwork for the feedback linearization method, applied to the soft robots with variable stiffness actuators in the antagonistic setup has been laid by the authors of Jovanović et al. (2017), Palli et al. (2008). In this section very same approach is used for pneumatic soft robot - the nonlinear system dynamics is transformed by the appropriate control law into the chain of integrators, so that system becomes linear.

10.4.1 Feedback linearization

Consider two degree-of-freedom soft robot with the position and pressure dynamics presented in the state-space form:

$$\begin{aligned}\dot{x} &= f(x) + g(x)\,u \\ y &= h(x)\end{aligned} \tag{10.12}$$

where outputs are $y = (q_1, q_2, \sigma_1, \sigma_2)^T$, inputs are $u = (p_{c,1,a}, p_{c,1,b}, p_{c,2,a}, p_{c,2,b})^T$, and states are $x = (q_1, q_2, \dot{q_1}, \dot{q_2}, p_{1,a}, p_{1,b}, p_{2,a}, p_{2,b})^T$. The first step implies differentiating each output until the input variable appears. If the sum of both outputs orders is equal to the number of states, then full linearization can be achieved. It is straightforward to calculate that the direct relation between outputs (position and stiffness) and commanded pressure is obtained when position is derived three times and stiffness once:

$$\begin{aligned}q_1^{(3)} &= L_f^3 h_{q,1}(x) + E_{1,1}p_{c,1,a} + E_{1,2}p_{c,1,b} + E_{1,3}p_{c,2,a} + E_{1,4}p_{c,2,b}\,, \\ q_2^{(3)} &= L_f^3 h_{q,2}(x) + E_{2,1}p_{c,1,a} + E_{2,2}p_{c,1,b} + E_{2,3}p_{c,2,a} + E_{2,4}p_{c,2,b}\,, \\ \dot{\sigma}_1 &= L_f h_{\sigma,1}(x) + E_{3,1}p_{c,1,a} + E_{3,2}p_{c,1,b} + E_{3,3}p_{c,2,a} + E_{3,4}p_{c,2,b}\,, \\ \dot{\sigma}_2 &= L_f h_{\sigma,2}(x) + E_{4,1}p_{c,1,a} + E_{4,2}p_{c,1,b} + E_{4,3}p_{c,2,a} + E_{4,4}p_{c,2,b}\,,\end{aligned} \tag{10.13}$$

where $E_{i,j}$ for $i = 1, \cdots, 4$, $j = 1, \cdots, 4$ is element of matrix E. As the sum of orders for both positions and stiffness is equal to the number of states, one can conclude that all states are fully observable as a result of having no zero dynamics. It can be concisely written as:

$$\begin{pmatrix} q^{(3)} \\ \dot{\sigma} \end{pmatrix} = \begin{pmatrix} L_f^3 h_q(x) \\ L_f h_\sigma(x) \end{pmatrix} + E \begin{pmatrix} p_{c,1,a} \\ p_{c,1,b} \\ p_{c,2,a} \\ p_{c,2,b} \end{pmatrix}, \tag{10.14}$$

with the control input:

$$\begin{pmatrix} p_{c,1,a} \\ p_{c,1,b} \\ p_{c,2,a} \\ p_{c,2,b} \end{pmatrix} = E^{-1} \left(- \begin{pmatrix} L_f^{(3)} h_q(x) \\ L_f h_\sigma(x) \end{pmatrix} + \begin{pmatrix} v_{q,1} \\ v_{q,2} \\ v_{\sigma,1} \\ v_{\sigma,2} \end{pmatrix} \right) , \tag{10.15}$$

where $v_{q,1}$, $v_{q,2}$, $v_{\sigma,1}$ and $v_{\sigma,2}$ are newly-introduced inputs, chosen such that for given desired trajectory of position $q_{d,i}$ and stiffness $\sigma_{d,i}$ following polynomials are Hurwitz:

$$\begin{gathered} v_{q,i} = q_{d,i}^{(3)} + K_{q,2}(\ddot{q}_{d,i} - \ddot{q}_i) + K_{q,1}(\dot{q}_{d,i} - \dot{q}_i) + K_{q,0}(q_{d,i} - q_i) \, , \\ v_{\sigma,i} = \dot{\sigma}_{d,i} + K_{\sigma,0}(\sigma_{d,i} - \sigma_i) \, . \end{gathered} \tag{10.16}$$

10.4.2 Simulation Results and Discussion

The proposed control approach for soft-robots has been validated in Matlab/Simulink environment on a two DoF soft robot arm actuated by antagonistic McKibben artificial muscles. Recalling the well-known dynamic model of robot, the inertial matrix of the robot arm dynamic model is given by

$$B = \begin{bmatrix} B_{11} & B_{12} \\ B_{21} & B_{22} \end{bmatrix} , \tag{10.17}$$

where $B_{11} = I_1 + m_1(\frac{1}{2}l_1)^2 + I_2 + m_2 l_1^2 + m_2(\frac{1}{2}l_2)^2 + m_2 l_1 l_2 \cos q_2$, $B_{12} = I_2 + m_2(\frac{1}{2}l_2)^2 + \frac{1}{2}m_2 l_1 l_2 \cos q_2$, $B_{21} = B_{12}$, $B_{22} = \frac{1}{2}m_2 l_2^2 + I_2$ with I_n being the identity matrix of dimension n. The Coriolis and centrifugal force matrix $C(q, \dot{q})$ and the gravity vector G are

$$C(q,\dot{q}) = \begin{bmatrix} h\dot{q}_2 & h(\dot{q}_1 + \dot{q}_2) \\ -h\dot{q}_1 & 0 \end{bmatrix} \begin{bmatrix} \dot{q}_1 \\ \dot{q}_2 \end{bmatrix} , \; G = \begin{bmatrix} (\frac{1}{2}m_1 l_1 g + m_2 l_1 g)\cos q_1 + \frac{1}{2}m_2 l_2 g \cos q_1 + q_2 \\ \frac{1}{2}m_2 l_2 g \cos q_1 + q_2 \end{bmatrix} . \tag{10.18}$$

The dynamic model parameters of the robot are the following: $m_1 = 0.44$ kg and $m_2 = 0.35$ kg are masses, $l_1 = 0.33$ m and $l_2 = 0.225$ m are link lengths, $I_1 = 0.004\text{kgm}^2$ and $I_2 = 0.0015\text{kgm}^2$ are link inertias, for both degrees of freedom.

Regarding the feedback linearization approach, all roots of the Hurwitz polynomials $v_{q,1}$, $v_{q,2}$, $v_{\sigma,1}$, and $v_{\sigma,2}$ have been chosen equal to -1, while the gains of the decoupling adaptive controller are set to $\Lambda = 1$, $K_d = 1$, and $K_\pi = 20$. As already discussed in Palli et al. (2008), position and stiffness reference trajectories need to be differentiable up to the third and first order, respectively, so that their asymptotic tracking can be achieved. The simulations have been designed in a way that robustness of methods is verified with respect to dynamic parameter uncertainty, when both position and stiffness of the soft robot's joints are varying. The uncertainty of parameters is set to 1% since the apparent difference between those two approaches can already be noticed.

As shown in Fig. 10.14 (a) and (c), feedback linearization and decoupling adaptive control have a similar performance when parameters are precisely known, achieving satisfactory tracking of both position and stiffness. It can also be observed that when the feedback linearization approach is used, stiffness does not get affected at all by the variations of position, while small transient effects occur for the case of the adaptive approach. The source for these transients may lay in the calculation of actuator matrix pseudoinverse.

However, when the values of dynamic model parameters are reduced by 1% compared to their real value, the difference in performance achieved by the two methods becomes quite noticeable. In accordance with the previous results in the literature, the position is tracked with a constant error when the feedback linearization approach is used Fig. 10.14 (b). On the

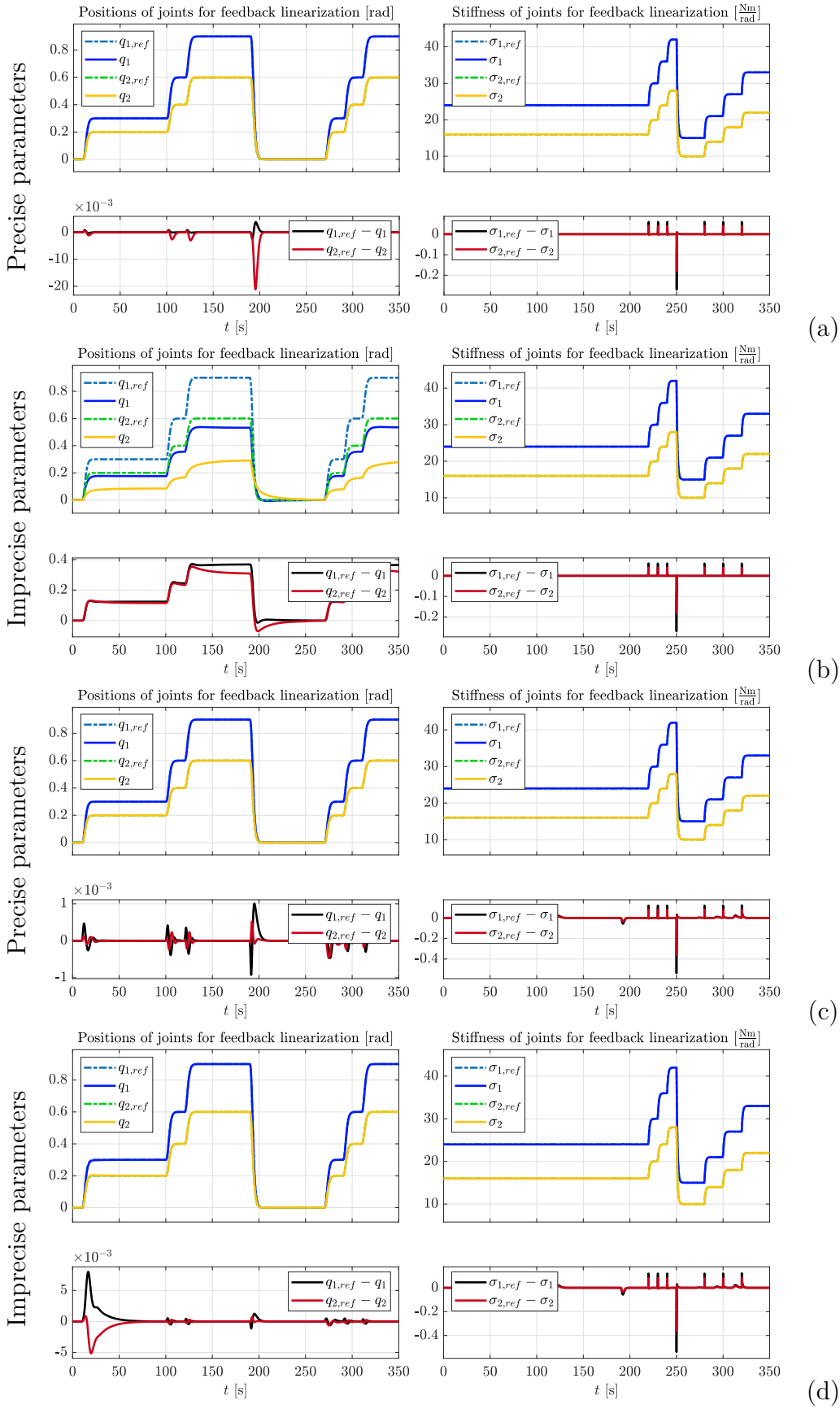

Figure 10.14: Positions and stiffnesses of joints for feedback linearization approach with precise (a) and 1 % imprecise (b) dynamic parameters, and adaptive approach with precise (c) and 1 % imprecise (d) parameters

other hand, the adaptive control scheme manages to cope with the uncertainty of parameters, once those dynamic parameters are learned, and achieves good performance in tracking desired position and stiffness references, Fig. 10.14 (d). The tracking of stiffness is not affected by the uncertainty of dynamic parameters, as there is no mutual dependency. Indeed, the robustness of the feedback linearization approach can be improved by raising the gain values as shown in Potkonjak et al. (2011), but high gains affect the natural compliance of a soft robot and make practical implementation challenging.

10.5 Conclusion

In this section a novel approach for adaptive and decoupling control of position and stiffness in pneumatic soft-robots has been presented. The approach achieves the desired decoupling by using the control degree of freedom, laying in the kernel of known part of the actuator matrix, plus an additional dynamic compensation that is made available by the introduction of the stiffness dynamics. The approach has been validated first via simulations and through experiments with a two-degree-of-freedom robot soft robot. Validation has shown that joint position and stiffness are effectively tracked in different use-cases. A formal proof of the stability of the tracking error for the approach has also been provided.

The solution has shown to have several advantages. First, it is robust to model uncertainties and, if stiffness reference is constant or slowly-varying, also to actuator uncertainties. Secondly, it requires computation of only the first time derivative of stiffness and of the second time derivative of position. No further differentiation is needed, thus simplifying practical implementations. Third, it allows joint stiffness to be controlled in closed loop, thereby making the system more capable of following various position trajectory profiles, as shown in experiments. Practically, this means that joints can achieve faster movements (even with lower stiffness) when compared to the open-loop case, hence potentially improving the safety of soft robots when used for human-robot interaction.

The main limitation of the current approach stems in the assumption that part of the actuator model is known, which has required performing an initial identification phase. However, we believe that the approach can be generalized for fully unknown actuator matrices, as well as for different classes of pneumatically and electrically driven soft robots. This objective can be achieved e.g. by using stiffness estimators, which would allow better estimation of the stiffness and thus more effective closed-loop control. A second limitation of the current hardware is related to the present mechanical coupling among joint pulleys, shafts, and muscles, which is unable to effectively support fast motions without experiencing slippage and inducing measurement errors. Albeit slower experiments have been shown, we are confident that better results can be achieved with a future hardware upgrade by adopting better mechanical solutions for such connections and using more consistent materials for the artificial muscles. With the same objective of achieving faster motions, but with a different type of actuators, some seminal work has already been initiated by Lukic et al. (2019), with an electric antagonistic VSA setup characterized by more reliable mechanical structures and faster natural dynamics.

It is also worth saying that the scalability of the proposed method, and in fact that of other adaptive control approaches, relies on the derivation of the regressor form of a robot's dynamics. To this respect, very recently, novel approaches, such as that by Marcucci et al. (2017a), have introduced automatic generation methods, aiming at reducing the amount of information needed to model and control a robot manipulator, and thus also potentially improving the efficiency of the proposed solution.

Chapter 11

Soft articulated robots with electro-mechanic drives

This chapter presents a decoupled nonlinear adaptive control for sfot articulated robots with the electro-mechanical drive. Similarly to the line of research by Palli et al. (2008), vectors of links position q and joints stiffness σ are chosen as system outputs on which the loop is closed. The proposed approach, however, differs in multiple ways.

The first contribution is that the adaptive control law is used for controlling the considered system in the cascaded way. Therefore, parametric uncertainties on both motor and link side are addressed. The inner-loop controller is designed to achieve the asymptotic tracking of the desired motors positions while the outer-loop one takes care of position and stiffness tracking, such that when $q_{i,j} \longrightarrow q_{i,j,des}$, then $q_i \longrightarrow q_{i,des}$ and $|\sigma_i - \sigma_{i,des}| < \epsilon$. The extensive research on cascade strategy including the one for rigid robots driven by AC motors is sublimed by Ortega et al. (2013), while the following sections differ in a way that robots have an antagonistic VSA drive. Secondly, the decoupling property of the proposed technique is achieved by leveraging on the explicit relation between stiffness and flexibility torques generated from motors which leads, eventually, to the necessity of only first order derivative of the position variable. To obtain an explicit relation, one needs to assume that the flexibility torque has a sine hyperbolic dependency on the transmission deflection. This is indeed often the case in the existing solutions (qbmove Centro Piaggio (2011)). Finally, compared to the recent solution of decoupling motion and stiffness (Mengacci et al. (2020)), the herein shown approach takes into account also dynamics of actuators.

The chapter starts by modifying the model of a soft articulated robot in order to satisfy the assumption on the explicit stiffness-flexibility torque relation. It continues by proposing the PD plus feedforward term based control that assumes the accurate knowledge of system parameters, and finishes by presenting the novel control approach based on the adaptive technique.

11.1 Design of the control law

To decouple the position and stiffness control, it becomes necessary to express the first derivative of stiffness as a function of local flexibility torques. Therefore, it is straightforward to conclude that the model of flexibility torque should satisfy the following condition

$$\frac{\partial^2 \tau_j^e}{\partial \phi_j^2} = k\, \tau_j^e \,,$$

where $j = a, b$ denote agonist and antagonist drive. The solution of this differential equation leads to the conclusion that τ_j^e should comprise functions of the exponential type. Moreover,

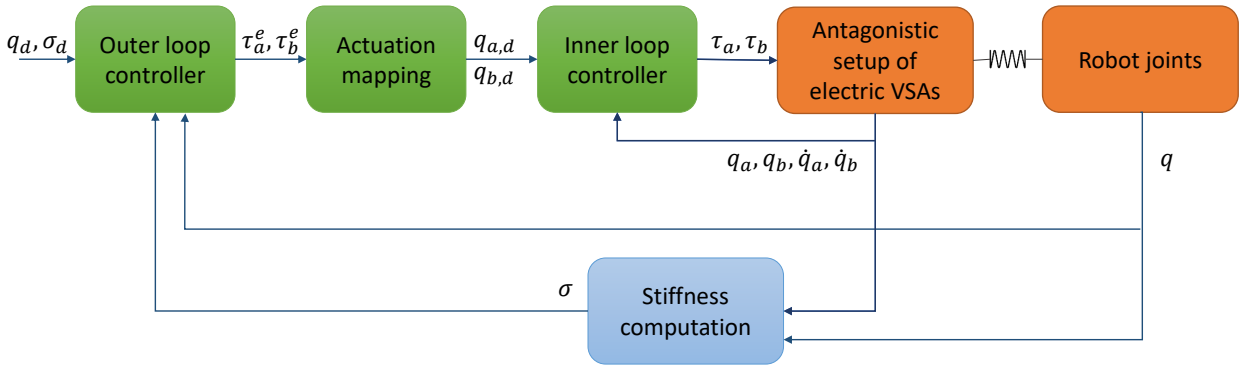

Figure 11.1: Depiction of the proposed cascaded control.

building upon the assumption that τ_j^e is odd and function of the transmission deflection ϕ_j, the sine hyperbolic representation of flexibility torque is adopted

$$\tau_j^e = \frac{k_j}{2} e^{a_j \phi_j} - \frac{k_j}{2} e^{-a_j \phi_j} = k_j \sinh a_j \phi_j \,.$$

with k_j and a_j being free parameters.

Accordingly, the total flexibility torque states

$$\tau^e = \tau_a^e(\phi_a) + \tau_b^e(\phi_b) = k_a \sinh(a_a \phi_a) + k_b \sinh(a_b \phi_b) \,,$$

which by definition leads to the following expressions for stiffness in robot i-th joint and its time derivative

$$\begin{aligned} \sigma &= k_a a_a \cosh(a_a \phi_a) + k_b a_b \cosh(a_b \phi_b) \,, \\ \dot{\sigma} &= k_a a_a^2 \sinh(a_a \phi_a) \dot{\phi}_a + k_b a_b^2 \sinh(a_b \phi_b) \dot{\phi}_b \\ &= a_a^2 \tau_a^e(\phi_a) \dot{\phi}_a + a_b^2 \tau_b^e(\phi_b) \dot{\phi}_b \,. \end{aligned}$$

Therefore, a full model of a robot driven by the electric VSAs states

$$B(q)\,\ddot{q} + C(q,\dot{q})\dot{q} + G(q) = -\tau_a^e(\phi_a) - \tau_b^e(\phi_b) \,, \tag{11.1a}$$

$$\dot{\sigma} = a_a^2 \tau_a^e(\phi_a) \dot{\phi}_a + \alpha_b^2 \tau_b^e(\phi_b) \dot{\phi}_b \,, \tag{11.1b}$$

$$B_a\,\ddot{q}_a + D_a\,\dot{q}_a - \tau_a^e(\phi_a) = \tau_a \,, \tag{11.1c}$$

$$B_b\,\ddot{q}_b + D_b\,\dot{q}_b - \tau_b^e(\phi_b) = \tau_b \,. \tag{11.1d}$$

The block diagram of the proposed control is presented in Fig. 11.1.

11.1.1 PD augmented control

Consider, for the beginning, a PD augmented control of soft robot driven by electro-mechanical VSAs, which assumes the knowledge of parameters. Therefore, first a theorem considering the inner loop control is derived, followed by the one of the outer loop.

Inner loop control of motors positions

Theorem 6. *Given an antagonistic setup of direct current motors, whose dynamics is described by Eq. 11.1c and 11.1d, the global asymptotic tracking of trajectories* $q_{a,d} : [0, \infty) \longrightarrow \mathbb{R}^n$ *and*

$q_{b,d} : [0, \infty) \longrightarrow \mathbb{R}^n$ *is achieved with the following control law*

$$\begin{array}{rcl} \tau_a & = & D_a\dot{q}_a - \tau_a^e(\phi_a) + \\ & & B_a\left(\ddot{q}_{a,d} - k_{p,a}(q_a - q_{a,d}) - k_{d,a}(\dot{q}_a - \dot{q}_{a,d})\right) , \\ \tau_b & = & D_b\dot{q}_b - \tau_b^e(\phi_b) + \\ & & B_b\left(\ddot{q}_{b,d} - k_{p,b}(q_b - q_{b,d}) - k_{d,b}(\dot{q}_b - \dot{q}_{b,d})\right) . \end{array} \tag{11.2}$$

where k_p and k_d are proportional and derivative gains, respectively.

Proof. Since the proof is equivalent for both motors, below is shown the procedure for the agonistic set of drives only.

Consider the Lyapunov function candidate

$$V_a = \frac{1}{2} s_a^T s_a \, ,$$

where $s_a = \dot{q}_a - \dot{q}_{a,d} + \Lambda_a(q_a - q_{a,d})$, and whose time derivative is

$$\dot{V}_a = s_a^T \dot{s}_a = s_a^T \left(\ddot{q}_a - \ddot{q}_{a,d} + \Lambda_a(\dot{q}_a - \dot{q}_{a,d})\right) .$$

Replacing $\ddot{q}_a$ with its value obtained from the model in Eq. 11.1c yields:

$$\dot{V}_a = s_a^T \left(B_a^{-1}(-D_a\dot{q}_a + \tau_a^e + \tau_a) - \ddot{q}_{a,d} + \Lambda_a(\dot{q}_a - \dot{q}_{a,d})\right) .$$

and substituting the control law proposed in Eq. 11.2 leads to

$$\dot{V}_a = -s_a^T k_a s_a \, ,$$

for $k_{d,a} = \Lambda_a + k_a$ and $k_{p,a} = \Lambda_a k_a$. The convergence of tracking error to zero is ensured since the second time derivative of Lyapunov candidate V_a is lower bounded. □

Outer loop control of link position and joint stiffness

Once convergence of the inner loop is obtained, the fact that $q_a \to q_{a,d}$ and $q_b \to q_{b,d}$ ensures the achievability of local flexibility torques necessary for the position and stiffness control via the following relation

$$\begin{array}{l} q_{a,d} = q - \frac{1}{a_a}\text{asinh}(\frac{\tau_a^e}{k_a}) \\ q_{b,d} = q - \frac{1}{a_b}\text{asinh}(\frac{\tau_b^e}{k_b}) \end{array} \, , \tag{11.3}$$

which is smooth and invertible.

Therefore, the derivation of the outer-loop decoupled control law of position and stiffness follows.

Theorem 7. *To achieve the asymptotic tracking of the desired links positions $q_d : [0, \infty) \longrightarrow \mathbb{R}^n$ with $q_d(t) \in C^2$ and bounded-error tracking of joints stiffness $\sigma_d(t) : [0, \infty) \longrightarrow \mathbb{R}^n$, such that $\sigma_d(t) \in C^1$, the following local elastic torques have to be applied to Eq. 11.1a and 11.1b:*

$$\begin{pmatrix} \tau_a^e \\ \tau_b^e \end{pmatrix} = \begin{pmatrix} -1 & -1 & \dots & 0 & 0 \\ \vdots & \vdots & \ddots & \vdots & \vdots \\ 0 & 0 & \dots & -1 & -1 \\ \gamma_1^a + \Delta_1 & \gamma_1^b - \Delta_1 & \dots & 0 & 0 \\ \vdots & \vdots & \ddots & \vdots & \vdots \\ 0 & 0 & \dots & \gamma_n^a + \Delta_n & \gamma_n^b - \Delta_n \end{pmatrix}^{-1} \begin{pmatrix} C\dot{q} + G + B(\ddot{q}_d - k_d\dot{e} - k_p e) \\ \\ \dot{\sigma}_d - k_\sigma e_\sigma \end{pmatrix}, \tag{11.4}$$

where $\gamma_i^a = a_{a,i}^2(\dot{q}_i - \dot{q}_{a,i})$, $\gamma_i^b = a_{b,i}^2(\dot{q}_i - \dot{q}_{b,i})$, Δ_i *is the constant term,* k_p, k_d, *and* k_σ *are positive definite diagonal matrices determining the convergence rate of position and stiffness tracking errors, respectively, position sliding variable is defined as* $s = \dot{q} - \dot{q}_r$, $\dot{q}_r = \dot{q}_d - \Lambda e$, *and* $e = q - q_d$; *stiffness tracking error is* $e_\sigma = \sigma - \sigma_d$.

Proof. Consider the following Lyapunov function candidate

$$V = V_q + V_\sigma = \frac{1}{2}s^T s + \frac{1}{2}e_\sigma^T e_\sigma \,,$$

and, for the beginning, focus on the position part, whose time derivative is

$$\dot{V}_q = s^T \dot{s} = s^T(\ddot{q} - \ddot{q}_d + \Lambda\dot{e}) \,.$$

Substituting the link dynamics, it follows

$$\dot{V}_q = s^T \left(B(q)^{-1}(-C(q,\dot{q})\dot{q} - G(q) - \tau^e(\phi_a, \phi_b)) - \ddot{q}_d + \Lambda\dot{e} \right) .$$

and the introduction of the control law:

$$\tau^e = -\left(C\dot{q} + G + B(\ddot{q}_d - k_p(q - q_d) - k_d(\dot{q} - \dot{q}_d))\right) , \tag{11.5}$$

leads to the negative semi-definite Lie derivative of a Lyapunov candidate

$$\dot{V} = -s^T k s \,,$$

where $k_d = \Lambda + k$ and $k_p = k$. The inspection of its second time derivative confirms that the error is asymptotically converging to zero.

Secondly, the Lie derivative of Lyapunov candidate stiffness part states

$$\dot{V}_\sigma = e_\sigma^T \dot{e}_\sigma = e_\sigma^T(\dot{\sigma} - \dot{\sigma}_d) \,,$$

and, following the same principle as in the previous, it comes to

$$\dot{V} = e_\sigma^T(a_a^2(\dot{q} - \dot{q}_a)\tau_a^e + a_b^2(\dot{q} - \dot{q}_b)\tau_b^e - \dot{\sigma}_d) \,.$$

Finally, the substitution of

$$a_a^2(\dot{q} - \dot{q}_a)\tau_a^e + a_b^2(\dot{q} - \dot{q}_b)\tau_b^e = \dot{\sigma}_d - k_\sigma e_\sigma \,, \tag{11.6}$$

leads to

$$\dot{V} = -e_\sigma^T k_\sigma e_\sigma \,.$$

It can be observed from Equations 11.5 and 11.6 that the control for position and stiffness is indeed coupled. This becomes more apparent when these two equations are expressed in the matrix form. For the sake of simplicity consider the single degree-of-freedom case:

$$\begin{pmatrix} -1 & -1 \\ a_a^2(\dot{q}-\dot{q}_a) & a_b^2(\dot{q}-\dot{q}_b) \end{pmatrix} \begin{pmatrix} \tau_a^e \\ \tau_b^e \end{pmatrix} = \begin{pmatrix} C(q,\dot{q})\dot{q} + G(q) + B(\ddot{q}_d - k_d\dot{e} - k_p e) \\ \dot{\sigma}_d - k e_\sigma \end{pmatrix} \tag{11.7}$$

Thus, to determine the explicit control law for τ_a^e and τ_b^e the inversion has to be performed leading to

$$\begin{pmatrix} \tau_a^e \\ \tau_b^e \end{pmatrix} = \begin{pmatrix} -1 & -1 \\ a_a^2(\dot{q}-\dot{q}_a) & a_b^2(\dot{q}-\dot{q}_b) \end{pmatrix}^{-1} \begin{pmatrix} C(q,\dot{q})\dot{q} + G(q) + B(\ddot{q}_d - k_d\dot{e} - k_p e) \\ \dot{\sigma}_d - k_\sigma e_\sigma \end{pmatrix}$$

However, one can notice from the previous that the matrix subject to inversion may become singular when the elements of the last row become equal, i.e. $a_a^2(\dot{q}-\dot{q}_a) = a_b^2(\dot{q}-\dot{q}_b)$. In order to avoid the ill condition without distorting the position of the robot, the following equilibrium of the net momenta needs to be achieved:

$$\Delta(\tau_a^e - \tau_b^e) = 0\,,$$

where $\Delta = \mathrm{diag}(\Delta_i)$, implying the control law in Eq. 11.4. □

Remark 9. *By observing the determinant of matrix*

$$\begin{pmatrix} -1 & -1 & \dots & 0 & 0 \\ \vdots & \vdots & \ddots & \vdots & \vdots \\ 0 & 0 & \dots & -1 & -1 \\ \gamma_1^a + \Delta_1 & \gamma_1^b - \Delta_1 & \dots & 0 & 0 \\ \vdots & \vdots & \ddots & \vdots & \vdots \\ 0 & 0 & \dots & \gamma_n^a + \Delta_n & \gamma_n^b - \Delta_n \end{pmatrix}$$

it is straighforward to conclude that the singularity can be avoided for Δ_i that is chosen as

$$\Delta_i = a_i^2 |\dot{q}_{i,j,max}|\,,$$

where $j = a, b$ denotes agonistic and antagonistic drive, respectively.

Remark 10. *According to Theorem 7, the position tracking error converges to zero, however, a bounded stiffness tracking error appears due to the Δ term. One can deal with it by increasing*

the gain k_σ or by using an integrator term. In the latter case, the control law gains the form

$$\begin{pmatrix} \tau_a^e \\ \tau_b^e \end{pmatrix} = \begin{pmatrix} -1 & -1 & \dots & 0 & 0 \\ \vdots & \vdots & \ddots & \vdots & \vdots \\ 0 & 0 & \dots & -1 & -1 \\ \gamma_1^a + \Delta_1 & \gamma_1^b - \Delta_1 & \dots & 0 & 0 \\ \vdots & \vdots & \ddots & \vdots & \vdots \\ 0 & 0 & \dots & \gamma_n^a + \Delta_n & \gamma_n^b - \Delta_n \end{pmatrix}^{-1} \times \begin{pmatrix} C\dot{q} + G + B(\ddot{q}_d - k_d\dot{e} - k_p e) \\ \\ \dot{\sigma}_d - k_\sigma e_\sigma - k_I \int e_\sigma \mathrm{d}t \end{pmatrix}, \tag{11.8}$$

with k_I being the positive definite matrix.

11.1.2 Decoupled Nonlinear Adaptive Control

The adaptive control approach allows to manage the soft robot system even in the circumstances when the dynamic parameters of link and motors are uncertain. Again, a cascaded formulation of the control is adopted, with link position and stiffness being controlled in the outer loop, while motors positions are controlled within the inner loop.

Inner loop control of motors positions

Theorem 8. *The global asymptotic tracking of the desired trajectories $q_{a,d} : [0, \infty) \longrightarrow \mathbb{R}^n$ and $q_{b,d} : [0, \infty) \longrightarrow \mathbb{R}^n$, such that $q_{a,d}, q_{b,d} \in C^2$ is achieved via the following control laws*

$$\begin{aligned} \tau_a &= Y_a\hat{\pi}_a - \tau_a^e - k_a s_a \,, \\ \dot{\hat{\pi}}_a &= -k_{\pi_a} Y_a^T s_a \,, \\ \tau_b &= Y_b\hat{\pi}_b - \tau_b^e - k_b s_b \,, \\ \dot{\hat{\pi}}_b &= -k_{\pi_b} Y_b^T s_b \,, \end{aligned} \tag{11.9}$$

where $k_{\pi_a} = \mathrm{diag}(k_{\pi_{1,a}}, k_{\pi_{2,a}})$ and $k_{\pi_b} = \mathrm{diag}(k_{\pi_{1,b}}, k_{\pi_{2,b}})$ determine the rate of parameter estimate convergence.

Proof. For the convenience, consider only the agonistic set of drives and take the Lyapunov function candidate

$$V_a = \frac{1}{2} s_a^T B_a s_a + \frac{1}{2} \tilde{\pi}_a^T k_{\pi_a} \tilde{\pi}_a \,,$$

whose Lie derivative is equal to

$$\begin{gathered} \dot{V}_a = s_a^T B_a \dot{s}_a + \tfrac{1}{2} s_a^T \dot{B}_a s_a - \tilde{\pi}_a^T k_{\pi_a} \dot{\hat{\pi}}_a = \\ s_a^T B_a (\ddot{q}_a - \ddot{q}_{a,d} + \Lambda_a \dot{e}_a) - \tilde{\pi}_a^T k_{\pi_a} \dot{\hat{\pi}}_a \,. \end{gathered}$$

where $\dot{B}_a$ is null since it is a constant matrix. Substituting the acceleration in the derivative of Lyapunov function candidate as follows

$$\begin{aligned} \dot{V}_a &= s_a^T B_a \left(B_a^{-1}(-D_a\dot{q}_a + \tau_a^e + \tau_a) - \ddot{q}_{a,d} + \Lambda_a \dot{e}_a \right) - \tilde{\pi}_a^T k_{\pi_a} \dot{\hat{\pi}}_a \\ &= s_a^T \left(-B_a(\ddot{q}_{a,d} - \Lambda_a \dot{e}_a) - D_a\dot{q}_a + \tau_a^e + \tau_a \right) - \tilde{\pi}_a^T k_{\pi_a} \dot{\hat{\pi}}_a \\ &= s_a^T \left(-Y_a\pi_a + \tau_a^e + \tau_a \right) - \tilde{\pi}_a^T k_{\pi_a} \dot{\hat{\pi}}_a \end{aligned}$$

and adopting the control laws in Eq. 11.9, leads to

$$\dot{V}_a = s_a^T(-Y_a\tilde{\pi}_a - k_a s_a) - \tilde{\pi}_a^T k_{\pi_a}\dot{\hat{\pi}}_a = \\ -s_a^T k_a s_a - \tilde{\pi}_a^T(Y_a^T s_a + k_{\pi_a}^{-1}\dot{\hat{\pi}}_a)$$

Finally, it stands that $\dot{V}_a = -k_a s_a^2$. □

Outer loop control of link positions and joint stiffnesses

Once convergence of the inner loop is obtained, the fact that $q_a \to q_{a,d}$ and $q_b \to q_{b,d}$ ensures the achievability of local flexibility torques necessary for the position and stiffness control via the following relation

$$\begin{array}{l} q_{a,d} = q - \frac{1}{a_a}\text{asinh}(\frac{\tau_a^e}{k_a^e}) \\ q_{b,d} = q - \frac{1}{a_b}\text{asinh}(\frac{\tau_b^e}{k_b}) \end{array} , \tag{11.10}$$

which is smooth and invertible.

Theorem 9. *Assume that the Propositions 1, 2, 3 and 4 hold. Then, the desired trajectories of links positions and joints stiffness $q_d : [0,\infty) \longrightarrow \mathbb{R}^n$ with $q_d(t) \in C^2$ and $\sigma_d(t) : [0,\infty) \longrightarrow \mathbb{R}^n$, such that $\sigma_d \in C^1$ are effectively tracked by adopting the following control laws*

$$\begin{pmatrix} \tau_a^e \\ \tau_b^e \end{pmatrix} = \begin{pmatrix} -1 & -1 & \dots & 0 & 0 \\ \vdots & \vdots & \ddots & \vdots & \vdots \\ 0 & 0 & \dots & -1 & -1 \\ \gamma_1^a + \Delta_1 & \gamma_1^b - \Delta_1 & \dots & 0 & 0 \\ \vdots & \vdots & \ddots & \vdots & \vdots \\ 0 & 0 & \dots & \gamma_n^a + \Delta_n & \gamma_n^b - \Delta_n \end{pmatrix}^{-1} \times \begin{pmatrix} Y(q,\dot{q},\dot{q}_r,\ddot{q}_r)\hat{\pi} - ks \\ \\ \dot{\sigma}_d - k_\sigma e_\sigma \end{pmatrix},$$

$$\dot{\hat{\pi}} = -k_\pi Y^T s\,, \tag{11.11}$$

where $Y(q,\dot{q},\dot{q}_r,\ddot{q}_r)\hat{\pi} = \hat{B}(q)\ddot{q}_r + \hat{C}(q,\dot{q})\dot{q}_r + \hat{G}(q)$ stands, with Y being a regressor matrix and $\hat{\pi}$ the vector of the uncertain parameters.

Proof. Consider the Lyapunov function candidate

$$V = V_q + V_\sigma\,,$$

where

$$V_q = \frac{1}{2}s^T B s + \frac{1}{2}\tilde{\pi}^T k_\pi \tilde{\pi}\,, \text{ and } V_\sigma = \frac{1}{2}e_\sigma^T e_\sigma\,.$$

The Lie derivative of the position term is derived as

$$\begin{array}{rcl} \dot{V}_q & = & s^T B(q)\dot{s} + \frac{1}{2}s^T\dot{B}(q)s - \tilde{\pi}k_\pi\dot{\hat{\pi}} \\ & = & s^T B(q)(\ddot{q} - \ddot{q}_d + \Lambda\dot{e}) + \frac{1}{2}s^T\dot{B}(q)s - \tilde{\pi}k_\pi\dot{\hat{\pi}} = \\ & = & s^T B(q)(B(q)^{-1}(-C(q,\dot{q})\dot{q} - G(q) - \tau_e) - \ddot{q}_d + \Lambda\dot{e}) + \frac{1}{2}s^T\dot{B}(q)s - \tilde{\pi}k_\pi\dot{\hat{\pi}} \\ & = & s^T(-C(q,\dot{q})\dot{q} - G(q) - B(q)(\ddot{q}_d - \Lambda\dot{e}) - \tau_e) + \frac{1}{2}s^T\dot{B}(q)s - \tilde{\pi}k_\pi\dot{\hat{\pi}}\,. \end{array}$$

where the skew-symmetry property can smoothly be used to avoid the appearance of $\dot{B}(q)$, since

$$s^T(\frac{1}{2}(\dot{B} - 2C) + C)s = s^T C s\,.$$

This further leads to

$$\dot{V} = s^T(-\tau_e - B(q)\ddot{q}_r - C(q,\dot{q})\dot{q}_r - G(q)) - \tilde{\pi}k_\pi\dot{\hat{\pi}}\,.$$

Now, exploiting the elastic torque from Eq. 11.11 the derivative of Lyapunov function becomes

$$\dot{V} = s^T(Y\hat{\pi} - Y\pi - ks) - \tilde{\pi}k_\pi\dot{\hat{\pi}} = -s^Tks - s^T(Y\tilde{\pi} + \tilde{\pi}k_\pi\dot{\hat{\pi}})$$

and substituting the parameters update law from the same Eq. 11.11, it finally stands $\dot{V} = -s^Tks$.

Concerning the stiffness part of Lyapunov function candidate, the procedure of finding its derivative is equivalent to the one in the previous section.

Finally, the following relation stands

$$\begin{pmatrix} -1 & -1 \\ a_a^2(\dot{q}-\dot{q}_a) & a_b^2(\dot{q}-\dot{q}_b) \end{pmatrix}\begin{pmatrix}\tau_a^e \\ \tau_b^e\end{pmatrix} = \begin{pmatrix} Y(q,\dot{q},\dot{q}_r,\ddot{q}_r)\hat{\pi} - ks \\ \dot{\sigma}_d - ke_\sigma \end{pmatrix} \tag{11.12}$$

whose ill condition occurs when $\alpha_a^2(\dot{q}-\dot{q}_a) = \alpha_b^2(\dot{q}-\dot{q}_b)$ which, again, can be cured by following the principle described above and introducing the Δ term. □

Remark 9 holds for the adaptive approach as well, while Remark 10 is slightly modified:

Remark 11. *According to Theorem 9, the position tracking error converges to zero, however, a bounded stiffness tracking error appears due to the Δ term. One can deal with it by increasing the gain k_σ or by using an integrator term. In the latter case, the control law gains the form*

$$\begin{pmatrix}\tau_a^e \\ \tau_b^e\end{pmatrix} = \begin{pmatrix} -1 & -1 & \dots & 0 & 0 \\ \vdots & \vdots & \ddots & \vdots & \vdots \\ 0 & 0 & \dots & -1 & -1 \\ \gamma_1^a + \Delta_1 & \gamma_1^b - \Delta_1 & \dots & 0 & 0 \\ \vdots & \vdots & \ddots & \vdots & \vdots \\ 0 & 0 & \dots & \gamma_n^a + \Delta_n & \gamma_n^b - \Delta_n \end{pmatrix}^{-1} \times \begin{pmatrix} Y(q,\dot{q},\dot{q}_r,\ddot{q}_r)\hat{\pi} - ks \\ \\ \dot{\sigma}_d - k_\sigma e_\sigma - k_I\int e_\sigma \mathrm{d}t \end{pmatrix},$$

$$\dot{\hat{\pi}} = -k_\pi Y^T s\,, \tag{11.13}$$

with k_I being the positive definite matrix.

11.2 Simulation results

The simulations in this section show performance of a two degree-of-freedom soft robot when augmented PD and adaptive control are applied. The main difference stems in the fact that adaptive controller does not require the knowledge of parameters. It will be observed that the introduction of an integral term leads to the reduced error in stiffness tracking.

Considering q_1 and q_2 as robot configuration variables, inertia, Coriolis matrix, and gravity vector have the same form as in the previous chapter, where pneumatically driven soft robot was observed, while the numerical values of the dynamic parameters are presented in Tab 11.1. Moreover, motors dynamics is determined by parameters in Tab. 11.2 and expressed via the

following differential equations

$$\begin{pmatrix} b_{1,a} & 0 \\ 0 & b_{2,a} \end{pmatrix} \begin{pmatrix} \ddot{q}_{1,a} \\ \ddot{q}_{2,a} \end{pmatrix} + \begin{pmatrix} d_{1,a} & 0 \\ 0 & d_{2,a} \end{pmatrix} \begin{pmatrix} \dot{q}_{1,a} \\ \dot{q}_{2,a} \end{pmatrix} - \begin{pmatrix} \tau^e_{1,a} \\ \tau^e_{2,a} \end{pmatrix} = \begin{pmatrix} \tau_{1,a} \\ \tau_{2,a} \end{pmatrix}$$

$$\begin{pmatrix} b_{1,b} & 0 \\ 0 & b_{2,b} \end{pmatrix} \begin{pmatrix} \ddot{q}_{1,b} \\ \ddot{q}_{2,b} \end{pmatrix} + \begin{pmatrix} d_{1,b} & 0 \\ 0 & d_{2,b} \end{pmatrix} \begin{pmatrix} \dot{q}_{1,b} \\ \dot{q}_{2,b} \end{pmatrix} - \begin{pmatrix} \tau^e_{1,b} \\ \tau^e_{2,b} \end{pmatrix} = \begin{pmatrix} \tau_{1,b} \\ \tau_{2,b} \end{pmatrix}$$

Finally, the model of a soft robot is completed with the mapping between motors and links positions, and generated flexibility torque as follows

$$\tau^e_{1,a} = k_{1,a} \sinh a_{1,a}(q_1 - q_{1,a}) \, , \tau^e_{1,b} = k_{1,b} \sinh a_{1,b}(q_1 - q_{1,b}) \, ,$$
$$\tau^e_{2,a} = k_{2,a} \sinh a_{2,a}(q_2 - q_{2,a}) \, , \tau^e_{2,b} = k_{2,b} \sinh a_{2,b}(q_2 - q_{2,b}) \, ,$$

where $a_{i,j}$ and $k_{i,j}$ are spring coefficients, provided in Tab. 11.2.

To show the performance of the augmented PD and adaptive control, positions of both joints are commanded to follow the sinusoidal trajectories $q_d = 1 + 0.5 \sin \frac{\pi}{10} t$, while the desired stiffnesses in joints are set to $\sigma_{1,d} = 8 + 3 \sin \frac{\pi}{8} t$ and $\sigma_{2,d} = 4 + \sin \frac{\pi}{8} t$.

The PD augmented control is first implemented by exploiting Eq. 11.2 and Eq. 11.4, with the results shown in Fig. 11.2, and then by including the integral term within stiffness control (Eq. 11.8) which is shown in Fig. 11.3. The control gains are chosen such that the condition of inner loop being faster than the outer loop is satisfied. Therefore, the inner-loop control gains are $k_{p,a} = k_{p,b} = 50$ and $k_{d,a} = k_{d,b} = 25$. Without the integral term, the outer-loop ones are $k_p = 25$, $k_d = 10$, $k_\sigma = 150$. Otherwise, the gains are $k_p = 0.05$, $k_d = 0.75$, $k_\sigma = 30$, and $k_i = 15$. It can be observed that the desired positions of both motors are well tracked in the inner loop, as well as the link position in the outer loop. Due to the existence of $\Delta_i = 70$, the mean of stiffness tracking error reduces to null value only when the integral action is used.

The second set of simulations considers the nonlinear adaptive controller which uses Eq. 11.9 and Eq. 11.11 to manage position and stiffness, as presented in Fig. 11.4, while the results when an integral term (as in Eq. 11.13) is added are shown in Fig. 11.5. Following the similar reasoning as in case of the augmented PD control, the inner-loop control gains are chosen as $k_{p,a} = k_{p,b} = k_{d,a} = k_{d,b} = 0.1$, $k_{\pi_{1,a}} = 6 \cdot 10^{-4}$, $k_{\pi_{1,b}} = 10^{-4}$, $k_{\pi_{2,a}} = 10^{-3}$, and $k_{\pi_{2,b}} = 10^{-4}$. Without the integral term, outer-loop control gains are $k_p = 0.1$, $k_d = 0.5$, $k_\pi = 0.2$, and $k_\sigma = 20$. Elseways, they are $k_p = 0.1$, $k_d = 0.1$, $k_\pi = 7$, $k_\sigma = 20$, and $k_i = 25$. Again, the term $\Delta_i = 145$ introduces the non-zero mean value which is erased with the means of integral action.

The regressor matrix $Y(q, \dot{q}, \dot{q}_r, \ddot{q}_r)$ has the same form as the one considered in the previous chapter (Eq. 10.9), while regressor matrices of motor system are

$$Y_j = \begin{pmatrix} \ddot{q}_{1,j,d} - \Lambda \dot{e}_{1,j} & \dot{q}_{1,j,d} & 0 & 0 \\ 0 & 0 & \ddot{q}_{2,j,d} - \Lambda \dot{e}_{2,j} & \dot{q}_{2,j,d} \end{pmatrix} ,$$

where $j = a, b$. It is noteworthy that in both cases there is no initial knowledge about dynamic and motor parameters, i.e. $\pi(0) = 0$, $\pi_{i,a}(0) =$, and $\pi_{i,a}(0) =$. Compared to the augmented PD approach, a larger tracking error occurs in the beginning due to the lack of parameter knowledge, however, it is compensated as the parameters are *learned*.

11.3 Conclusion

This chapter has addressed the control of electro-mechanically actuated soft articulated robots with antagonistic VSAs. The two versions of cascade-based strategy have been used to

Table 11.1: Definition and nominal values of the geometric and inertial parameters of the two-link soft robot. The real values of these parameters are assumed unknown when applying adaptive control.

Param.	Value	Unit	Description
m_1	0.26	kg	First link mass
m_2	0.26	kg	Second link mass
l_1	0.09	m	First link length
l_2	0.09	m	Second link length
I_1	0.0021	kgm^2	First link inertia
I_2	0.0021	kgm^2	Second link inertia

Table 11.2: Definition of the actuator model's parameters.

Param.	Value	Unit	Description
$b_{1,a}$	0.001	kgm^2	Agonistic motors inertia
$b_{1,b}$	0.001	kgm^2	Antagonistic motors inertia
$d_{1,a}$	10^{-6}	kgm^2	Agonistic motors damping
$d_{1,b}$	10^{-6}	kgm^2	Antagonistic motors damping
$a_{1,a}$	6.7328	kgm^2	Agonistic motors spring coefficient
$k_{1,b}$	0.0227	kgm^2	Antagonistic motors spring coefficient
$a_{2,a}$	6.9602	kgm^2	Agonistic motors spring coefficient
$k_{2,b}$	0.0216	kgm^2	Antagonistic motors spring coefficient

simultaneously and independently manage link position and joint stiffness in closed loop – augmented PD controller and nonlinear adaptive control. Both approaches achieve the asymptotic tracking of position and have bounded error when it comes to stiffness tracking, which can be compensated by taking into account the integral of stiffness error. Performance of the proposed controllers is verified on a two-degree-of-freedom soft robot within the simulation environment and it is shown that tracking of the desired position and stiffness trajectories with sinusoidal evolution has been effectively achieved.

The advantages of the proposed method are compliant to the ones in the previous chapter. The adaptive control provides the robustness to the uncertain dynamic parameters and it is only required to compute the first derivative of stiffness and the second derivative of position. Besides imposing the desired dynamics of links position and joints stiffness, this chapter also considers the dynamics of the actuation system, thus providing the broader solution. The main limitation comes from the fact that the direct relation between stiffness and flexibility torque is required, as well as the knowledge of its analytic form. Future work will be devoted to the experimental verification of the results.

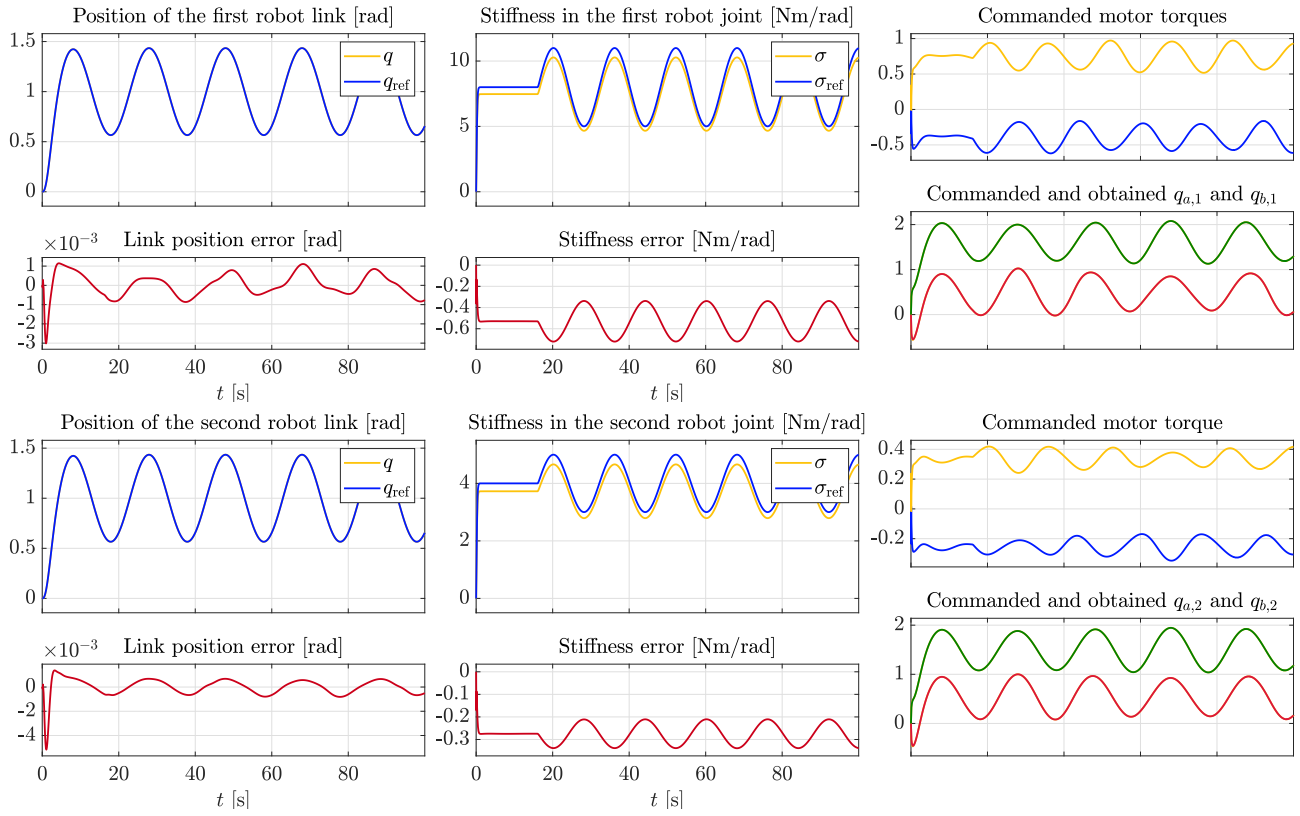

Figure 11.2: Simulation #1 (Augmented PD Control of a 2-DoF setup without the integral term) - The top and bottom rows show the behavior of the first and second joint, respectively. The desired link positions is effectively tracked (leftmost figures), while there is a bounded error in stiffness tracking, slightly larger for the first joint (middle figures). The good performance is achieved when it comes to tracking the commanded motors positions (rightmost figures). It is worth remarking that commanded motor torques have a smooth trajectory.

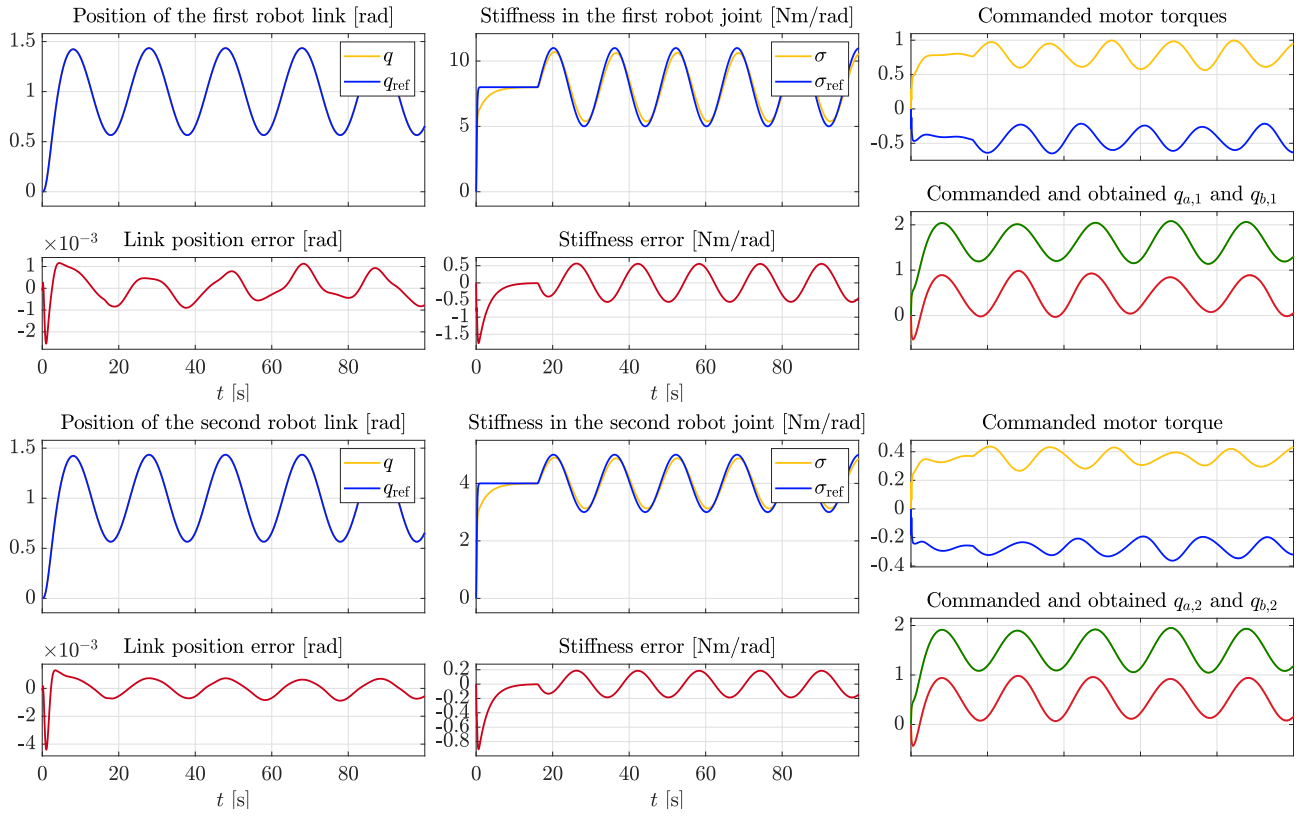

Figure 11.3: Simulation #2 (Augmented PD Control of a 2-DoF setup with the integral term) - The top and bottom rows show the behavior of the first and second joint, respectively. It can be observed that the desired link positions and joint stiffnesses are effectively tracked (leftmost and middle figures). The good performance is achieved when it comes to tracking the commanded motors positions (rightmost figures). Again, commanded motor torques have a smooth trajectory.

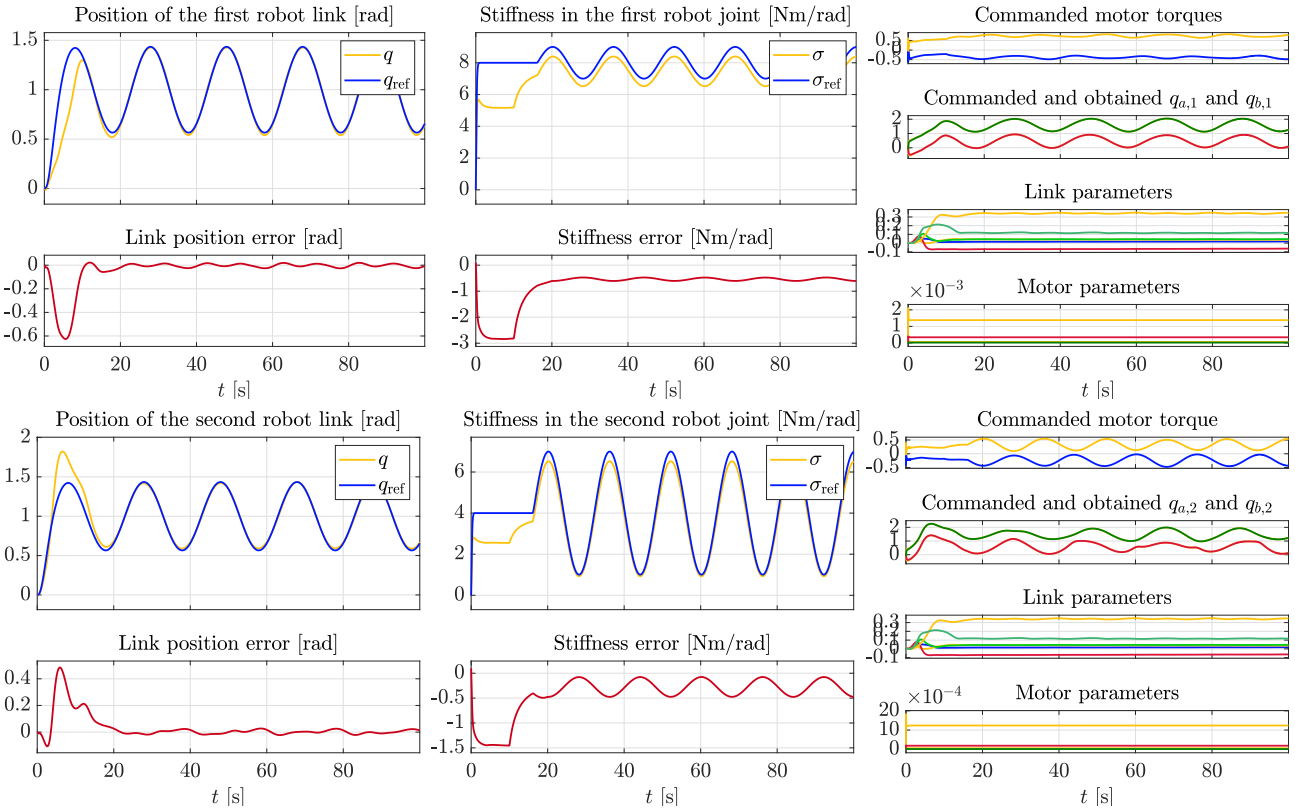

Figure 11.4: Simulation #3 (Nonlinear Adaptive Control of a 2-DoF setup without the integral term) - The top and bottom rows show the behavior of the first and second joint, respectively. After the initial time segment when adaptive controller is updating the parameters, link positions are successfully tracked (leftmost figures), while there exists a bounded error in stiffness tracking (middle figures). The estimated parameters of both link and motor dynamics remain bounded (rightmost figures).

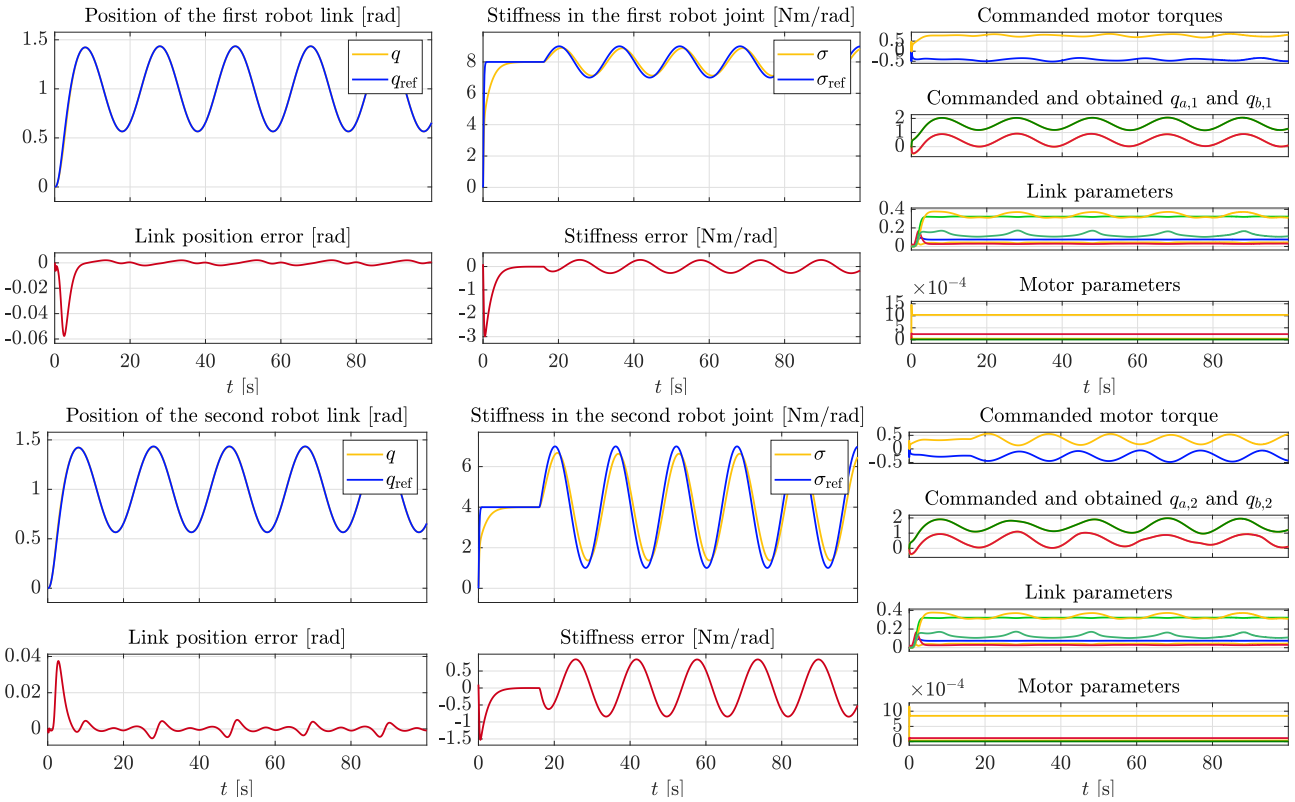

Figure 11.5: Simulation #4 (Nonlinear Adaptive Control of a 2-DoF setup with the integral term) - The top and bottom rows show the behavior of the first and second joint, respectively. After the short initial time segment when adaptive controller is updating the parameters, link positions and joint stiffnesses are successfully tracked (leftmost and middle figures). The estimated parameters of both link and motor dynamics remain bounded (rightmost figures).

Chapter 12

Soft-bodied robots

The PCC approach is nowadays an established technique in kinematic control of continuum soft robots Webster III and Jones (2010). More recently, it has been proven to be effective also for open loop dynamic control Falkenhahn et al. (2015). A step further has been done in Della Santina et al. (2020b); Katzschmann et al. (2019) where the PCC dynamics has been connected with the one of a rigid robot subject to a set of embeddable holonomic constraints. In this way, model-based feedback controllers developed for rigid robots, such as feedback linearization approach and PD plus feedforward term, could be easily extended to the PCC case.

The aforementioned controllers share the same weakness: they all rely heavily on accurate knowledge of soft robot dynamic parameters, which is generally not available in the practice of soft robotics. This challenge is herein tackled by adopting nonlinear adaptive control, built upon the technique pioneered in Slotine and Li (1991). This framework has already been applied to articulated soft robots Tonietti and Bicchi (2002); Trumić et al. (2020c), and to kinematic control of continuum soft robots Wang et al. (2016). Yet, dynamic control of continuum soft robots is substantially more challenging problem.

The main contribution of this chapter is the following:

- a robust closed-loop position controller for a soft-bodied robot, which is based on the nonlinear adaptive control theory;
- extensive simulations - including 3D and non constant curvature soft robots - proving the effectiveness and the robustness of the controller.

12.1 Design of the control law

Adaptive control is a technique robust to model uncertainties due to imprecise knowledge of system parameters Slotine and Li (1991). It ensures the asymptotic tracking of desired joint trajectories via dynamic adaptation of a set of parameters. The method's applicability relies on the dynamics' linearity with respect to suitable parameters, i.e. the ability to write it as the product of a regressor matrix Y and a constant parameter vector π. In its basic formulation, it also requires a full actuation.

First, it is shown that the linearity property is preserved in the newly proposed model. As the dynamics in (3.4) is that of a standard rigid robot, it is linear with respect to a parameter vector π_ξ, i.e. $Y_\xi(\xi, \dot{\xi}, \ddot{\xi})\,\pi_\xi = \tau_\xi$, for some matrix Y_ξ. This implies that analogous decompositions hold for each addend appearing in (3.4): $B_\xi(\xi)\,\ddot{\xi} = Y_{B_\xi}(\xi, \ddot{\xi})\,\pi_{B_\xi}$, $C_\xi(\xi, \dot{\xi})\,\dot{\xi} = Y_{C_\xi}(\xi, \dot{\xi})\,\pi_{C_\xi}$, and $G_\xi(\xi) = Y_{G_\xi}(\xi)\,\pi_{G_\xi}$. It can also be observed that $m(q)$ linearly depends on $L_{0,i}$ and thus it holds $J_m(q) = Y_m(q)\,\pi_m$ for suitable Y_m and π_m. Moreover, the left hand-side of (3.6) can be

easily written as

$$J_m^T B_\xi(\xi)\,\ddot{\xi} + J_m^T C(\xi,\dot{\xi})\,\dot{\xi} + J_m^T G(\xi) + K\,q + D\,\dot{q}\,.$$

Its first addend can be factorized as follows:

$$\begin{aligned} J_m^T B_\xi(\xi)\,\ddot{\xi} &= \pi_m^T Y_m^T Y_{B_\xi}(\xi,\ddot{\xi})\,\pi_{B_\xi} = \\ &= \pi_m^T Y_m^T Y_{B_\xi}(m(q), \dot{J}_m\,\dot{q} + J_m\,\ddot{q})\,\pi_{B_\xi}\,, \end{aligned}$$

where (3.3) and (3.5) have been used. By using similar reasoning as in Property 2 from Marcucci et al. (2017b), one can find suitable Y_B and π_B such that $J_m^T B_\xi(m(q))\,\ddot{\xi} = Y_B(q,\dot{q},\ddot{q})\,\pi_B$. With similar steps, the second and third addends can be written as follows:

$$\begin{aligned} J_m^T C(\xi,\dot{\xi})\,\dot{\xi} &= \pi_m^T Y_m^T Y_{C_\xi}(m(q), \dot{J}_m\,\dot{q} + J_m\,\ddot{q})\,\pi_{C_\xi} = \\ &= Y_C(q,\dot{q})\,\pi_C\,, \\ J_m^T G(\xi) &= \pi_m^T Y_m^T Y_{G_\xi}(\xi)\,\pi_{G_\xi} = \\ &= J_m^T Y_{G_\xi}(m(q))\,\pi_{G_\xi} = Y_G(q)\,\pi_G\,. \end{aligned}$$

Decomposing also $K\,q = Y_K(q)\,\pi_K$ and $D\,\dot{q} = Y_D(\dot{q})\,\pi_D$, and summing up the three addends above yields:

$$Y(q,\dot{q},\ddot{q})\,\pi = A(q)\,\tau\,, \tag{12.1}$$

with regressor matrix $Y = (Y_B, Y_C, Y_G, Y_K, Y_D)$ and parameter vector $\pi = (\pi_B^T, \pi_C^T, \pi_G^T, \pi_K^T, \pi_D^T)^T$.

Leveraging on Prop. 5 and 6, the following result is ready to be derived:

Theorem 10 (Adaptive Control of soft-bodied robots)**.** *Given a soft-bodied robot as in (3.6), the dynamic control law*

$$\begin{aligned} \dot{\hat{\pi}} &= K_\pi Y^T(q,\dot{q},\dot{q}_r,\ddot{q}_r)\,\sigma\,, \\ \tau &= A(q)^\dagger\,(Y(q,\dot{q},\dot{q}_r,\ddot{q}_r)\,\hat{\pi} + K_d\,\sigma)\,, \end{aligned}$$

where $\hat{\pi}$ is the parameter estimate vector, $\dot{q}_r = \dot{q}_d + \Lambda(q_d - q)$, $\sigma = \dot{q}_d - \dot{q} + \Lambda(q_d - q)$, K_π, Λ and K_d are free positive definite matrices, and $A(q)^\dagger$ is the pseudo-inverse of $A(q)$, ensures asymptotic tracking of any desired trajectory vector signal $q_d(t) \in \mathcal{C}^2$.

Proof. In order to apply the adaptive approach proposed in Slotine and Li (1991), which avoids using the second time-derivative of q, first the reference speed $\dot{q}_r$ is introduced and the robot dynamics is rewritten as

$$B(q)\,\ddot{q}_r + C(q,\dot{q})\,\dot{q}_r + G(q) + K\,q + D\,\dot{q} = A(q)\,\tau\,.$$

By exploiting the linearity property shown in (12.1), one can write the left hand-side of the above expression as the product of a regressor matrix $Y(q,\dot{q},\dot{q}_r,\ddot{q}_r)$ and the corresponding parameter vector π.

Additionally, a new input $\tau^* = A(q)\,\tau$ can be defined. Being $A(q)$ exactly known (and indeed independent of any robot's parameters) and also invertible, except at isolated points, the adaptive control law described in Slotine and Li (1991) can be applied via τ^*, and then translated back to τ by using the pseudo-inverse of $A(q)$, i.e. as $\tau = A(q)^\dagger\,\tau^*$. The rest of the proof straightforwardly follows from Slotine and Li (1991). □

The block scheme of the proposed controller is presented in Fig. 12.1.

In a realistic scenario, position and speed information for all configurations can be obtained via commercial motion-capture systems, embedded proprioceptive sensors, or a combination of them Della Santina et al. (2020c). In such approaches, the kinematic map from Della Santina

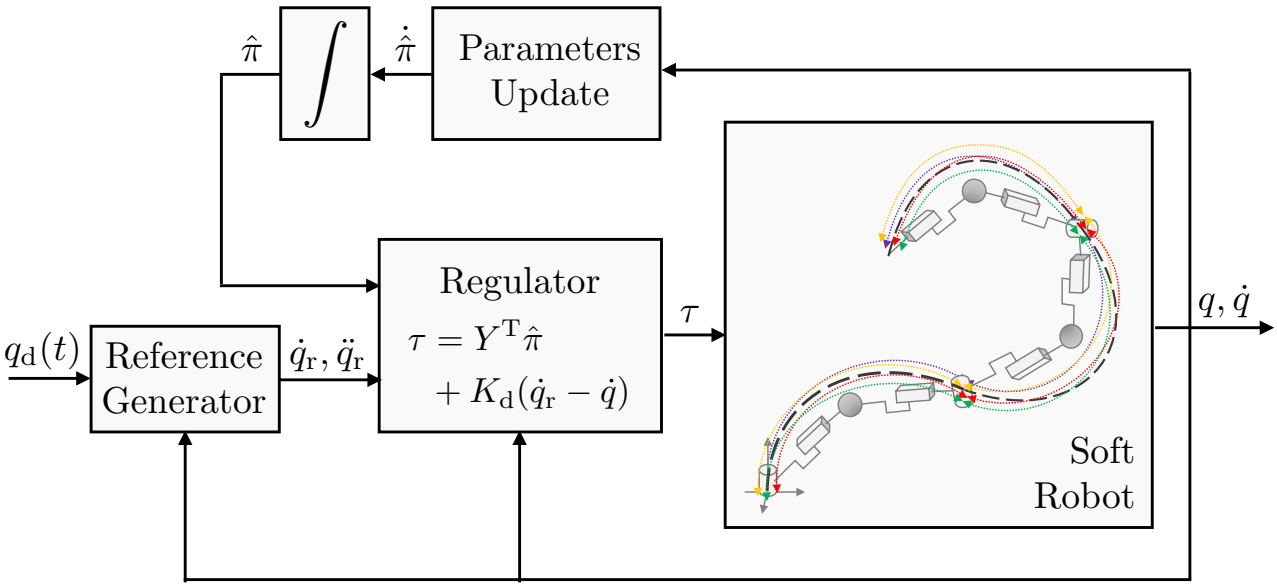

Figure 12.1: Block scheme of the control algorithm introduced in this work. The soft robot with piecewise constant curvature is matched to a dynamically equivalent augmented rigid robot. This model is then used to derive an adaptive controller able to implement trajectory tracking in configuration space without the knowledge of any of the soft robot's physical parameters.

et al. (2020a) has been adopted. Though not being based on the augmented formulation, it provides an equivalent information from the sensing viewpoint.

12.2 Simulation results

The performance and robustness of the proposed control method are validated here by considering three setups: a planar soft-bodied robot modeled with the PCC approximation, a soft inverted pendulum with affine curvature, and a 3D soft robot. All robot's parameters including mass, length, stiffness, and damping of each segment are assumed as completely unknown.

12.2.1 Planar Soft Manipulator

As a first case, consider a planar soft robot composed of four independently-actuated and equal segments with length $L = 0.1$ m, mass $m = 10$ g, stiffness $k = 1$ Nm/rad, and damping $\beta = 0.1$ Nm·s/rad. The robot's base frame is chosen so that its tip points downwards and is aligned with gravity when all joint angles are null. To ensure kinematics and dynamic equivalence on the plane, each segment is modeled as a four-DoF rigid robot according to the augmented formulation presented in Della Santina et al. (2020b). Since the PCC-based planar formulation has no singularity and discontinuity issues, one can use here the bending angle θ_i as a configuration variable.

The controller uses a regressor matrix $Y \in \mathbb{R}^{4\times 173}$ built on such a model, with an initial parameter vector value of $\hat{\pi}(0) = 0_{173}$. In Fig. 12.2 are presented the results obtained when the robot is required to track the reference signals $\theta_{d,i} = M_i \sin(\omega t + \varphi_i)$, with $\omega = 1$ rad/s and M_i and φ_i being the i-th entries of the vectors $M = \left(\frac{\pi}{8}, \frac{\pi}{6}, \frac{\pi}{3}, \frac{\pi}{2}\right)$ rad and $\varphi = (0, \frac{\pi}{2}, \frac{\pi}{3}, \pi)$ rad, respectively. Figure 12.2 illustrates the results obtained with lower and higher control gains, while Fig. 12.3 presents more realistic results by including noise, external disturbance and an initial tracking error of $(1, -1, 1, -1)^T$ rad.

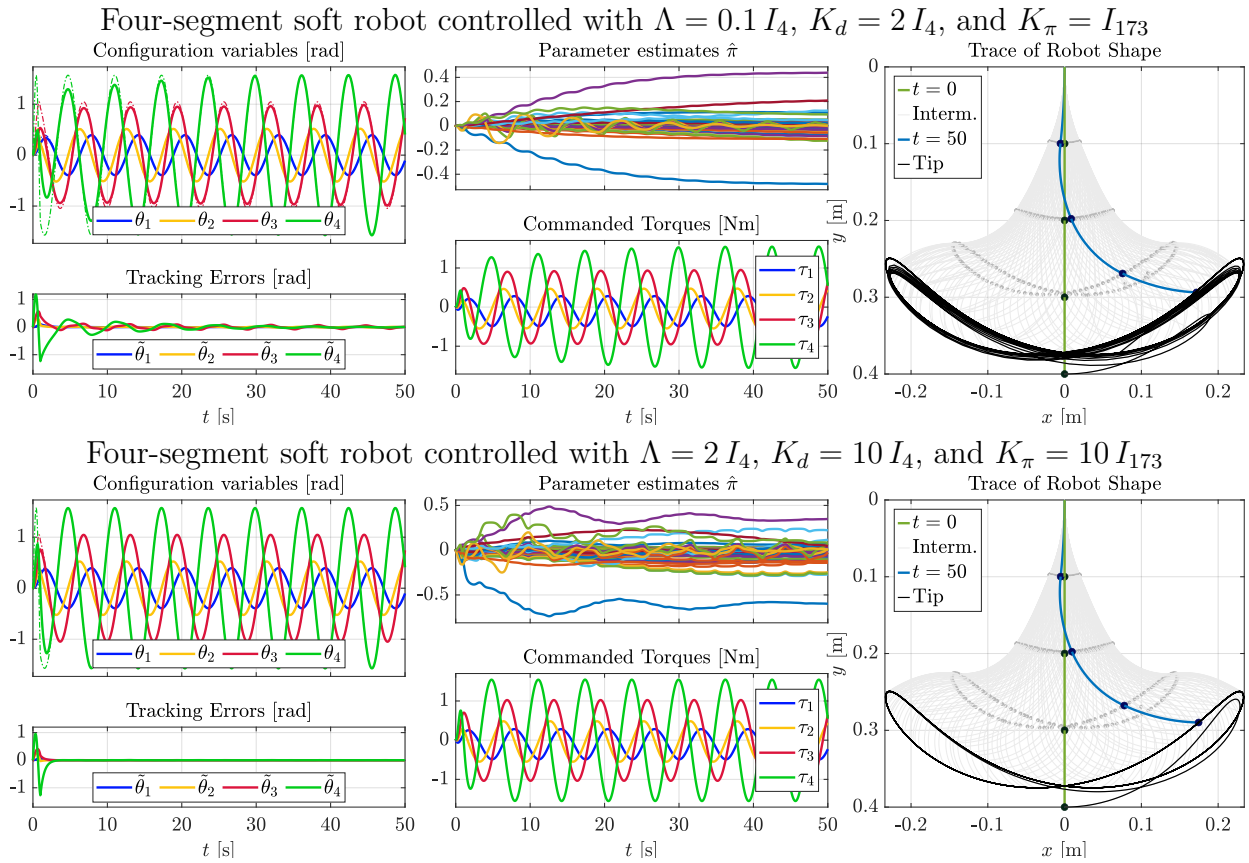

Figure 12.2: Scenario #1: From left to right, the two rows report the temporal evolution of the configuration variables (dashed lines indicate the desired trajectories) and the corresponding tracking errors $\tilde{\theta}_i = \theta_{i,d} - \theta_i$, the estimated parameters and commanded torques, and a trace of the robot's shape. As expected from theory, higher control gains allow a faster tracking convergence and a more precise tracking since the beginning. It can be noticed that the parameter estimates nicely behave and remain bounded.

12.2.2 Soft inverted pendulum with affine curvature

As a second example, consider a continuum soft robot behaving as a soft inverted pendulum under the effect of gravity Della Santina (2020). Let $L = 1$ m, $m = 1$ kg, $k = 1$ Nm/rad, and $\beta = 0.1$ Nm·s/rad be its length, mass, stiffness, and damping, respectively. Having defined the system's configuration vector as $\theta = (\theta_0, \theta_1)^T$, the instantaneous robot's shape can be described by the affine curvature $\kappa_s(t, s) = \theta_0(t) + \theta_1(t)\, s$, where $s \in [0, 1]$ parameterizes the position along the main axis of the pendulum, in such a way that Ls is the arc length of the path connecting the base to the point s through the main axis. The soft pendulum's dynamics can then be modeled as

$$B(\theta)\, \ddot{\theta} + C(\theta, \dot{\theta})\, \dot{\theta} + G(\theta) + k\, H\, \theta + \beta\, H\, \dot{\theta} = H \begin{pmatrix} 1 \\ 0 \end{pmatrix} \tau\,,$$

with $B(\cdot)$, $C(\cdot)$, and $G(\cdot)$ being derived by appropriately summing up the infinitesimal mass elements (Della Santina (2020)), $H \in \mathbb{R}^{2\times 2}$ with $H_{i,j} = 1/(i + j - 1)$ is the Hankel matrix. It is notable that this model generalizes the PCC-based one described in Ch. 3, for which it stands $\theta_0 \equiv 0$.

Let the regressor matrix Y be constructed according to the procedure described in Sec. 12.1,

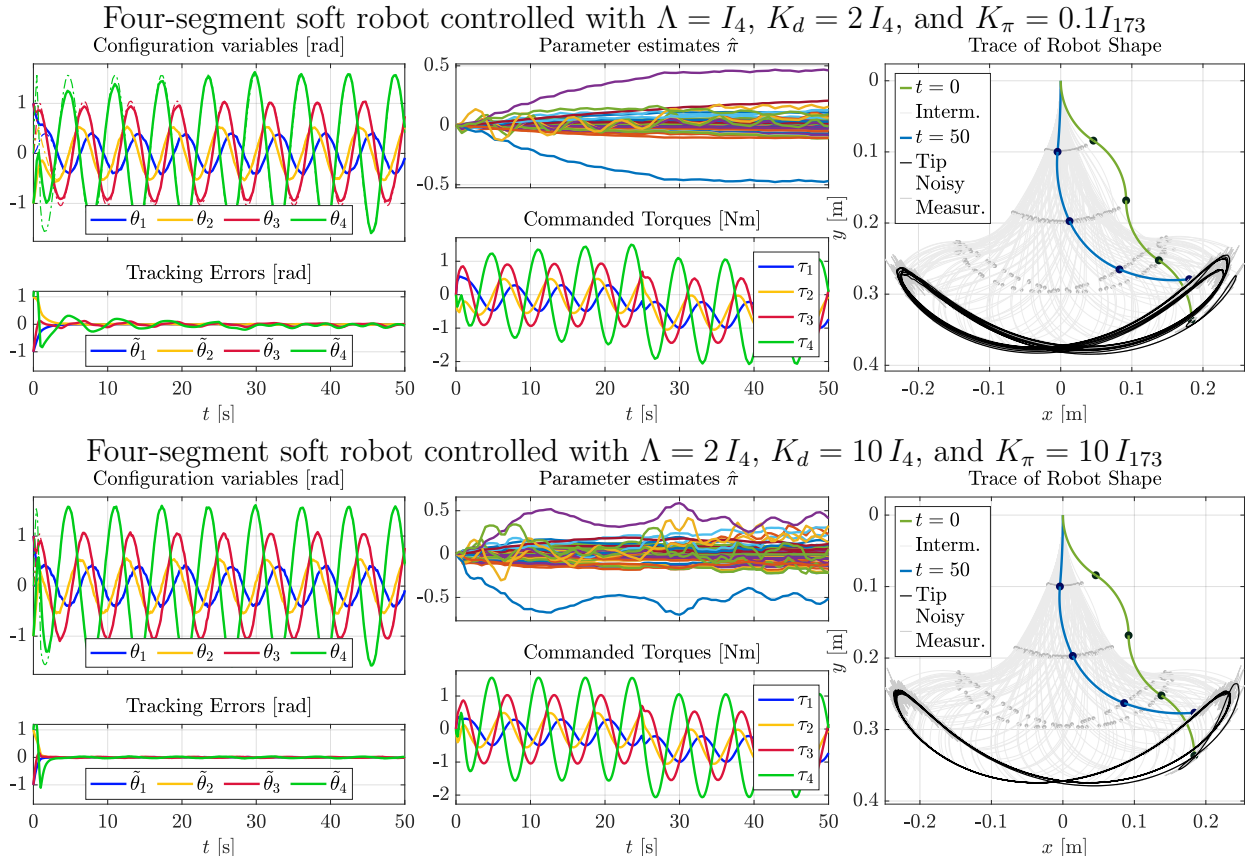

Figure 12.3: Scenario #2: The two rows report, from left to right, the configuration variable evolution (dashed lines indicate the desired trajectories) and the corresponding tracking errors $\tilde{\theta}_i = \theta_{i,d} - \theta_i$, the estimated parameters and commanded torques, and a trace of the robot's shape. A persistent constant force of 0.5 N is applied from $t = 25$ s on each segment, simulating an external disturbance. The measurement of each configuration variable is affected by Gaussian white noise with zero mean value and standard deviation of 0.032 rad. As expected from theory, higher control gains allow a faster tracking convergence and a more precise tracking since the beginning. It can be noticed that the parameter estimates nicely behave and remain bounded. The approach is robust also to the presence of external disturbance and measurement noise.

for the case of a planar single segment. This yields to $Y(\theta_0, \dot{\theta}_0, \dot{\theta}_{0,r}, \ddot{\theta}_{0,r}) = (y_1, y_2, \theta_0, \dot{\theta}_{0,r})$, where

$$\begin{aligned} y_1 &= \frac{\ddot{\theta}_{0,r}}{16}\left(\left(\mathrm{sinc}'\left(\frac{\theta_0}{2}\right)\right)^2 + 4\,\mathrm{sinc}^2\left(\frac{\theta_0}{2}\right) + 16\right) + \\ &+ \frac{\dot{\theta}_{0,r}\dot{\theta}_0}{16}\,\mathrm{sinc}'\left(\frac{\theta_0}{2}\right)\left(\mathrm{sinc}''\left(\frac{\theta_0}{2}\right) + 2\,\mathrm{sinc}\left(\frac{\theta_0}{2}\right)\right), \\ y_2 &= -\tfrac{1}{4}\left(2\,\mathrm{sinc}\left(\frac{\theta_0}{2}\right)\cos\left(\frac{\theta_0}{2}\right) + \mathrm{sinc}'\left(\frac{\theta_0}{2}\right)\sin\left(\frac{\theta_0}{2}\right)\right), \end{aligned}$$

and to a parameter vector $\pi = (mL^2, mgL, k, \beta)^T$. Fig. 12.4 illustrates the results obtained with a soft inverted pendulum with low ($k = 1$ Nm/rad) and medium stiffness ($k = 4$ Nm/rad), which is controlled to the upright position with control gains $K_\pi = 0.01$, $K_d = 0.05$, and $\Lambda = 0.3$, while Fig. 12.5 depicts the case when noise and external disturbance are affecting the system. The soft pendulum is regulated to the upright position by a controller with gains $\Lambda = 0.2$, $K_d = 0.05$, and $K_\pi = 0.01\,I_4$, and the stiffer one with gains $\Lambda = 0.1$, $K_d = 0.1$, and $K_\pi = 0.05\,I_4$. In both cases the initial tracking error is $(\pi/4, -\pi/4)^T$ rad. It should be noted that the small value of the external disturbance is only chosen so as to keep the response times of both pendulums short, while a bigger value would lead to a longer settling time but would be successfully handled

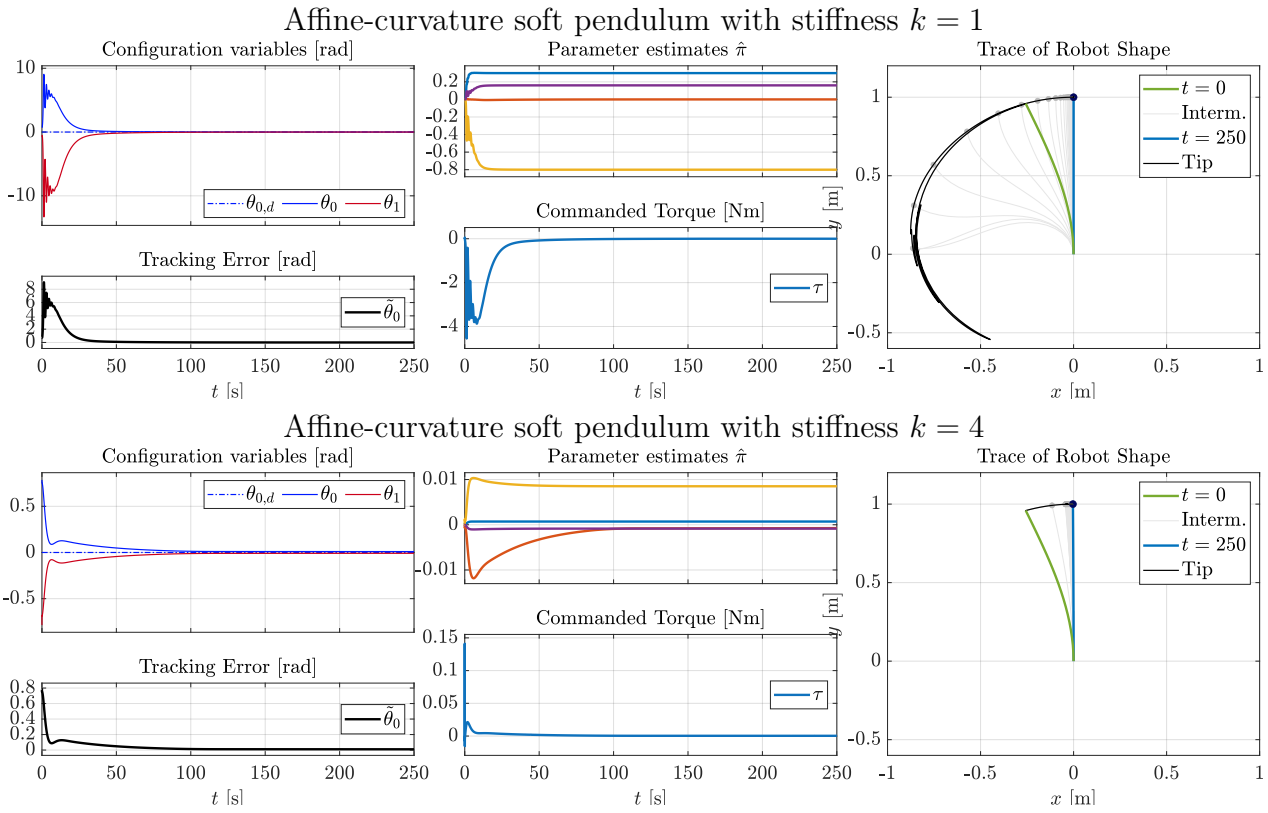

Figure 12.4: Scenario #3: Affine-curvature soft pendulum subject to gravity. The proposed controller allows asymptotically stabilizing the robot to the upright position both with a lower and a higher stiffness.

by the approach.

12.2.3 Soft Manipulator in 3D space

Finally, this work considers a generic soft-bodied robot composed of four CC segments in a 3D space whose model is described by Eq. 3.6. The four segments are assumed to be identical and characterized by $L_{i,0} = 1$ m, $m_i = 1$ kg, $k_i = 1$ Nm/rad, $\beta_i = 0.1$ Nms/rad, for $i = \{1, 2, 3, 4\}$. Deriving and using an adaptive controller based on such a model is challenging due to the large number of involved functions and parameters. One can proceed therefore by building it based on the simplified model presented in Della Santina et al. (2020a). The desired reference signals for both segments are sinusoidal, the controller gains are $\Lambda = 7\, I_{12}$, $K_d = 13\, I_{12}$, and $K_\pi = 2\, I_{60}$, the regressor matrix is $Y \in \mathbb{R}^{12\times 60}$, and the initial parameter vector is $\hat{\pi}(0) = 0_{60}$. The obtained results are first shown in Fig. 12.6 assuming the perfect sensory conditions and lack of external disturbances, while Fig. 12.7 reports a system performance when the noise and disturbances are affecting it, and when the initial tracking error is 0.05 m for each of the three configuration variables of the first two segments, and -0.05 m for those of the other two.

12.3 Conclusion

This section presented a novel solution for the control of soft-bodied robot position. Based on the nonlinear adaptive control theory, the approach enables a successful tracking performance even when significant parametric uncertainties exist. Validation of the method has been carried out on various robot configurations, thus proving also its robustness. A still open

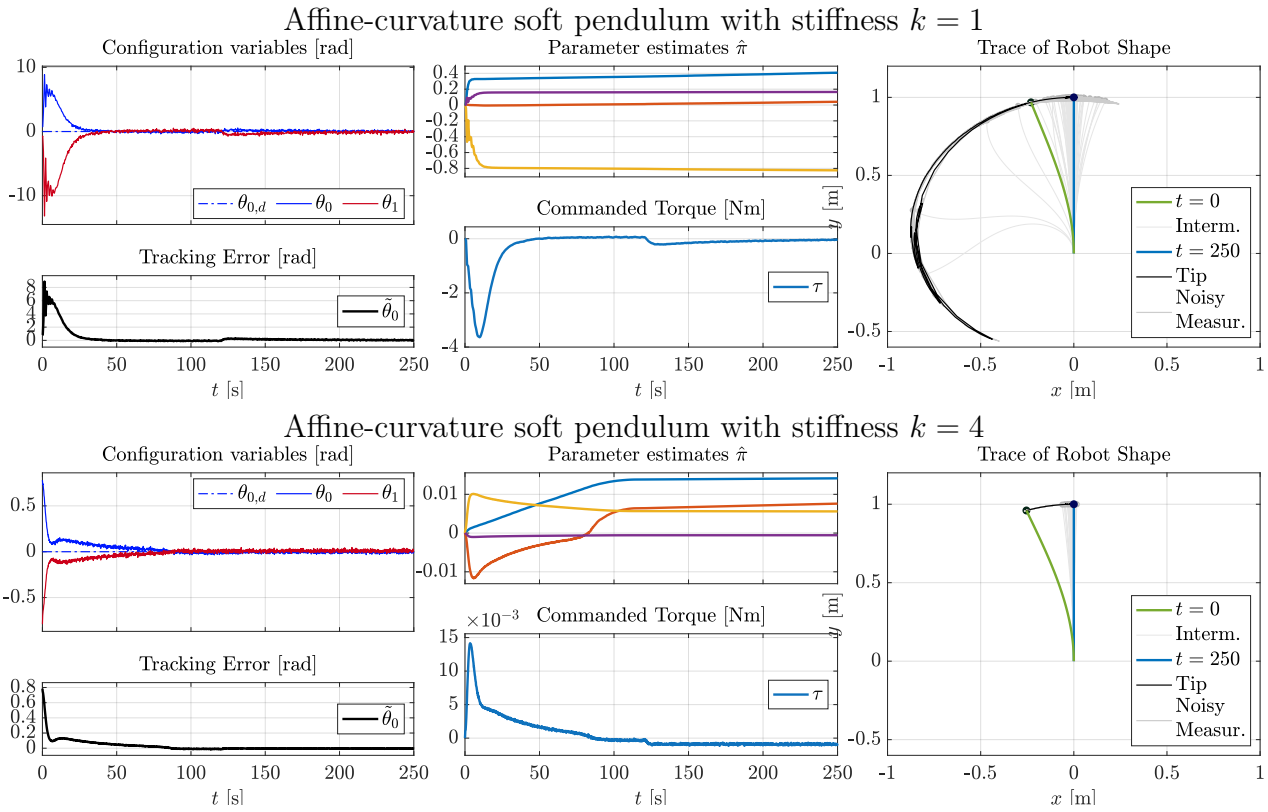

Figure 12.5: Scenario #4: Affine-curvature soft pendulum subject to gravity. The proposed controller allows asymptotically stabilizing the robot to the upright position both with a lower and a higher stiffness. The standard deviation of the measurement noise is 0.032 rad, and a persistent constant disturbance of $5 \cdot 10^{-3}$ N is applied from $t = 125$ s.

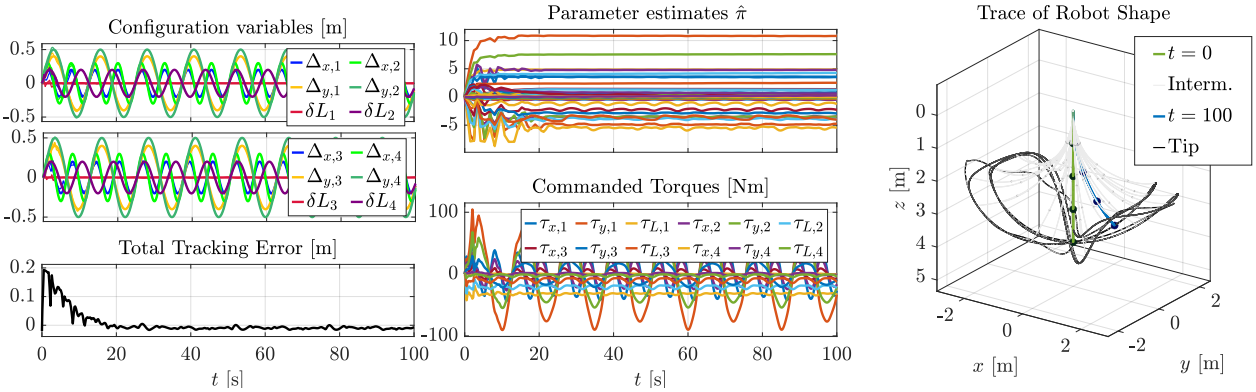

Figure 12.6: Scenario #5: Four-segment 3D soft-bodied robot tracking sinusoidal references. A Gaussian white noise with zero mean value and standard deviation of 0.032 m affects all configuration measures, and a persistent constant force of amplitude 5 N is applied on each segment from $t = 50$ s. The total tracking error is computed as the 2-norm of the vector composed of the tracking errors along all components. The simulation shows the controller's ability to adapt the parameter estimates, even with noise and disturbances, so as to track the desired signals.

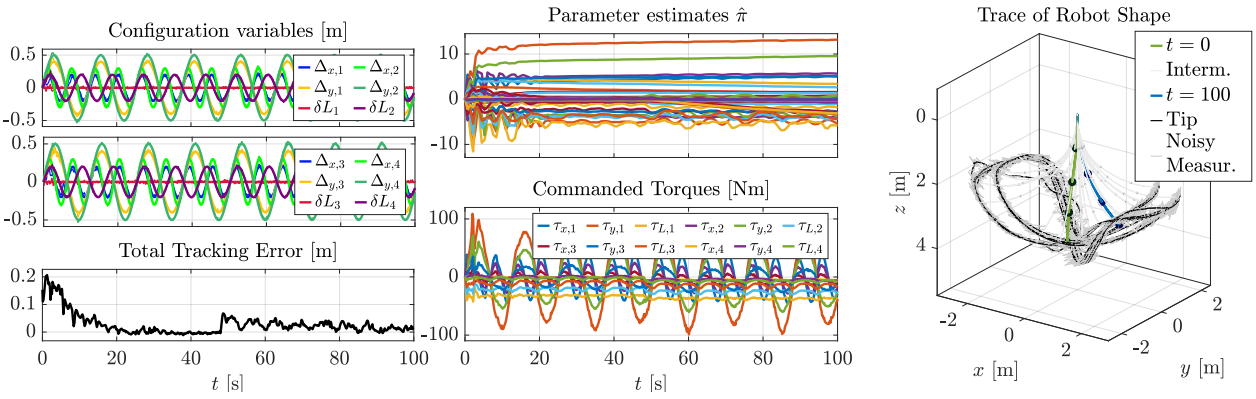

Figure 12.7: Scenario #6: Four-segment 3D soft-bodied robot tracking sinusoidal references. A Gaussian white noise with zero mean value and standard deviation of 0.032 m affects all configuration measures, and a persistent constant force of amplitude 5 N is applied on each segment from $t = 50$ s. The total tracking error is computed as the 2-norm of the vector composed of the tracking errors along all components. The simulation shows the controller's ability to adapt the parameter estimates, even with noise and disturbances, so as to track the desired signals.

question concerning the applicability of the proposed method is connected to the maximum number of segments used to represent a given soft-bodied robot. To this respect, thanks to the dynamic equivalence herein established, the proposed work can benefit from studies seeking for the minimum information required for an adaptive controller to accurately regulate a soft-robot (Marcucci et al. (2017b)). It should also be noticed that the regressor is evaluated off-line and once before the actual control action is executed. The results presented in this work show the ability of the method to reject external disturbance and cope with measurement noise. Future work will be devoted to testing the algorithm with real experiments, where the state space is truly infinite dimensional, and extending it to black box uncertainties.

Summary Conclusions

Soft robots have been projected to become the advanced technological solutions that would take the maximum of inspiration from the biological systems and, consequently, their benefits. The advantageous features are achieved either by employing variable stiffness actuators to drive soft articulated robots or leveraging the morphological flexibility to accomplish different postures of soft-bodied robots. This thesis has been dedicated to improving the performance of such robots by tackling the challenges of stiffness estimation and exploiting robust control techniques.

The first part commenced by briefly describing the representative examples of soft articulated and soft-bodied robots. It was followed by the mathematical description of robots considered within the thesis, i.e. pneumatically and electro-mechanically driven soft articulated robots with antagonistic VSAs and general soft-bodied robots modeled under the PCC hypothesis and assumption of having the affine curvature.

The second part of the thesis was devoted to developing the stiffness estimation approaches with the prime aim to reduce the required sensory information and the number of parameters to be tuned, as well as to avoid the observability issues. It is shown via experiments that effective results can be achieved for electro-mechanically driven robots. Both the invasive and non-invasive approaches allowed accurate stiffness estimation for multi-degree-of-freedom robots in real-time even when the link position is steady, while requiring only the knowledge of links and motors positions in the non-invasive case, as well as commanded torque signal in the invasive case.

Compared to the state-of-the-art solutions, there was no need for force/torque and velocity sensors, while the estimators were not dependent on the input signals' nature. Moreover, simulations showed the successful estimation of stiffness in pneumatically actuated joints. The main disadvantage comes from the fact that accurate knowledge of dynamic parameters, whether on the motor or link side, is required. Thus, future work will consider the robust estimation of stiffness and overall impedance in soft robots, and address the transfer of knowledge to the estimation of stiffness in human limbs.

The third part was focused on the adaptive control of soft robots. The decoupling property of the proposed techniques allowed the simultaneous and independent control of position and stiffness for soft articulated robots, while the adaptive property enabled the robustness to parametric uncertainty. The well-known benefits of closed-loop control were shown via numerous experiments executed on a pneumatic robot and in the simulations for electro-mechanical soft articulated robots. It could also be observed that the main limitation stems from the fact that knowledge of the actuation matrix (in the case of pneumatic robots) and analytic form of stiffness-torque relation (in the case of electric robots) is required. Moreover, the adaptive controller demonstrated the successful applicability to various soft-bodied robots, ranging from planar to three-dimensional ones, modeled under PCC or affine curvature assumptions. Future research will be devoted to the experimental verification of those approaches on setups of soft-bodied robots and electric soft-articulated robots, as well as to closing the loop with stiffness observers.

Bibliography

ABB (2019) Yumi—irb 14000. `http://new.abb.com`. Accessed: 2020-09-30.

Ajoudani A, Zanchettin AM, Ivaldi S, Albu-Schäffer A, Kosuge K and Khatib O (2018) Progress and prospects of the human–robot collaboration. *Autonomous Robots* : 1–19.

Albu-Schäffer A and Bicchi A (2016) Actuators for soft robotics. In: Siciliano B and Khatib O (eds.) *Springer handbook of robotics*, chapter 21. Springer, pp. 243–282.

Albu-Schäffer A, Haddadin S, Ott C, Stemmer A, Wimböck T and Hirzinger G (2007a) The dlr lightweight robot: design and control concepts for robots in human environments. *Industrial Robot: an international journal* 34(5): 376–385.

Albu-Schaffer A and Hirzinger G (2002) Cartesian impedance control techniques for torque controlled light-weight robots. In: *Robotics and Automation, 2002. Proceedings. ICRA'02. IEEE International Conference on*, volume 1. IEEE, pp. 657–663.

Albu-Schäffer A, Ott C and Hirzinger G (2007b) A unified passivity-based control framework for position, torque and impedance control of flexible joint robots. *The international journal of robotics research* 26(1): 23–39.

Albu-Schäffer A and Petit COF (2012) Energy shaping control for a class of underactuated euler-lagrange systems. *IFAC Proceedings Volumes* 45(22): 567–575.

Angelini F, Della Santina C, Garabini M, Bianchi M, Gasparri GM, Grioli G, Catalano MG and Bicchi A (2018) Decentralized trajectory tracking control for soft robots interacting with the environment. *IEEE Transactions on Robotics* .

Best CM, Gillespie MT, Hyatt P, Killpack M, Rupert L and Sherrod V (2016a) Model predictive control for pneumatically actuated soft robots. *IEEE Robotics & Automation Magazine* 2(9): 31.

Best CM, Gillespie MT, Hyatt P, Rupert L, Sherrod V and Killpack MD (2016b) A new soft robot control method: Using model predictive control for a pneumatically actuated humanoid. *IEEE Robotics & Automation Magazine* 23(3): 75–84.

Bicchi A and Tonietti G (2002) Design, realization and control of soft robot arms for intrinsically safe interaction with humans. In: *Proc. IARP/RAS Workshop on Technical Challenges for Dependable Robots in Human Environments*. pp. 79–87.

Centro Piaggio U (2018) `http://www.centropiaggio.unipi.it/`. Accessed: 2020-09-30.

Cherelle P, Grosu V, Beyl P, Mathys A, Van Ham R, Van Damme M, Vanderborght B and Lefeber D (2010) The maccepa actuation system as torque actuator in the gait rehabilitation robot altacro. In: *2010 3rd IEEE RAS & EMBS International Conference on Biomedical Robotics and Biomechatronics*. IEEE, pp. 27–32.

Cherubini A, Passama R, Crosnier A, Lasnier A and Fraisse P (2016) Collaborative manufacturing with physical human–robot interaction. *Robotics and Computer-Integrated Manufacturing* 40: 1–13.

Chou CP and Hannaford B (1996) Measurement and modeling of mckibben pneumatic artificial muscles. *IEEE Transactions on robotics and automation* 12(1): 90–102.

De Luca A and J Book W (2016) Robots with flexible element. In: Siciliano B and Khatib O (eds.) *Springer handbook of robotics*, chapter 11. Springer, pp. 243–282.

De Luca A and Lucibello P (1998) A general algorithm for dynamic feedback linearization of robots with elastic joints. In: *Robotics and Automation, 1998. Proceedings. 1998 IEEE International Conference on*, volume 1. IEEE, pp. 504–510.

De Santis A, Siciliano B, De Luca A and Bicchi A (2008) An atlas of physical human–robot interaction. *Mechanism and Machine Theory* 43(3): 253–270.

Della Santina C (2020) Soft inverted pendulum with affine curvature. *IEEE Robotics and Automation Letters* 1(1): 000–111.

Della Santina C, Bianchi M, Grioli G, Angelini F, Catalano M, Garabini M and Bicchi A (2017) Controlling soft robots: balancing feedback and feedforward elements. *IEEE Robotics & Automation Magazine* 24(3): 75–83.

Della Santina C, Bicchi A and Rus D (2020a) On an improved state parametrization for soft robots with piecewise constant curvature and its use in model based control. *IEEE Robotics and Automation Letters* 5(2): 1001–1008.

Della Santina C, Katzschmann RK, Bicchi A and Rus D (2020b) Model-based dynamic feedback control of a planar soft robot: Trajectory tracking and interaction with the environment. *The International Journal of Robotics Research* 39(4): 490–513.

Della Santina C, Truby RL and Rus D (2020c) Data–driven disturbance observers for estimating external forces on soft robots. *IEEE Robotics and Automation Letters* 5(4): 5717–5724.

Dietrich A, Ott C and Albu-Schäffer A (2015) An overview of null space projections for redundant, torque-controlled robots. *The International Journal of Robotics Research* 34(11): 1385–1400.

Diolaiti N, Melchiorri C and Stramigioli S (2005) Contact impedance estimation for robotic systems. *IEEE Transactions on Robotics* 21(5): 925–935.

DLR (2007) `https://dlr.de`. Accessed: 2020-09-30.

Dynamic Robotics Laboratory OSU (2007) `https://mime.oregonstate.edu/research/drl/robots/bimasc/`. Accessed: 2020-09-30.

Fagiolini A, Trumić M and Jovanović K (2020) An input observer-based stiffness estimation approach for flexible robot joints. *IEEE Robotics and Automation Letters* 5(2): 1843–1850.

Falkenhahn V, Hildebrandt A, Neumann R and Sawodny O (2015) Model-based feedforward position control of constant curvature continuum robots using feedback linearization. In: *2015 IEEE International Conference on Robotics and Automation (ICRA)*. IEEE, pp. 762–767.

Flacco F (2012) *Modeling and control of robots with compliant actuation*. PhD Thesis, Sapienza University of Rome.

Flacco F and De Luca A (2011) Stiffness estimation and nonlinear control of robots with variable stiffness actuation. *IFAC Proceedings Volumes* 44(1): 6872–6879.

Flacco F, De Luca A, Sardellitti I and Tsagarakis NG (2012a) On-line estimation of variable stiffness in flexible robot joints. *Intl. Journal of Robotics Research* 31(13): 1556–1577.

Flacco F, Kröger T, De Luca A and Khatib O (2012b) A depth space approach to human-robot collision avoidance. In: *2012 IEEE International Conference on Robotics and Automation*. IEEE, pp. 338–345.

Franka Emika (2011) `http://franka.de`. Accessed: 2020-09-30.

Fras J, Noh Y, Macias M, Wurdemann H and Althoefer K (2018) Bio-inspired octopus robot based on novel soft fluidic actuator. In: *2018 IEEE International Conference on Robotics and Automation (ICRA)*. IEEE, pp. 1583–1588.

Garabini M, Passaglia A, Belo F, Salaris P and Bicchi A (2011) Optimality principles in variable stiffness control: The vsa hammer. In: *Intl. Conf. on Intelligent Robots and Systems*. IEEE, pp. 3770–3775.

Gavrilović M and Marić M (1969) Positional servo-mechanism activated by artificial muscles. *Medical and Biological Engineering* 7(1): 77–82.

Grazioso S, Di Gironimo G and Siciliano B (2019) A geometrically exact model for soft continuum robots: The finite element deformation space formulation. *Soft robotics* 6(6): 790–811.

Grebenstein M, Albu-Schäffer A, Bahls T, Chalon M, Eiberger O, Friedl W, Gruber R, Haddadin S, Hagn U, Haslinger R et al. (2011) The dlr hand arm system. In: *2011 IEEE International Conference on Robotics and Automation*. IEEE, pp. 3175–3182.

Grioli G and Bicchi A (2010) A non-invasive real-time method for measuring variable stiffness. In: *Robotics: Science and Systems*. pp. 1–8.

Grioli G, Wolf S, Garabini M, Catalano M, Burdet E, Caldwell D, Carloni R, Friedl W, Grebenstein M, Laffranchi M, Lefeber D, Stramigioli S, Tsagarakis N, Van Damme M, Vanderborght B, Albu-Schäffer A and Bicchi A (2015) Variable stiffness actuators: The user's point of view. *The International Journal of Robotics Research* 34(6): 727–743.

Haddadin S, De Luca A and Albu-Schäffer A (2017) Robot collisions: A survey on detection, isolation, and identification. *IEEE Transactions on Robotics* 33(6): 1292–1312.

Haddadin S, Krieger K, Albu-Schäffer A and Lilge T (2018) Exploiting elastic energy storage for "blind" cyclic manipulation: Modeling, stability analysis, control, and experiments for dribbling. *IEEE Transactions on Robotics* 34(1): 91–112.

Hirzinger G, Sporer N, Albu-Schaffer A, Hahnle M, Krenn R, Pascucci A and Schedl M (2002) Dlr's torque-controlled light weight robot iii-are we reaching the technological limits now? In: *Proceedings 2002 IEEE International Conference on Robotics and Automation (Cat. No. 02CH37292)*, volume 2. IEEE, pp. 1710–1716.

Hogan N (1985) Impedance control: An approach to manipulation: Part ii—implementation. *Journal of dynamic systems, measurement, and control* 107(1): 8–16.

Hou M and Patton RJ (1998) Input observability and input reconstruction. *Automatica* 34(6): 789–794.

Hu Y, Eljaik J, Stein K, Nori F and Mombaur K (2016) Walking of the icub humanoid robot in different scenarios: implementation and performance analysis. In: *2016 IEEE-RAS 16th International Conference on Humanoid Robots (Humanoids)*. IEEE, pp. 690–696.

Huang X, Kumar K, Jawed MK, Ye Z and Majidi C (2019) Soft electrically actuated quadruped (seaq)—integrating a flex circuit board and elastomeric limbs for versatile mobility. *IEEE Robotics and Automation Letters* 4(3): 2415–2422.

Hurst JW, Chestnutt JE and Rizzi AA (2010) The actuator with mechanically adjustable series compliance. *IEEE Transactions on Robotics* 26(4): 597–606.

Ikuta K, Ishii H and Nokata M (2003) Safety evaluation method of design and control for human-care robots. *The International Journal of Robotics Research* 22(5): 281–297.

Jovanović K, Lukić B and Potkonjak V (2017) Feedback linearization for decoupled position/stiffness control of bidirectional antagonistic drives. *Facta Universitatis, Series: Electronics and Energetics* 31(1): 51–61.

Karavas N, Ajoudani A, Tsagarakis N, Saglia J, Bicchi A and Caldwell D (2015) Tele-impedance based assistive control for a compliant knee exoskeleton. *Robotics and Autonomous Systems* 73: 78–90.

Katzschmann RK, Della Santina C, Toshimitsu Y, Bicchi A and Rus D (2019) Dynamic motion control of multi-segment soft robots using piecewise constant curvature matched with an augmented rigid body model. In: *2019 2nd IEEE International Conference on Soft Robotics (RoboSoft)*. IEEE, pp. 454–461.

Kautsky J, Nichols NK and Van Dooren P (1985) Robust pole assignment in linear state feedback. *International Journal of control* 41(5): 1129–1155.

Keppler M, Lakatos D, Ott C and Albu-Schäffer A (2016) A passivity-based approach for trajectory tracking and link-side damping of compliantly actuated robots. In: *Robotics and Automation (ICRA), 2016 IEEE International Conference on*. IEEE, pp. 1079–1086.

Keppler M, Lakatos D, Ott C and Albu-Schäffer A (2018) Elastic structure preserving (esp) control for compliantly actuated robots. *IEEE Transactions on Robotics* 34(2): 317–335.

Khatib O (1987) A unified approach for motion and force control of robot manipulators: The operational space formulation. *IEEE Journal on Robotics and Automation* 3(1): 43–53.

KUKA (2015) `http://kuka.com`. Accessed: 2020-09-30.

Lentini G, Settimi A, Caporale D, Garabini M, Grioli G, Pallottino L, Catalano MG and Bicchi A (2019) Alter-ego: A mobile robot with a functionally anthropomorphic upper body designed for physical interaction. *IEEE Robotics & Automation Magazine* 26(4): 94–107.

Li T, Li G, Liang Y, Cheng T, Dai J, Yang X, Liu B, Zeng Z, Huang Z, Luo Y et al. (2017) Fast-moving soft electronic fish. *Science Advances* 3(4): e1602045.

Liao B, Zang H, Chen M, Wang Y, Lang X, Zhu N, Yang Z and Yi Y (2020) Soft rod-climbing robot inspired by winding locomotion of snake. *Soft Robotics* .

Ljung L (1999) System identification: theory for the user. *PTR Prentice Hall, Upper Saddle River, NJ* : 1–14.

Lukic B, Jovanovic K and Sekara T (2019) Cascade control of antagonistic vsa-an engineering control approach to a bio-inspired robot actuator. *Frontiers in neurorobotics* 13: 69.

Lukić BZ, Jovanović KM and Kvaščcev GS (2016) Feedforward neural network for controlling qbmove maker pro variable stiffness actuator. In: *Neural Networks and Applications (NEUREL), 2016 13th Symposium on*. IEEE, pp. 1–4.

Marcucci T, Della Santina C, Gabiccini M and Bicchi A (2017a) Towards minimum-information adaptive controllers for robot manipulators. In: *2017 American Control Conference (ACC)*. IEEE, pp. 4209–4214.

Marcucci T, Della Santina C, Gabiccini M and Bicchi A (2017b) Towards minimum-information adaptive controllers for robot manipulators. In: *2017 American Control Conference (ACC)*. IEEE, pp. 4209–4214.

Medrano-Cerda GA, Bowler CJ and Caldwell DG (1995) Adaptive position control of antagonistic pneumatic muscle actuators. In: *Proceedings 1995 IEEE/RSJ International Conference on Intelligent Robots and Systems. Human Robot Interaction and Cooperative Robots*, volume 1. IEEE, pp. 378–383.

Ménard T, Grioli G and Bicchi A (2014) A stiffness estimator for agonistic–antagonistic variable-stiffness-actuator devices. *IEEE Transactions on Robotics* 30(5): 1269–1278.

Mengacci R, Angelini F, Catalano MG, Grioli G, Bicchi A and Garabini M (2020) On the motion/stiffness decoupling property of articulated soft robots with application to model-free torque iterative learning control. *The International Journal of Robotics Research* : 0278364920943275.

Mironchenko A and Prieur C (2019) Input-to-state stability of infinite-dimensional systems: recent results and open questions. *arXiv preprint arXiv:1910.01714* .

Ortega R, Perez JAL, Nicklasson PJ and Sira-Ramirez HJ (2013) *Passivity-based control of Euler-Lagrange systems: mechanical, electrical and electromechanical applications*. Springer Science & Business Media.

Ott C, Albu-Schaffer A, Kugi A and Hirzinger G (2008) On the passivity-based impedance control of flexible joint robots. *IEEE Transactions on Robotics* 24(2): 416–429.

Palli G, Melchiorri C and De Luca A (2008) On the feedback linearization of robots with variable joint stiffness. In: *2008 IEEE international conference on robotics and automation*. IEEE, pp. 1753–1759.

Palli G, Melchiorri C, Wimbock T, Grebenstein M and Hirzinger G (2007) Feedback linearization and simultaneous stiffness-position control of robots with antagonistic actuated joints. In: *Robotics and Automation, 2007 IEEE International Conference on*. IEEE, pp. 4367–4372.

Petit F, Daasch A and Albu-Schäffer A (2015) Backstepping control of variable stiffness robots. *IEEE Transactions on Control Systems Technology* 23(6): 2195–2202.

Piazza C, Catalano MG, Godfrey SB, Rossi M, Grioli G, Bianchi M, Zhao K and Bicchi A (2017) The softhand pro-h: a hybrid body-controlled, electrically powered hand prosthesis for daily living and working. *IEEE Robotics & Automation Magazine* 24(4): 87–101.

Polygerinos P, Correll N, Morin SA, Mosadegh B, Onal CD, Petersen K, Cianchetti M, Tolley MT and Shepherd RF (2017) Soft robotics: Review of fluid-driven intrinsically soft devices; manufacturing, sensing, control, and applications in human-robot interaction. *Advanced Engineering Materials* 19(12): 1700016.

Potkonjak V, Svetozarevic B, Jovanovic K and Holland O (2011) The puller-follower control of compliant and noncompliant antagonistic tendon drives in robotic systems. *International Journal of Advanced Robotic Systems* 8(5): 143–155.

qbmove Centro Piaggio (2011) QbMove Maker Pro datasheet. `https://www.qbrobotics.com`. Accessed: 2019-09-01.

Ruderman M, Bertram T and Iwasaki M (2014) Modeling, observation, and control of hysteresis torsion in elastic robot joints. *Mechatronics* 24(5): 407–415.

Rus D and Tolley MT (2015) Design, fabrication and control of soft robots. *Nature* 521(7553): 467.

Saberi A, Stoorvogel AA and Sannuti P (2000) Exact, almost and optimal input decoupled (delayed) observers. *International Journal of Control* 73(7): 552–581.

Sadati SH, Naghibi SE, Shiva A, Michael B, Renson L, Howard M, Rucker CD, Althoefer K, Nanayakkara T, Zschaler S et al. (2019) Tmtdyn: A matlab package for modeling and control of hybrid rigid–continuum robots based on discretized lumped systems and reduced-order models. *The International Journal of Robotics Research* : 0278364919881685.

Sain M and Massey J (1969) Invertibility of linear time-invariant dynamical systems. *IEEE Trans. on automatic control* 14(2): 141–149.

Sardellitti I, Medrano-Cerda G, Tsagarakis NG, Jafari A and Caldwell DG (2012) A position and stiffness control strategy for variable stiffness actuators. In: *Intl. Conference on Robotics and Automation*. IEEE, pp. 2785–2791.

Siciliano B and Khatib O (2008) *Springer handbook of robotics*. Springer Science & Business Media.

Slotine JJE and Li W (1991) *Applied nonlinear control*. Prentice hall Englewood Cliffs, NJ.

Spong MW (1989) Adaptive control of flexible joint manipulators. *Systems & Control Letters* 13(1): 15–21.

Sundaram S (2012) Lecture notes in fault-tolerant and secure control systems.

Sundaram S and Hadjicostis CN (2007) Delayed observers for linear systems with unknown inputs. *IEEE Transactions on Automatic Control* 52(2): 334–339.

Sundaram S and Hadjicostis CN (2008) Partial state observers for linear systems with unknown inputs. *Automatica* 44(12): 3126–3132.

Thieffry M, Kruszewski A, Duriez C and Guerra TM (2018) Control design for soft robots based on reduced-order model. *IEEE Robotics and Automation Letters* 4(1): 25–32.

Thuruthel TG, Falotico E, Manti M and Laschi C (2018) Stable open loop control of soft robotic manipulators. *IEEE Robotics and Automation Letters* 3(2): 1292–1298.

Tonietti G and Bicchi A (2002) Adaptive simultaneous position and stiffness control for a soft robot arm. In: *IEEE/RSJ International Conference on Intelligent Robots and Systems*, volume 2. IEEE, pp. 1992–1997.

Trumić M, Della Santina C, Jovanović K and Fagiolini A (2020a) Adaptive control of soft robots based on an enhanced 3d augmented rigid robot matching. *Control Systems Letters* : 1–6.

Trumić M, Jovanović K and Fagiolini A (2018) Kernel-based nonlinear adaptive control of stiffness and position in pneumatic soft robots. In: *Automatica.it*. SIDRA, pp. 1–2.

Trumić M, Jovanović K and Fagiolini A (2019) Flexibility torque estimation in articulated soft robots. In: *Automatica.it*. SIDRA, pp. 1–2.

Trumić M, Jovanović K and Fagiolini A (2020b) Comparison of model-based simultaneous position and stiffness control techniques for pneumatic soft robots. In: *International Conference on Robotics in Alpe-Adria Danube Region*. Springer, pp. 218–226.

Trumić M, Jovanović K and Fagiolini A (2020c) Decoupled nonlinear adaptive control of position and stiffness for pneumatic soft robots. *The International Journal of Robotics Research* : 1–19.

Trumić M, Jovanović K and Fagiolini A (2020) Towards safer collaboration - closing the loop on position and stiffness of soft articulated robots. In: *Italian Robotics and Intelligent Machines Conference*. I-RIM 3D, pp. 1–2.

University of Heidelberg (2018) `https://nacht-der-forschung-heidelberg.de/event/interactive-robotics-demonstrations/`. Accessed: 2020-09-30.

Valcher ME (1999) State observers for discrete-time linear systems with unknown inputs. *IEEE Transactions on Automatic Control* 44(2): 397–401.

Van Ham R, Sugar TG, Vanderborght B, Hollander KW and Lefeber D (2009) Compliant actuator designs. *IEEE Robotics & Automation Magazine* 16(3).

Verrelst B, Van Ham R, Vanderborght B, Daerden F, Lefeber D and Vermeulen J (2005) The pneumatic biped "lucy" actuated with pleated pneumatic artificial muscles. *Autonomous Robots* 18(2): 201–213.

Wang H, Yang B, Liu Y, Chen W, Liang X and Pfeifer R (2016) Visual servoing of soft robot manipulator in constrained environments with an adaptive controller. *IEEE/ASME Transactions on Mechatronics* 22(1): 41–50.

Webster III RJ and Jones BA (2010) Design and kinematic modeling of constant curvature continuum robots: A review. *The International Journal of Robotics Research* 29(13): 1661–1683.

Willemse CJ and van Erp JB (2019) Social touch in human–robot interaction: Robot-initiated touches can induce positive responses without extensive prior bonding. *International journal of social robotics* 11(2): 285–304.

Wolf S, Grioli G, Eiberger O, Friedl W, Grebenstein M, Höppner H, Burdet E, Caldwell DG, Carloni R, Catalano MG et al. (2016) Variable stiffness actuators: Review on design and components. *IEEE/ASME transactions on mechatronics* 21(5): 2418–2430.

Biography

Maja Trumić was born on September 18th, 1993. in Bor, where she finished elementary and high school. She enrolled at the School of Electrical Engineering in Belgrade in 2012 at the Department of Signals and Systems and graduated in 2016 with an average grade of 9.76, defending the bachelor thesis titled "Design of an autopilot for a self-guided short-range air-to-ground missile". The same year she started master studies at the School of Electrical Engineering in Belgrade at the same department and finished a year later with an average grade of 10 and a master thesis titled "Analysis of vibration signals from low power motors using wavelet analysis". In the 2017/2018 academic year, she enrolled in bilateral doctoral studies at the School of Electrical Engineering in Belgrade, in the module System Control and Signal Processing, and at the University of Palermo, within the program Information and Communication Technologies. During her doctoral studies at the School of Electrical Engineering, she passed ten exams with an average grade of 10.00.

In her undergraduate studies, Maja Trumić acquired knowledge through internships at the Military Technical Institute in Belgrade in 2016 (three months) and the Bosch research center in Renningen, Germany, in the same year (four months). After successfully completing her internship, Maja Trumić was given the opportunity to work on a master thesis in 2017 within the Bosch plant in Bühl, Germany.

As part of bilateral doctoral studies, Maja spent eighteen months at the University of Palermo in "MIRPAlab" team as a doctoral student. During her doctoral studies, she attended courses in the area of adaptive control and optimization within the summer school in Bertinoro, Italy, organized by the Italian Society of Professors and Researchers in Automation (Società Italiana Docenti e Ricercatori in Automatica - SIDRA), as well as courses in nonlinear systems and control and robust and adaptive control of multivariable systems within the International Graduate School on Control, organized by The European Embedded Control Institute (EECI).

She has taken part in two national projects:

- TR-35003: "Ambient Intelligent Service Robots of Anthropomorphic Characteristics", a project of the Ministry of education, science and technological development, Republic of Serbia, 2011-2020, and
- ForNextCobot: "Mechanical Impedance Estimation and Planning for Next Generation Collaborative Robots", a project of PROMIS, Science Fund of the Republic of Serbia, as part of the Program for excellent projects of young researchers #6062528, 2020-2022,

and one international project HORIZON 2020 MINDtheGEPs-101006543: "Modifying Institution by Developing Gender Equality Plans", 2021-2025.

Maja Trumić is the awardee of the Dositej Scholarship - Fund for Young Talents of the Republic of Serbia in undergraduate and master studies, student scholarships of the Ministry of education, science, and technological development, and Zoran Đinđić Internship Programme of German Business for the Countries of Western Balkans.

образац изјаве о ауторству

Изјава о ауторству

Име и презиме аутора Маја Трумић

Број индекса 2017/5019

Изјављујем

да је докторска дисертација под насловом

Естимација крутости и адаптивно управљање код попустљивих робота

- резултат сопственог истраживачког рада;
- да дисертација у целини ни у деловима није била предложена за стицање друге дипломе према студијским програмима других високошколских установа;
- да су резултати коректно наведени и
- да нисам кршио/ла ауторска права и користио/ла интелектуалну својину других лица.

Потпис аутора

У Београду, 26.04.2021.

_____

образац изјаве о истоветности штампане и електронске верзије докторског рада

Изјава о истоветности штампане и електронске верзије докторског рада

Име и презиме аутора Маја Трумић

Број индекса 2017/5019

Студијски програм Електротехника и рачунарство

Наслов рада Естимација крутости и адаптивно управљање код попустљивих робота

Ментор Коста Јовановић и Адриано Фађолини

Изјављујем да је штампана верзија мог докторског рада истоветна електронској верзији коју сам предао/ла ради похрањивања у **Дигиталном репозиторијуму Универзитета у Београду.**

Дозвољавам да се објаве моји лични подаци везани за добијање академског назива доктора наука, као што су име и презиме, година и место рођења и датум одбране рада.

Ови лични подаци могу се објавити на мрежним страницама дигиталне библиотеке, у електронском каталогу и у публикацијама Универзитета у Београду.

Потпис аутора

У Београду, 26.04.2021.

_____

образац изјаве о коришћењу

Изјава о коришћењу

Овлашћујем Универзитетску библиотеку „Светозар Марковић“ да у Дигитални репозиторијум Универзитета у Београду унесе моју докторску дисертацију под насловом:

Естимација крутости и адаптивно управљање код попустљивих робота

која је моје ауторско дело.

Дисертацију са свим прилозима предао/ла сам у електронском формату погодном за трајно архивирање.

Моју докторску дисертацију похрањену у Дигиталном репозиторијуму Универзитета у Београду и доступну у отвореном приступу могу да користе сви који поштују одредбе садржане у одабраном типу лиценце Креативне заједнице (Creative Commons) за коју сам се одлучио/ла.

1. Ауторство (CC BY)

2. Ауторство – некомерцијално (CC BY-NC)

3. Ауторство – некомерцијално – без прерада (CC BY-NC-ND)

4. Ауторство – некомерцијално – делити под истим условима (CC BY-NC-SA)

5. Ауторство – без прерада (CC BY-ND)

6. Ауторство – делити под истим условима (CC BY-SA)

(Молимо да заокружите само једну од шест понуђених лиценци.
Кратак опис лиценци је саставни део ове изјаве).

Потпис аутора

У Београду, 26.04.2021.

_____

1. **Ауторство**. Дозвољавате умножавање, дистрибуцију и јавно саопштавање дела, и прераде, ако се наведе име аутора на начин одређен од стране аутора или даваоца лиценце, чак и у комерцијалне сврхе. Ово је најслободнија од свих лиценци.

2. **Ауторство – некомерцијално**. Дозвољавате умножавање, дистрибуцију и јавно саопштавање дела, и прераде, ако се наведе име аутора на начин одређен од стране аутора или даваоца лиценце. Ова лиценца не дозвољава комерцијалну употребу дела.

3. **Ауторство – некомерцијално – без прерада**. Дозвољавате умножавање, дистрибуцију и јавно саопштавање дела, без промена, преобликовања или употребе дела у свом делу, ако се наведе име аутора на начин одређен од стране аутора или даваоца лиценце. Ова лиценца не дозвољава комерцијалну употребу дела. У односу на све остале лиценце, овом лиценцом се ограничава највећи обим права коришћења дела.

4. **Ауторство – некомерцијално – делити под истим условима**. Дозвољавате умножавање, дистрибуцију и јавно саопштавање дела, и прераде, ако се наведе име аутора на начин одређен од стране аутора или даваоца лиценце и ако се прерада дистрибуира под истом или сличном лиценцом. Ова лиценца не дозвољава комерцијалну употребу дела и прерада.

5. **Ауторство – без прерада**. Дозвољавате умножавање, дистрибуцију и јавно саопштавање дела, без промена, преобликовања или употребе дела у свом делу, ако се наведе име аутора на начин одређен од стране аутора или даваоца лиценце. Ова лиценца дозвољава комерцијалну употребу дела.

6. **Ауторство – делити под истим условима**. Дозвољавате умножавање, дистрибуцију и јавно саопштавање дела, и прераде, ако се наведе име аутора на начин одређен од стране аутора или даваоца лиценце и ако се прерада дистрибуира под истом или сличном лиценцом. Ова лиценца дозвољава комерцијалну употребу дела и прерада. Слична је софтверским лиценцама, односно лиценцама отвореног кода.